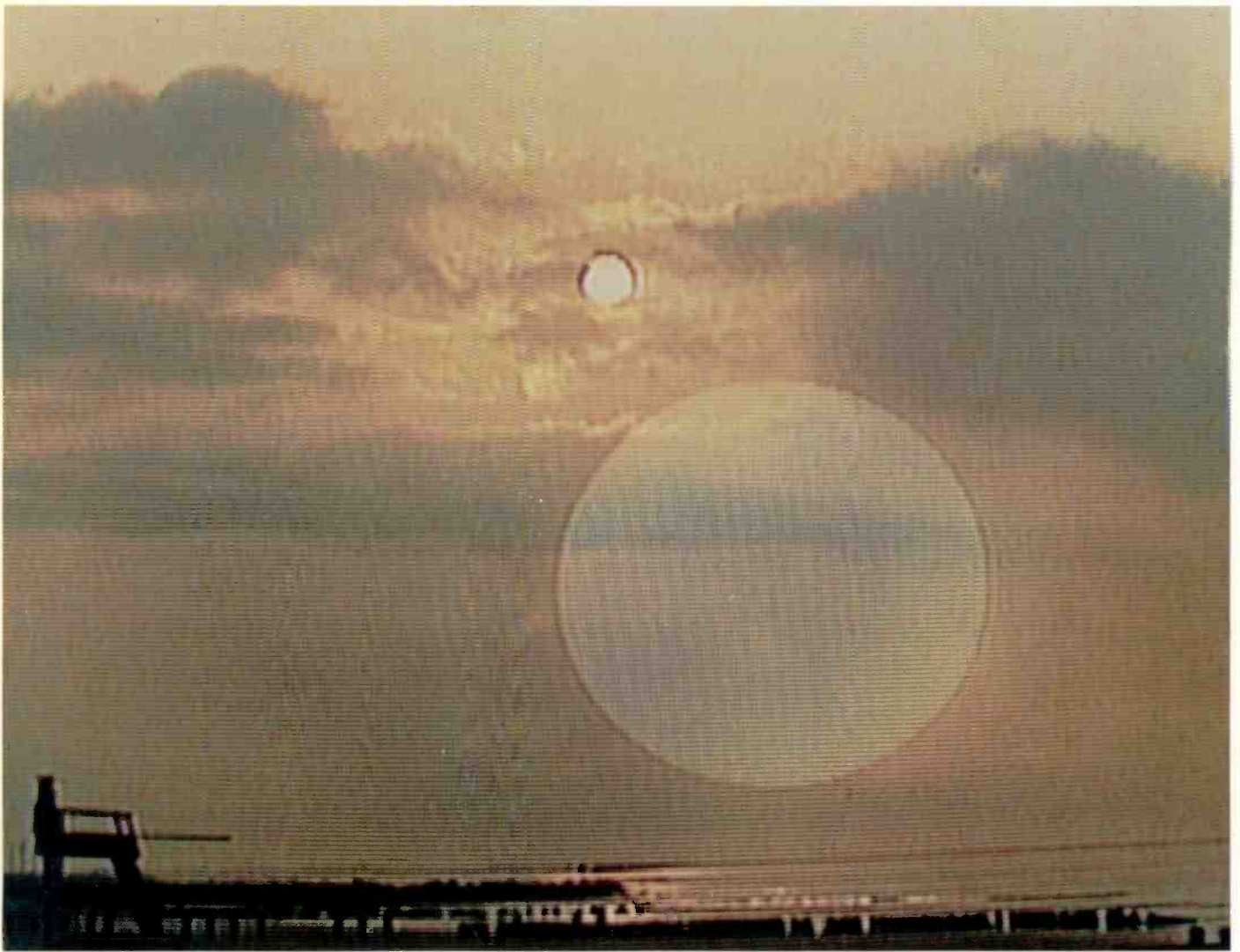


RCA Engineer

Vol. 29 No. 6 Nov./Dec. 1984



imaging technology

RCA Engineer

A technical journal published by the

RCA Technical Excellence Center □ 13 Roszel Road □ P. O. Box 432 □ Princeton, NJ 08540-0432 □ Tacnet: 226-3090

RCA Engineer Staff

Tom King Editor

Mike Lynch Associate Editor

Louise Carr Art Editor

Mike Sweeny Contributing Editor

Phyllis Grimm Secretary

Mike Booth Composition Specialist

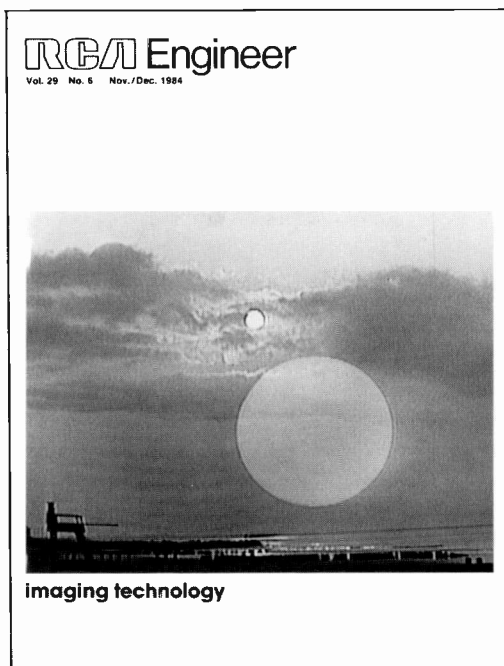
Editorial Advisory Board

Tony Bianculli Manager, Engineering Information, Technical Excellence Center □ **Jay Brandinger** Staff Vice-President, Systems Engineering, RCA Laboratories □ **Jim Carnes** Division Vice-President, Engineering, Consumer Electronics Division □ **John Christopher** Vice-President, Technical Operations, RCA

Americom □ **Jim Feller** Division Vice-President, Engineering, Government Systems Division □ **Mahlon Fisher** Division Vice-President, Engineering, Video Component & Display Division □ **Larry Gallace** Director, Product Assurance, Solid State Division □ **Arch Luther** Senior Staff Scientist, RCA Laboratories □ **Howie Rosenthal** Staff Vice-President, Engineering □ **Joe Steoger** Division Vice-President, Engineering, RCA Service Company □ **Bill Underwood** Director, Technical Excellence Center □ **Bill Webster** Vice-President, RCA Laboratories

Consulting Editors

Ed Burke Administrator, Marketing Information and Communications, Government Systems Division □ **Walt Dennen** Manager, Naval Systems Department Communications and Information, Missile and Surface Radar □ **John Phillips** Director, Business Development, RCA Service Company



Cape May, New Jersey, August 4, 1984, just after dawn.

Our cover is an off-monitor shot of a Broadcast Systems Division videotape entitled "A Director's Diary." This eight-minute tape, made with the CCD-1 broadcast camera, provides a striking commentary on the capabilities of the camera.

We chose the cover photo because it illustrates a unique capability of the CCD-1 camera—it can look directly at the sun, or any other bright light, without being damaged. In this case, only a neutral density filter was used. This shot was taken during a fade from a full-screen view of the sun to a long view of the seashore. The large transparent disk in the center is the fading closeup of the sun. Notice that even with the bright sun in the background, there is no loss of detail elsewhere in the picture. The rest of the photo sequence is on the inside back cover.

We want to thank **Andy Hilliard**, Broadcast Systems Division, for the videotape, and **Rod Borschardt**, RCA Laboratories, for his time and technical help.

□ To disseminate to RCA engineers technical information of professional value □ To publish in an appropriate manner important technical developments at RCA, and the role of the engineer □ To serve as a medium of interchange of technical information among various groups at RCA □ To create a community of engineering interest within the company by stressing the interrelated nature of all contributions □ To help publicize engineering achievements in a manner that will promote the interests and reputation of RCA in the engineering field □ To provide a convenient means by which the RCA engineer may review professional work before associates and engineering management □ To announce outstanding and unusual achievements of RCA engineers in a manner most likely to enhance their prestige and professional status.

Imaging Technology—RCA's traditional strength

I believe it is fair to say that of the five senses people use to communicate with one another or measure their surroundings, vision is the most dominant and most useful. In this time when our corporate strategy is to return to our core businesses, we should keep in mind that imaging technology is RCA's central unifying element. The strongest of all.

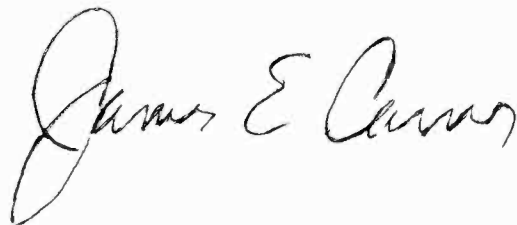
What is wonderfully amazing about imaging technology is that after all these years of endeavor to understand the basic human visual process, to use it as a tool and technique, and to invent, develop, manufacture, and market products that use imaging technology, we are nowhere near exhausting its potential.

This issue of *RCA Engineer* is a testament to that fact. Even as the business of building and selling NTSC television products grows at unexpected rates, we are nearing the threshold of a new era called high definition television—HDTV.

If an NTSC picture is worth a thousand words, then an HDTV picture will be worth ten thousand words. Again, as with NTSC, RCA will play a pivotal role in establishing HDTV standards—in part because of fundamental visual perception studies pursued at RCA Laboratories and reported in this issue. Other articles illustrate an interesting symbiotic relationship

between ICs and imaging: how CCD technology is beginning to fulfill its promise as an imaging tool, and how imaging technology affects the manufacture of ICs. Also discussed are pattern recognition and classification techniques, and signal processing techniques.

Few technologies are as central to the day-to-day needs of mankind as imaging technology. Few companies have played such a successful, central role in imaging as RCA has over the past 50 years. Few technologies stand on the threshold of broad new advances and growth. We have the tools, the expertise, the track record, the opportunity. It is up to all of us to bring all our talents to bear as we extend RCA's contributions in the years ahead.



James E. Carnes
Division Vice President, Engineering
Consumer Electronics Division

RCA Engineer

Vol. 29 | No. 6 November | December 1984

overview & tutorials

- 4** Electronic imaging with CCDs
G.W. Huges
- 11** Encoding and decoding wideband I chroma signals
R.T. Keen
- 15** U.S. color television fundamentals—a review
D.H. Pritchard

image processing & analysis

- 28** Perceptual analysis and simulation of color monitor displays
R.W. Klopfenstein | A.P. Pica | C.R. Carlson
- 33** Pyramid methods in image processing
E.H. Adelson | C.H. Anderson | J.R. Bergen | P. J. Burt | J.M. Ogden
- 42** Real-time dynamic range compression of electronic images
D.F. Dion | M.J. Cantella
- 47** Development of multispectral detector technology
J.R. Tower | B.M. McCarthy | R.T. Strong | L.E. Pellon | E.G. Watson | K.F. Kinnard
H. Elabd | A.G. Moldovan | P.A. Levine | D.M. Hoffman | W.M. Kramer | R.W. Longsdorff
- 56** Multifeature methods for target detection
W.E. Schaming | L.E. Toombs

general interest

- 60** Nickel-hydrogen batteries come of age
S.F. Schiffer
- 66** Fat Albert peers over the horizon
L. Mertens | J. Houyouse | P. Gelzinis

departments

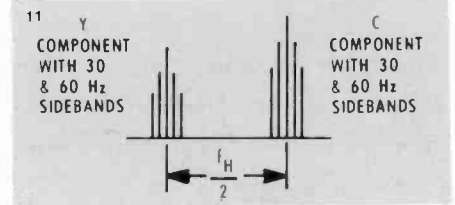
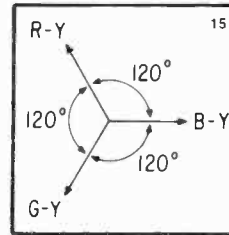
Patents, **73** | Pen and Podium, **75** | News and Highlights, **77**
Obituaries, **82**

**in this issue ...
imaging technology**

■ **Hughes:** "The RCA FT imager is unique in the commercial world in that it is thinned to 10 micrometers, laminated to optical glass for support, and backside-illuminated."

■ **Keen:** "Due to advances in charge-coupled device (CCD) applications (such as comb filtering), commercial television receivers are now able to accept and process all video information . . ."

■ **Pritchard:** "In consumer television, the detector response (except for scientific measurement purposes) consists of the spectral sensitivity of the 'standard' human eye."



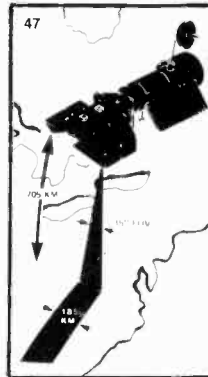
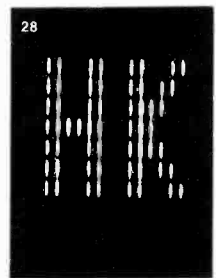
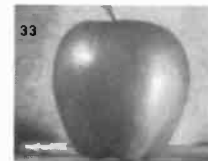
■ **Pica:** "An arbitrary image is analyzed for the purposes of JND analysis by taking its scaled transform and integrating the resulting power spectrum over successive channels of a one-octave bandwidth."

■ **Adelson:** "Because the pyramid is useful in so many tasks, we believe that it can bring some conceptual unification to the problems of representing and manipulating low-level visual information."

■ **Dion:** "Histogram equalization processing of an image statistically compresses the image by attenuating those gray level ranges within it that occur infrequently, while stretching those that occur frequently."

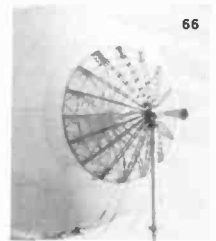
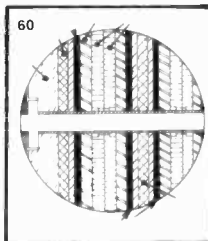
■ **Tower:** "At RCA, our work on the NASA VIS/NIR sensor builds directly on the CCD technology of the SID403 imager."

■ **Schaming/Toombs:** "Bayes' theorem is used to determine the probability that a pixel in the target window is actually a target pixel . . ."

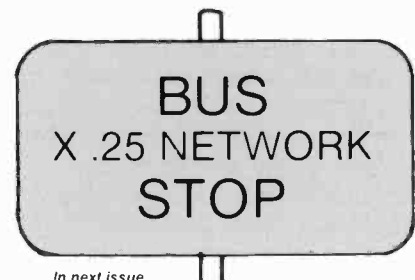


■ **Schiffer:** "We expect that the usable life of the batteries will exceed 10 years at relatively deep depths of discharge in orbit."

■ **Mertens:** "The aerostat system must be able to remain on station at 10,000 to 12,000 feet altitude for up to one week without refueling or other routine maintenance."



in future issues...
communications
automated testing
statistics in manufacturing
project management
sources of RCA technical information



In next issue

Electronic imaging with CCDs

Electronic imaging is at a major turning point due to the emergence of manufacturable, high-performance CCD imagers. The high sensitivity and complete elimination of lag in these devices allows CCD cameras to make high-quality images not available from tube cameras.

Almost since their invention in 1970,¹ charge-coupled devices (CCDs) have been hailed as the ideal solid-state replacement for beam-scanned imaging tubes in television cameras. While much progress has been made in the last 14 years, it is only recently that commercial CCD imagers have demonstrated performance characteristics good enough to rival tubes. The reasons for this are typical of emerging technologies and have to do with price and performance learning curves.

The slow development of CCD imagers is primarily due to the size and complexity of the chip, and to a lesser degree, continuing developments in tube technology. In spite of their apparent simple structure, full

Abstract: *CCD imagers for TV are just now becoming available in large quantities. Several solid-state cameras have been announced that are the first wave of a new generation of high-performance, low-cost cameras that will change the way in which video is used and perceived. This paper reviews the characteristics of various solid-state imager sensor types, and compares representative imagers that are in use today. Present applications of CCD image sensors and the future direction of imager and camera development are discussed.*

TV resolution imagers are VLSI chips and require VLSI manufacturing technology in order to make them at a reasonable yield. Integrated circuit manufacturers are just now beginning to be capable of making such large chips. Imaging tube technology has not been stagnant during the CCD development period, either. Imaging tubes have continued to improve, delivering better performance at a lower cost every year. As a result, CCD imagers of vidicon quality are just now becoming manufacturable for high volume applications.

From the present vantage point it appears that we have finally turned the corner and are on our way to a future in electronic imaging dominated by CCDs and other solid-state image sensors. Although almost all electronic vision needs are now being met by tubes, several significant new products were recently announced that foretell the future of the imaging business. RCA, Sony, and Toshiba have introduced compact, low-power, solid-state consumer color video cameras in this country. The Sony and Toshiba cameras use CCD imagers, while the Hitachi-made RCA camera uses an MOS image sensor. All of these cameras use a single image sensor mated with a suitable checkerboard-like color filter pattern to produce the color video signal. Sony and RCA have also started to market monochrome industrial CCD cameras. The SONY camera, in particular, is highly advanced in the use of custom LSI chips and miniaturized sur-

face-mounted circuit boards.² The most significant technological advance in the imaging area is the CCD broadcast television camera announced by RCA in April 1984.³ This camera uses three CCD sensors, one for each of the primary colors—red, green, and blue. By any measure, this is the highest-performance solid-state camera announced yet by any manufacturer in the world. It exceeds the performance of broadcast tube cameras in all areas of measurement except static resolution.⁴

Advantages of solid-state imagers

The pervasiveness of successful integrated circuit technology has raised our level of expectations for all solid-state devices. We automatically expect them to have certain advantages, such as low power consumption, high reliability, long life, and low price. These characteristics are also achievable with solid-state image sensors. More important, though, are other solid-state imager characteristics that enhance the desirability of these devices for electronic imaging.

Unlike tubes, solid-state imagers have excellent geometric registration (important for 3-chip color broadcast cameras and robotics), have no microphonic problems, and exhibit no burn-in from intense overloads. If the solid-state imager is a CCD of the right architecture, it can also be completely free from the lag or "sticking" problems inherent in photoconductive tubes,

and can deliver noise-free pictures at light levels much below those necessary for vidicons. On the other hand, all visible solid-state image sensors exhibit an undesirable phenomenon not seen in tubes. This problem is called highlight smear, and it occurs as an unwanted vertical bright line coincident with every pixel in highlight portions of the scene. It can be minimized to varying degrees depending upon the architecture chosen, but only in the case of the frame transfer imager, as used by RCA in its new broadcast camera, can it be eliminated completely with a mechanical shutter.

Solid-state imager architecture

Figure 1 schematically shows the five most common architectures used in monolithic solid-state imagers. In each, the cross-hatched areas represent the photosensitive part of the imager, and the segmented bars with arrows are the CCD registers.

Figure 1a shows the so-called MOS sensor.⁵ This device consists of an array of X-Y-addressed photodiodes with MOS readout circuits. Structurally, this imager resembles an MOS dynamic RAM, and in fact one of its main advantages is that it can be fabricated directly on a DRAM production line with no modifications in the process. This results in a significant manufacturing and cost advantage because of economies of scale and commonality of processes. Since this is a two-dimensional structure, the MOS readout circuits must be interleaved between the array of photodiodes, and not all of the imager area is photosensitive (it has less than 100 percent optical "fill factor"). In normal TV usage the photodiodes are operated in the vidicon mode, meaning that they are reset to some potential and allowed to stare at the scene for a period of time, typically 1/30 s.

The major disadvantage of this sensor is its low sensitivity and high random and fixed-pattern noise. The low sensitivity is due to a low optical fill factor of typically 25-33 percent, which prevents use of all the incident photons. More important, however, is the random and fixed-pattern noise associated with the high-capacitance buses used in the X-Y addressing scheme. In solid-state imagers, a temporal readout noise is present that is proportional to the squareroot of the reset capacitance. This noise is typically an order of magnitude larger in MOS sensors, which have large capacity buses, than in a well-designed CCD imager, where the reset capacitance

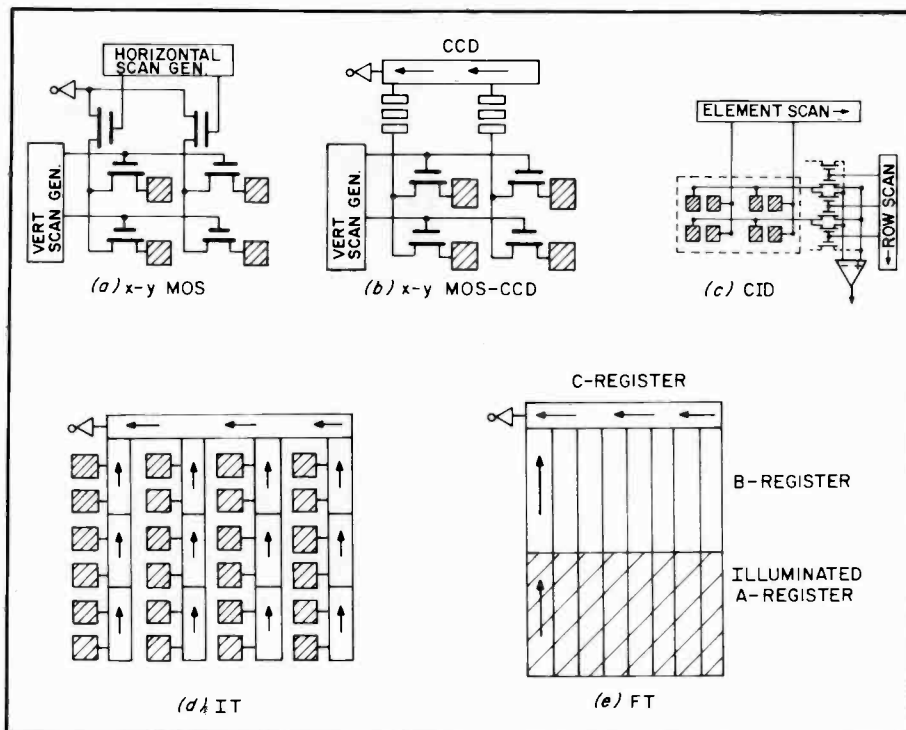


Fig. 1. Solid-state imager architectures: (a) MOS sensor; (b) Hybrid MOS/CCD sensor; (c) Charge Injection Device (CID); (d) Interline Transfer (IT) sensor; and (e) Frame Transfer (FT) sensor.

is only that of one gate and can be very small.

A fixed-pattern clock noise is also present in MOS sensors. A pattern of vertical lines appears in the picture at sufficiently low light levels due to capacitive pickup of the clock waveforms by the on-chip video circuitry. Extraordinary means are usually taken to minimize this noise, but in practice it is the dominant noise source in such an imager. In a CCD imager this clock pickup is limited to a single output node, and can be eliminated completely.

To overcome the noise limitations, MOS/CCD structures have been built as shown in Fig. 1b.^{6,7} This device uses a CCD register for horizontal scanning, which provides a means of transferring charge from the high-capacitance column electrodes to a low-capacitance CCD register. The presence of the CCD register eliminates any vertical lines due to clocking. The low-capacitance CCD readout, together with charge priming of the column electrodes, enables these devices to operate with random and fixed-pattern noise levels that fall between MOS and full CCD imagers. This imager is a contender for markets such as home video, where the ultimate in sensitivity may not be of primary importance.

Figure 1c shows a charge-injection (CID) type of imager.⁸ This device is also an X-Y-addressed imager, and has some of the

same characteristics as MOS imagers. Two advantages it has over CCDs are that it can be fabricated in semiconductor materials with poor charge-transfer efficiency (such as InSb, used for some types of IR imagers), and that it can be used in a non-destructive readout mode. In practice, however, this imager has not gained wide acceptance. Most manufacturers prefer to use either MOS sensors or CCD imagers.

Figure 1d shows the most commonly used CCD imager format, the interline transfer (IT) structure.⁹ In this device the photons are detected with p-n or MOS photodiodes that are embedded in an array of CCD column registers. Horizontal readout is accomplished with a CCD register, as shown. As in the MOS imager, the diodes are operated in the vidicon mode. After integration, the charge is dumped into the vertical registers during the vertical blanking time, and then shifted up to the horizontal register row by row during the horizontal blanking time. This allows all the transients of the vertical clocks and transfer pulses to be confined to the blanking times, where they are not visible in the image. Typically, the CCD registers are covered with an opaque shield to prevent photo generation of charge in the registers, and to minimize highlight smear. In practice, this shield is not 100-percent effective, and significant highlight smear is usually

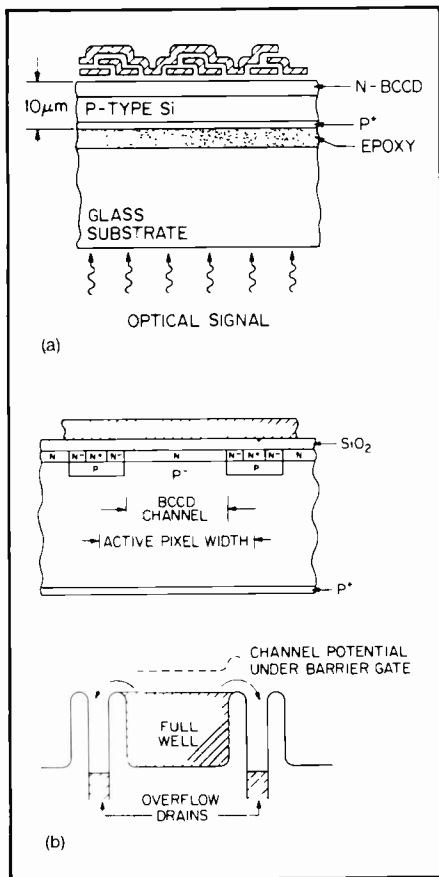


Fig. 2. RCA 403 × 512, thinned, backside-illuminated, 3-poly, FT imager. (a) Cross-sectional view perpendicular to the transfer direction showing the three-level polysilicon gates, buried-channel CCD, and details of glass lamination. (b) Cross-sectional view down the channel, showing buried overflow drains and potential profile.

seen. Another limitation of these sensors when photodiode detectors are used is a small but noticeable lag due to incomplete charge transfer from the photodiode. Structural modifications have been made that minimize this effect, but it still exists to some degree.¹⁰ Sony, to eliminate this problem entirely, uses a photogate detector made with a very thin polysilicon gate layer.² This is a compromise solution, and it limits the quantum efficiency in the blue due to optical absorption in the poly layer.

All of the imagers discussed thus far are illuminated from the front side and are made on conventional-thickness silicon wafers. They all provide some means for controlling blooming. The interline-transfer CCD and MOS imagers are the most common devices used in consumer one-chip cameras today. Except for the color filter layer, the rest of the device is fabricated by conventional IC wafer fabrication methods.

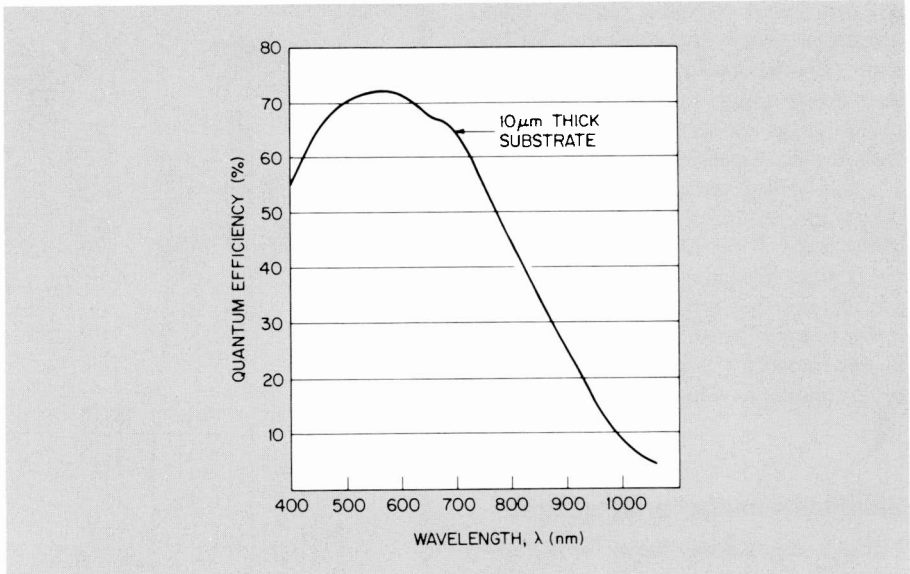


Fig. 3. Spectral response of RCA 40 × 512 FT imager with buried blooming drains.

Figure 1e shows the frame transfer (FT) architecture¹¹ used in RCA's new high-performance CCD broadcast camera. In operation, the A register is illuminated for the integration time, usually 1/60 of a second, and charge is generated there by photoexcitation across the silicon bandgap. During the vertical retrace this charge pattern is transferred up to storage register B. During the horizontal retrace, each line is transferred, one at a time, to horizontal register C, and then scanned out through the on-chip amplifier at the TV horizontal-line rate. Like the imagers discussed earlier, FT imagers can be operated with front-side illumination. However, to ensure good blue response, they use either thinned polysilicon or transparent CCD gates, or are made with the so-called virtual-phase structure that allows polysilicon apertures in certain regions of the device.¹²

The RCA FT imager is unique in the commercial world in that it is thinned to 10 micrometers, laminated to optical glass for support, and backside-illuminated. This allows good blue response, and since we have constructed it with buried blooming drains, we are able to achieve a 100-percent fill factor. The result is at least 60 percent quantum efficiency over the whole visible spectrum.¹³ Figure 2 shows cross-sectional views of the imager, and Fig. 3 is a typical quantum efficiency curve demonstrating the excellent optical response.

Performance and cost considerations of solid-state imagers

The variety of architectures being used for solid-state imagers is due to two primary

factors: performance requirements and cost. If a product is being designed for consumer use, and the ultimate in sensitivity is not required, then the MOS sensor might be the logical choice. With this technology, the sensor can be fabricated on a high-volume DRAM production line, thus taking advantage of the predictable yield and low period-costs of the facility.

If a consumer product is still the application, but sensitivity is considered a fairly important issue, then an IT CCD imager might be chosen. Like the MOS sensor, this device is frontside-illuminated, which simplifies wafer fabrication and allows the possibility of monolithic color filter fabrication in the process.

If the highest sensitivity and the complete absence of highlight smear and lag are absolute requirements, then the FT CCD approach might be chosen, as it was at RCA.

The best solid-state imagers are being used in either consumer one-chip cameras or broadcast three-chip cameras. Table I summarizes the important characteristics of the major imagers either in use today or announced for use in commercial color camera products in the U.S. Other, more advanced imagers have been announced in the research literature, but these have yet to be proven manufacturable, and have not been included here.

A precise comparison of the cost of these different imagers is not possible because of the proprietary nature of fabrication processes, yield, and factory operating cost. However, the most sensitive factor in cost for integrated circuits is chip area. The number of potential good chip sites

Table 1. Characteristics of major solid-state imagers in use today.

Mfgr.	No. of Pix. (H × V)	Format & Arch.	Noise (rms ϵ)	Chip Size (mm ²)	Sensitivity (@46dB S/N, f/1.4)	Lag	Smear
Hitachi ⁷	388 × 492	2/3" MOS/CCD	260	85	180 lux	small	yes
NEC ²⁵	384 × 490	2/3" IT-CCD	65	79		small	small
RCA	403 × 512	1/2" FT-CCD	55	82	8 lux	none	none†
SONY ²	384 × 491	2/3" IT-CCD	60	100	49 lux	none	yes
Toshiba ¹⁷	398 × 492	1/2" IT-CCD	65	51	204 lux*	small	yes

† with a mechanical shutter

* 1-chip color camera. Sensitivity for a monochrome camera will be higher.

on a silicon wafer is inversely proportional to chip area, and yield is almost exponentially dependent on it.¹⁴ Therefore, from a cost standpoint it is very important to keep size to a minimum.

A second generation of interline transfer imagers with higher resolution (typically 768H), higher fill factor (approximately 80 percent), and very low transfer smear are beginning to appear in the literature.¹⁵⁻¹⁶ MOS/CCD sensors with reduced noise levels are also planned. While the manufacturability of these devices is still in question, they, or variants of them, will undoubtedly be seen in future consumer products.

Like tubes, all solid-state imagers are made to fill the optical aperture of standard TV camera lenses. The most common lenses on the market are 2/3-inch, 1/2-inch, and Super-8 formats. RCA's FT imager is a 1/2-inch device, but its size is approximately that of a 2/3-inch IT imager. Most Japanese manufacturers are in production with 2/3-inch imagers at the present time, although Toshiba has announced a consumer color camera with a 1/2-inch imager,¹⁷ and a Super-8-format imager has been announced by Matsushita.¹⁸ These smaller imagers have a considerable cost advantage over the most common 2/3-inch imager size, but because of smaller pixels they also have less sensitivity. Nevertheless, they will undoubtedly fuel the low-end camera market in the future, leaving the larger, more sensitive chips to service the higher-performance markets.

Applications

In the commercial area there are three major camera market segments, each with somewhat different requirements. A broad

area called industrial cameras is dominated today by the industrial surveillance business. This market uses mostly black-and-white cameras, although color is beginning to make some inroads. At present there are only a few solid-state B&W cameras available with the sensitivity required for surveillance. RCA is a leader in this field, both in terms of market share¹⁹ and performance. The industrial automation and robotics market is currently a small segment of this industrial market, but it has the potential for eventually dominating it. The availability of low-cost, high-performance solid-state cameras should help this market develop at a much faster rate in the future. One of the requirements in the robotics area is a small, low-mass, high-performance camera that can be used at the end of movable robot arms. SONY appears to be aiming their latest small industrial camera at this kind of market.²

The market of interest to most people is the consumer home video market. All approaches to this market have been with cameras using only one imager chip with an integrated color filter. This color filter pattern typically is a checkerboard-like pattern, and it allows designers to trade off color information for resolution.

At the present time several manufacturers, including RCA, have introduced solid-state or CCD cameras for this market with varying degrees of performance. Most of these cameras are not quite sensitive enough yet to be used indoors under nighttime home lighting conditions, although CCD cameras have a distinct advantage here because of their higher sensitivity. These cameras are all presently priced at around \$1000, and require a somewhat cumbersome separate recorder for remote use. However, we expect that soon CCD and

other solid-state cameras will be available with self-contained camera and recorder in one compact unit. If such a product can be introduced with a standard tape format, high-volume sales will begin. This will undoubtedly allow this product to follow the classical consumer product learning curves. We can then expect to see a repeat of the videotape recorder phenomenon, with rapidly dropping prices and continual improvements in features and performance.

Broadcast television is an area in which CCD imagers really show their advantages. This is a high-performance market that demands the ultimate in performance from sensors. RCA has recently introduced a three-chip CCD electronic news-gathering (ENG) broadcast camera that outperforms all other cameras, including tube cameras, in all areas except static test-pattern resolution³ (see Fig. 4). The dynamic resolution for moving scenes is actually better than that of a tube camera because of the resolution-degrading smear of tubes. This camera uses three of the RCA 1/2-inch FT CCD sensors just described. These CCDs are organized with a 403(H) × 512 (V) pixel format, and operate in the field-integration mode whereby the integration time for each field is 1/60 s. This gives the camera a significant advantage over cameras with frame integration (1/30 s) due to the reduced field lag. The camera has absolutely no highlight smear when a rotating mechanical shutter is used, and delivers a substantial improvement in sensitivity and signal-to-noise ratio over tube cameras. It will deliver a "full level" signal with only 2.5 footlamberts of scene illumination¹³ (see Fig 5).

At the present time, this camera does not have as much horizontal resolution as the best tube cameras, but under dynamic



Fig. 4. NBC reporter Connie Chung interviewing a delegate at the 1984 Democratic Convention, using the RCA CCD-1 electronic news-gathering camera.

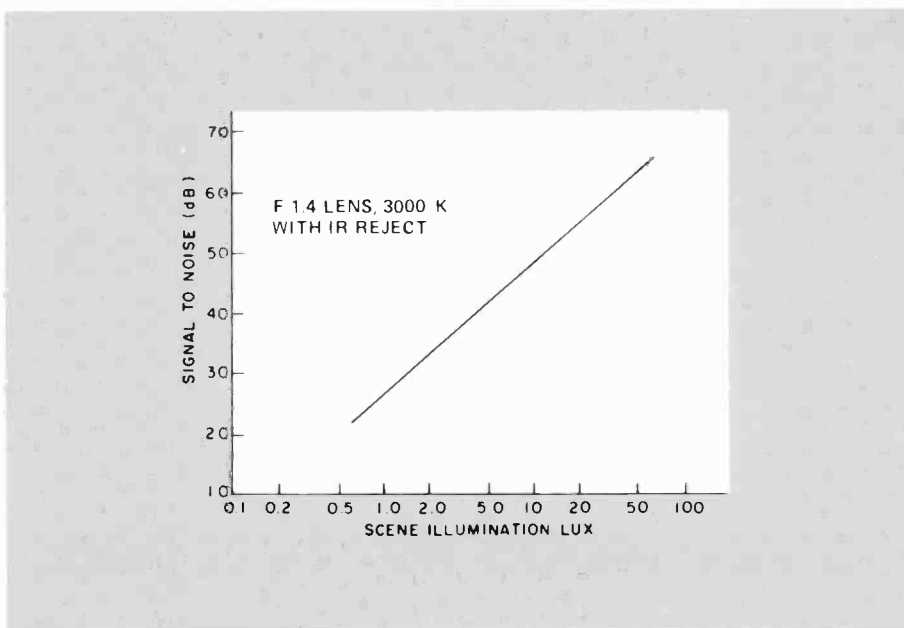


Fig. 5. Signal-to-noise ratio vs scene illumination for RCA 403 × 512 FT imager.

conditions (which is what television is used for anyway), it is far superior to any tube camera because of the complete absence of lag. This is shown graphically in Fig. 6. Since this camera uses a mechanical shutter to eliminate smear, it can be used to further advantage if the exposure time of the shutter is reduced. In this mode of operation it becomes a "flash frame" camera with excellent dynamic resolution characteristics not possible with tube cameras (see Fig. 7).

Future directions

It has been exciting to watch the rapid growth of the integrated circuit industry. The historical trend in silicon IC development has been to increasingly larger and denser circuits at a continually decreasing cost-per-gate. CCD imager development will not disappoint industry watchers in this regard.

Outside the commercial area there have been several promising research developments at RCA that will result in significant advances in imaging for remote sensing and for infrared imaging applications. RCA Labs and the Government Systems Division, Advanced Technology Labs have been under contract with NASA to develop line sensors for the visible/near-IR (VIS/NIR) and short-wave IR (SWIR) optical bands.²⁰ These sensors are designed for use in the next generation of LANDSAT instruments for remote sensing from satellites. The VIS/NIR imager is a four-band, mechanically butttable line sensor that uses RCA's thinned, backside-illuminated frame transfer technology and optical narrow-band interference filters. The SWIR imager is a two-band, Schottky-barrier, mechanically butttable line sensor that uses the Schottky-barrier CCD technology developed at RCA for thermal IR area imagers.²¹ In a free-flying satellite instrument these imagers will be butted to form line imagers for the VIS/NIR and SWIR bands of 12,000 pixels and 6,000 pixels, respectively. The performance projected for an instrument using both of these imagers will exceed the present LANDSAT instrument in spatial and spectral resolution, dynamic range, and sensitivity.

RCA Labs has also been at the forefront of infrared CCD (IRCCD) area imager development. We have pioneered the Schottky-barrier IRCCD approach to solid-state IR imaging, and have recently demonstrated large-area imagers with a format of 160(H) × 244(V) pixels that meets or exceeds the requirements of many military

and industrial IR imaging applications.²² Figure 8 shows night imagery recently taken with this imager.

For high-performance commercial visible imager applications, CCDs will be the imagers of choice because of their inherently better low-noise performance. MOS imagers may continue to be viable for low-cost applications, but will find it increasingly difficult to compete with CCDs as the industry learns how to produce them cost effectively.

Because of the large number of pixels required for full TV resolution and the minimum feature size of IC technology, solid-state imagers for television are at least as difficult to manufacture as 256k RAMs. If imager chip-area is also taken into consideration, then the comparison should be made with 1M RAMs.

Advances in IC fabrication technology are driven by the high-volume RAM market. When IC facilities complete their changeover to 6-inch, and eventually 8-inch, silicon wafers, chips as large and complex as imagers will become commonplace and inexpensive. As the IC world learns how to make 256k and 1M RAMs cheaply, solid-state imagers will follow right along. Some of the products that will use these imagers exist today, some are embryonic, and some have not yet been identified.

We expect the availability of inexpensive imagers and custom camera ICs to fuel the growth of the home video camera market. The growth of home video recording has been phenomenal, with 2 million VCRs sold in this country in 1982, 4 million in 1983, and 7 million projected for 1984.²³ While a comparable volume cannot be expected for cameras, a significant fraction is anticipated.

Until now, the use of CCD cameras in industrial and other non-TV applications has not been large. Cost, size, weight, and power are probably the major causes for this lack of development. In the future we will undoubtedly see a "camera on a chip" become available. When it does, we can expect to see many sensing applications unfold that are served by other means now, and some that we are not even aware of yet. These applications may not need full TV resolution, and they may not even be used with a human observer "in the loop."

At the other end of the cost and performance spectrum, high-resolution CCD imagers for electronic still photography²⁴ and high-definition TV (HDTV) will become a reality. A typical U.S. HDTV scenario calls for a 5:3 image format with



Fig. 6. Split-screen photo of TV monitor comparing superior lag characteristics of RCA broadcast CCD camera. Saticon tube camera is on left, RCA CCD camera is on right.

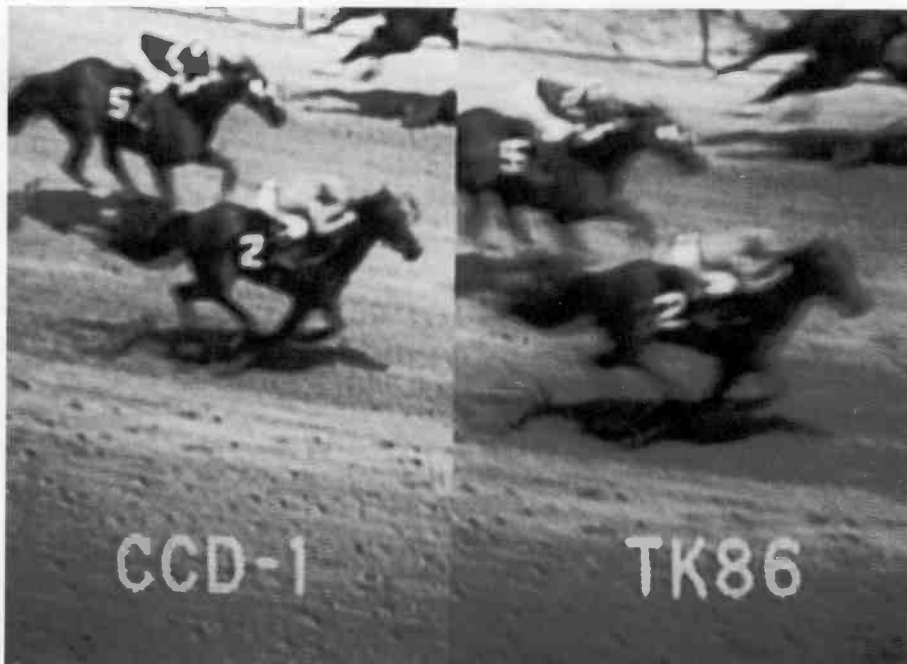


Fig. 7. Split-screen photo of TV monitor comparing "flash-frame" mode of operation of RCA CCD broadcast camera. RCA CCD-1 camera is on left, TK-86 saticon tube camera is on right.

approximately 1500(H) × 1050(V) pixels. Although a CCD imager of this size is not yet manufacturable to broadcast-TV specifications, the demands to produce such an imager will be great if HDTV is to live up to its promise. Beam-scanned vacuum-tube imagers are not adequate sensors for this task. Registration of the three tubes is a major problem. Even more importantly,

the small beam spot-size results in a significant reduction in sensitivity (or increase in capacitive lag) that is worse than in present broadcast tubes. Without a doubt, for CCD technologists HDTV will offer the greatest challenge of any present or planned commercial application. Advances in VLSI technology will ease the burden somewhat, but as they have in the past,



Fig. 8. TV monitor photo of night imagery taken with 160×244 Schottky barrier-IRCCD imager developed at RCA Laboratories.

CCD imagers will continue to be at the leading edge of integrated circuit technology.

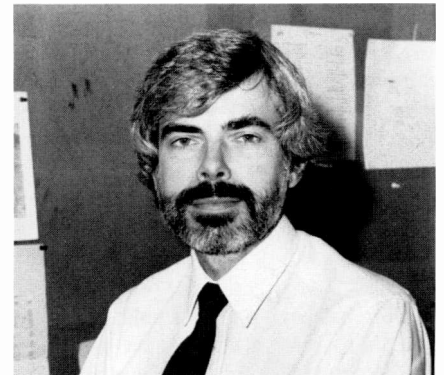
References

1. W.S.Boyle and G.E.Smith, "Charge Coupled Semiconductor Devices," *Bell System Technical Journal*, vol. 49, pp. 593, April 1970.
2. K. Yamagata et al., "Miniature CCD Camera and its Machine Vision Applications," Intl. Electronic Imaging Exposition & Conference, Boston MA, Sept. 10-13 1984.
3. D.J.Woywood, "The RCA CCD-I Broadcast Color Camera", National Association of Broadcasters Convention, Las Vegas, Nevada, April 29-May 2, 1984.
4. E.D.Savoye et. al., "High Sensitivity CCD Imagers for Television," 28th annual SPIE International Technical Symposium, August 19-24 1984, San Diego, CA.
5. M.Aoki et al., "2/3-inch Format MOS Single-Chip Color Imager," *IEEE Trans. Electron Devices*, vol. ED-29, pp. 745-750, April 1982.
6. S. Terakawa et al., "A New Organizational Area Image Sensor with CCD Readout Through Charge Priming Transfer," *IEEE Electron Devices Letters*, vol. EDL-1, pp. 86-88, May 1980.
7. S. Ohba et al., "MOS Imaging with Random Noise

Suppression," *IEEE International Solid-State Circuits Conference Digest*, p 26-27, 1984.

8. H.K.Burk and G.J.Michon, "Charge-Injection Imaging: Operating Techniques and Performance Characteristics," *IEEE J. Solid-State Circuits*, vol. SC-11, pp. 121-127, February 1976.
9. L. Walsh and R. H. Dyke, "A new Charge-Coupled Area Imaging Device," *Proc. of CCD Applications Conf.*, San Diego CA, pp. 21-22, Sept. 1973.
10. N. Teramishi et. al., "No Image Lag Photodiode Structure in the Interline CCD Image Sensor," *IEEE 1982 IEDM Technical Digest*, pp. 324-327.
11. C. Sequin and M. Tompsett, "Charge-Coupled Devices," *Adv. Electron Phys.*, Suppl. 8, (1975).
12. J. Hynccek, "Virtual Phase Technology: A New Approach to Fabrication of Large Area CCDs," *IEEE Trans. Electron Devices*, Vol. ED-28 (5), pp 483-489, 1981.
13. P. A. Levine et. al "High Performance Frame Transfer CCD Imager For Television Applications," Intl. Electronic Imaging Exposition & Conference, Boston MA, Sept. 10-13 1984.
14. W. J. Bertram, "Yield and Reliability," *VLSI Technology*, S. Sze, ed., McGraw Hill 1983, pp 599-612.
15. E. Oda et. al., "A CCD Image Sensor with 768×490 Pixels," 1983 *IEEE International Solid-State Circuits Conference Digest*, pp 264-265.
16. Y. Ishihara and K. Tanigaki, "A High Photosensitivity

- IL-CCD Image Sensor with Monolithic Resin Lens Array," *IEEE 1983 IEDM Technical Digest*, pp 497500.
17. K. Ooi et. al., "A New Frequency Interleaving CCD Color Video Camera," Intl. Electronic Imaging Exposition & Conference, Boston MA, Sept. 10-13 1984.
18. *Electronics magazine*, p. 71, September 8, 1983.
19. J.R. Tower et al., "Development of multispectral detector technology," *RCA Engineer*, this issue.
20. J. Tower et al., "Visible and Short Wave Infrared Push-broom Sensors for Remote Sensing Instruments," International Geophysical and Remote Sensing Symposium, Strasbourg, France, August 27-30 1984.
21. W.F.Kosonocky et al., "Performance Characteristics of Schottky Barrier Infrared Detector Arrays," Meeting of IRIS Specialty Group on Infrared Detectors, August 14-16, 1984, Seattle, WA.
22. *Electronics Week*, pp. 93-94, July 23, 1984
23. C. Cohen, "Experimental camera records color slides on small disc for display on TV set," *Electronics*, Vol 54 (18), pp 76-79.
24. Y. Ishihara et al., "Interline CCD Image Sensor with an Antiblooming Structure," *IEEE Trans. Ed-31* (1), pp. 83-88, Jan. 1984.



Gary Hughes is Head, CCD Imagers and Systems Research at RCA Laboratories. He joined RCA in 1973 as a Member of the Technical Staff, and has worked in various aspects of MOS IC technology since that time. Presently he is responsible for visible and infrared CCD imager research. In 1984 he received the David Sarnoff Award for contributing to the development of the CCD high-performance TV camera.

Contact him at:
RCA Laboratories
Princeton, N.J.
Tacnet: 222-3056

Encoding and decoding wideband I chroma signals

It has been over 25 years since the color television broadcast signal was defined. Now, with the help of the CCD comb filter, we can process all of it.

The National Television Systems Committee (NTSC) definitions for a broadcast color signal includes an extra color resolution called "wideband I." Until recently, this extra color resolution has not been used in any color receiver on the consumer market because signal processing techniques had not been refined enough to extract this extra information from the composite video signal. Due to advances in charge-coupled device (CCD) applications (such as comb filtering), commercial television receivers are now able to accept and process all the video information presented to the receiver according to the NTSC standards.

NTSC color signal broadcast standards

Dalton Pritchard's article, also in this issue, will help those of you who may be a little rusty on the fundamentals of television

Abstract: *The color portion of an NTSC standard broadcast video signal consists of two phase-modulated signals. One is of a wider bandwidth than the other and is a vestigial sideband signal. How do we accurately reproduce a vestigial phase-modulated sideband signal? With a little understanding of the construction of the signal, it becomes clear.*

broadcast signals. Briefly, a broadcast video signal is composed of two parts; a luminance signal (referred to as "Y") that contains the black-and-white picture, and a chrominance signal (referred to as "C") that adds color. This chrominance signal is broken down into two subsets; an "I" signal ("in-phase"), and "Q" signal ("quadrature"). It has been determined experimentally that the eye is more sensitive to those colors along what is termed the "I axis" than those along the "Q axis." The "I" signal contains those colors that are "in-phase" with your eye. On a vectorscope display, the I axis occurs at 123° and the Q axis occurs at 33° . The reference signal (chroma burst) occurs at 180° .

The total chrominance signal is modulated on a subcarrier at 3.579545 MHz, but it is modulated in two ways. The phase of the subcarrier represents the hue (or the particular color) to be displayed. This is the reason for having two chrominance signals. A phase-modulated signal is best represented and reproduced when two modulators and two demodulators are used whose two carriers (the same frequency) operate 90° out of phase with respect to each other. The I and Q signals are encoded in this matter. They are also modulated by amplitude to represent the intensity (or saturation) of the color.

Because of the way in which television signals are synchronized, we can think of the signal as being "sampled," but at two rates. The first is at the horizontal scan rate, which is approximately 15734 Hz. Therefore, there will be power sidebands at every harmonic of 15734 Hz, decreasing

in amplitude as frequency increases. The second sampling rate is at the vertical scan rate, which is approximately 59.94 Hz. This creates power sidebands around every horizontal sideband, as shown in Fig. 1. The same principle holds true for the modulated chrominance signal. Since it is sampled in the same manner as the luminance signal, it produces power sidebands in the same fashion. In the frequency domain, the luminance signal and chrominance signal would then have equally spaced power sidebands. This situation is unacceptable. However, if we locate the chrominance subcarrier at an odd half harmonic of the horizontal rate, there is no contention between the sidebands. In other words, if we locate the color subcarrier right at a harmonic of the horizontal rate, then the luminance power sidebands and chrominance sidebands overlap each other, and it is virtually impossible to properly separate the two signals. If we put the chrominance subcarrier half-way between two harmonics of the horizontal rate, the power sidebands of the chrominance information is "interlaced" with the luminance information. The chrominance signal is strategically placed at $455/2$ times the horizontal scanning frequency. This is located between the 227th and 228th harmonic of the horizontal rate. We now have an interlaced signal. In the time domain, this means that if we have a screen that is nothing but a field full of one particular color, the chrominance subcarrier (located at 3579545 Hz) is 180° (or half of a cycle) out of phase from one line to the next. We can fit exactly 227.5 cycles into a horizontal

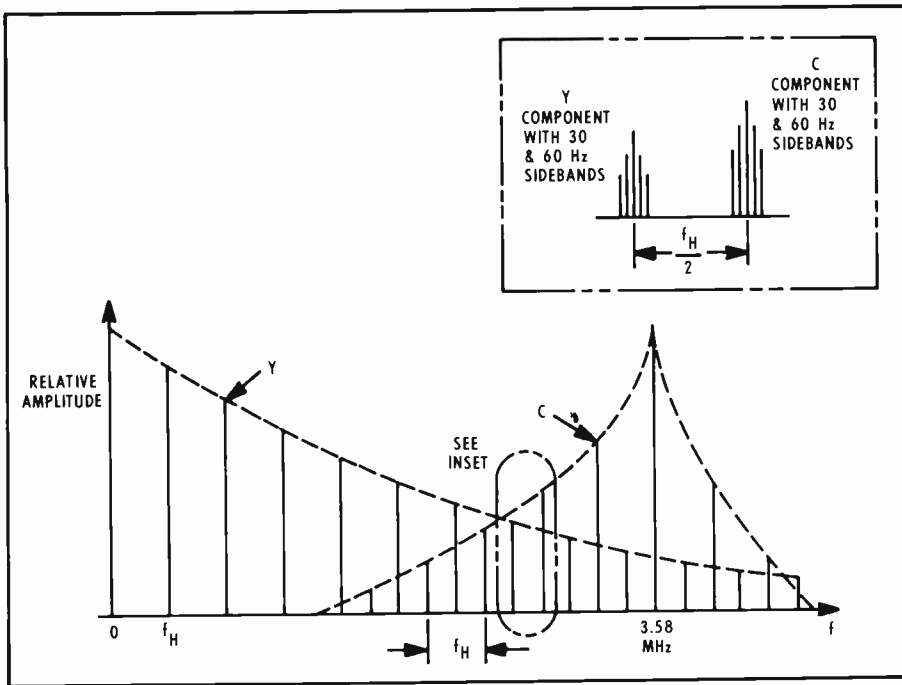


Fig. 1. Power sideband interleaving.

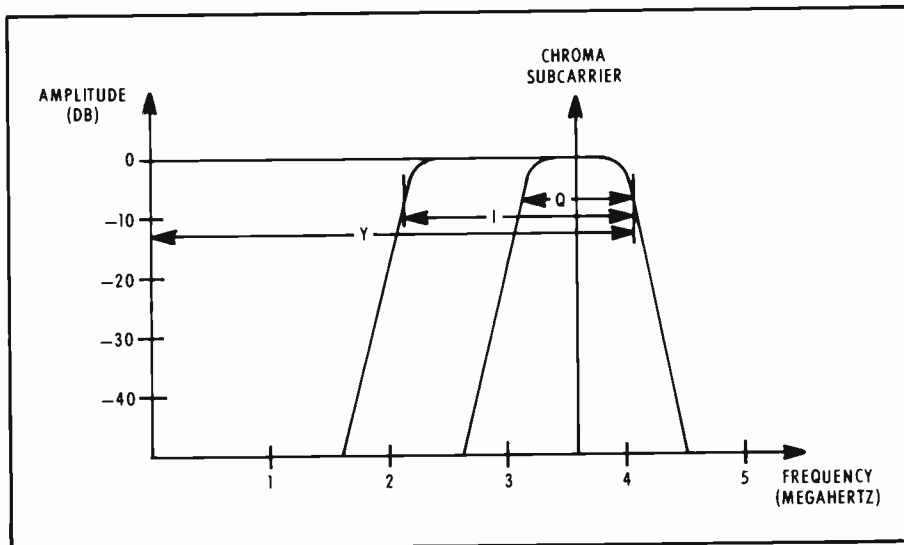


Fig. 2. NTSC-defined Y, I, and Q bandwidths.

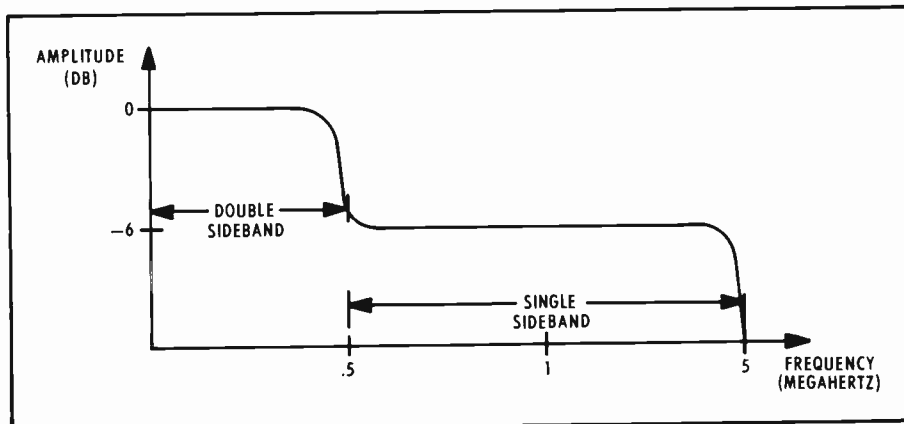


Fig. 3. Demodulated I bandwidth and shape

line if we do not have to blank the signal every line for sync.

The NTSC definitions for television signals include the specific bandwidths of the black-and-white and color signals. A diagram is shown in Fig. 2. Because of the interlacing explained above, the luminance and two chrominance signals can all occupy a total bandwidth of approximately 4.5 MHz. The luminance signal occupies the whole area, but the chrominance bandwidths are much less. The modulated Q signal occupies a region 500 kHz above and 500 kHz below the subcarrier frequency. When demodulated, this gives a total bandwidth of 500 kHz for the Q signal. The modulated I signal, on the other hand, occupies 500 kHz above and 1500 kHz below the subcarrier frequency. When demodulated, this will give a bandwidth of 500 kHz (at the -6 dB point), but then will remain at -6 dB out to 1.5 MHz. This effect is shown in Fig. 3. This type of modulation is commonly known as "vestigial sideband" modulation, where around the subcarrier the signal will have double sidebands, but farther out will be reduced to a single sideband.

Standard chroma demodulation

The normal approach to separating the chrominance information from the luminance information is to divide the IF video output into two different paths. One path has a bandreject filter (or trap) at 3.58 MHz, thus taking the chrominance signal out of the composite signal, and leaving luminance. The other path will have a bandpass filter centered around 3.58 MHz with a total bandwidth of 1 MHz, leaving chrominance. This is somewhat of an oversimplification, because when the chrominance and luminance signals are interleaved there will be luminance trapped in the bandpassed chrominance signal, and chrominance trapped in the bandrejected luminance signal. Examples of the effects seen on the screen are:

- A referee's uniform appears to have colors running through it.
- The edge of a striped detergent box has an unclear edge; rather, it looks like a zipper is running along the edge.
- The same box has little dark dots running through it at the same rate as the zipper.

These effects occur because the standard luminance/chrominance separation process doesn't separate the sidebands, it just sep-

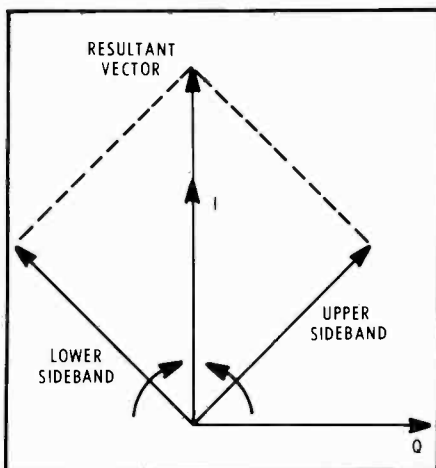


Fig. 4. Double sideband example.

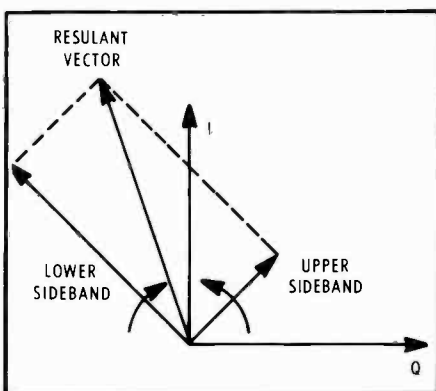


Fig. 5. Double sideband example (upper sideband attenuated).

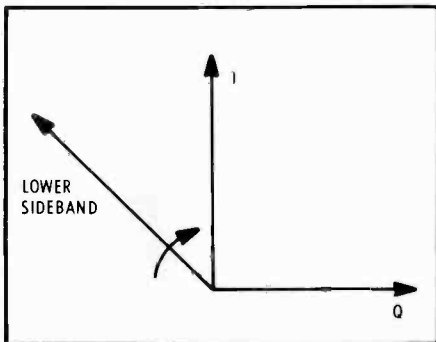


Fig. 6. Single sideband example.

arates out the chrominance bandwidth area. This is why we cannot get all of the available sideband I signal. The lower sideband of the 3579545 Hz subcarrier extends down to 2.08 MHz. By bandrejecting this section, the black-and-white portion of the picture is severely limited in resolution. Also, we get even more luminance information in the chrominance channel, causing "unrealistic" colors. Therefore, in a bandpass/bandreject scheme, the color signal is limited to $\pm 500\text{kHz}$ from the subcarrier. This is termed an equiband system

because the upper and lower sidebands are equal in bandwidth. Any wideband I information will probably be interpreted as a luminance signal.

To separate the luminance and chrominance signals properly, it is possible to make filters that have peaks at every sideband and nulls in between sidebands. The overall response would appear to have a "comb" shape to it. To implement such a filter with resistors, capacitors, and inductors would be expensive and take up a lot of space, and device tolerances would make it difficult to control. The advent of CCDs has made this type of filter practical.

The availability of an economic comb filter has changed the whole world of chrominance processing. The 3.58 bandpass/bandreject circuitry is not needed any longer. The problem of luminance information being present in the chrominance channel and chrominance information being present in the luminance channel has been nearly eliminated. The power sidebands are virtually separate, and it is possible to allow the luminance channel bandwidth to extend up to 4.0 MHz with almost no phase distortion, while the chrominance channel is totally available to us. The three problems listed above disappear, even if we demodulate in an equiband demodulator. But what about that extra 1 MHz of chrominance signal that extends from 2.08 MHz to 3.08 MHz?

Wideband I demodulation considerations

In order to properly use the wideband I signal, a comb filter must be used to separate the chrominance from the luminance. Other problems come about if the separated chrominance is simply demodulated from there, then added back in with the luminance.

The chrominance signal still must be band-limited. It has been determined experimentally that below 2.08 MHz, there will still be luminance information in the area where one would expect to see chrominance information. Therefore, we need to add a high-pass filter. Also, because of IF response, transmitter response, and other system responses, the upper sideband of the chrominance subcarrier will be drastically rolled off due to the 4.5 MHz sound carrier being removed from the video signal by a trap. To compensate for this, we can peak that sideband a little more than the lower sideband.

Why must the upper sideband be peaked,

and what other problems do we encounter when we try to demodulate wideband I? Let's look at a phasor representation of the chrominance sidebands with respect to the subcarrier. Figure 4 shows two vectors rotating in opposite directions, equal in amplitude and opposite in phase. These two vectors represent the upper and lower sideband signals. Take an arbitrary example—3469405 Hz and 3689684 Hz. These frequencies are seven times the horizontal rate (approximately 110 Hz) above and below the subcarrier. The 3469405-Hz signal vector is the one that is rotating in a clockwise direction, whereas the 3689684 Hz signal vector is rotating in a counterclockwise direction. They always add up vectorially to a single phase when demodulated, as shown in the diagram. This is the I phase. Suppose that the upper sideband begins to attenuate with respect to the lower sideband. A typical set of frequencies might be 3028846 Hz and 4130244 Hz, which are 35 times the horizontal rate above and below the subcarrier. At this point, due to the 4.5 MHz sound trap, the upper sideband will probably be attenuated. The diagram in Fig. 5 shows what happens when these two signals are added (demodulated) together. Even though the original signal may have been strictly I phase, the resultant signal is beginning to have a component that the Q demodulator will try to claim.

If we go all the way, there is only lower sideband I, and no upper sideband at all. This could occur at a frequency of 2478147 Hz, which is 70 times the horizontal rate below the subcarrier. The upper sideband would have to occur at 4680943 Hz, which is not allowed in the NTSC bandwidth definitions. Now only one vector rotates in a clockwise direction, and it appears to have no significant phase information at all, as shown in Fig. 6. The NTSC definitions say that there can be no Q information at all in this region, so we can restore this seemingly "random phase" signal to its approximate original value. We do this by demodulating the chrominance with both I-phase and Q-phase signals as in an equiband system, filtering the demodulated Q signal to 500 kHz, and filtering the demodulated I signal to 1.5 MHz. A block diagram is shown in Fig. 7.

It would, of course, be very rare to see a sinusoidal waveform on the screen consisting of I color information. This rarely happens. However, there are certain instances where the effects of using the demodulated wideband I signal are rather evident. The most prominent is when one

picture is inserted into another. This often occurs in game shows, sports shows, and news broadcasts. The inserted picture will usually have a colored border, such as red or yellow. With a television set that only demodulates equiband chrominance (± 500 KHz from the subcarrier for both I and Q signals), the upright supports of the colored border will be paler (less intense) than the top and bottom segments of the colored border. This is because the small bandwidth of an equiband system restricts the transitional response of any color signal presented to the system. The upright supports of such a box are usually rather thin, so the chrominance demodulating system cannot respond quickly to such a signal. If we allow the demodulators to use the single sideband portion of the I signal, the system has a frequency response virtually out to 1.5 MHz instead of 0.5 MHz. This allows the system to respond to the rapid changes required to reproduce these upright sections of a border. Another example is the display of a brightly colored piece of clothing, such as a shirt. In an equiband system, if the person wearing this shirt were to walk away from the camera, the color would begin to fade. In a wideband I demodulation scheme, the bright colors would be retained longer as the person walked away. The obvious question here is, "Why not make the chrominance bandwidth equal to the luminance bandwidth and have even better color response?" The answer is actually twofold. First, the total bandwidth specified by the NTSC for a television channel does not allow us to have both 4 MHz of luminance response and 4 MHz of chrominance response in a 4.5-MHz bandwidth. The circuitry necessary to decode such a signal would be expensive. Also, the human eye has its own inherent bandwidth limitations for chrominance and luminance information. Luminance information is sensed and sent to the brain by the rods, and color information is sensed and sent to the brain by the cones. The human eye cannot see as much detail in color as it can in black and white, so it seems rather futile to broadcast extra information in color if we cannot see it. We can easily measure it, but that doesn't make it practical.

As was stated earlier, as the color signal deviates farther in frequency from the color subcarrier, the signal goes from double sideband to single sideband. If we look at the phasor diagrams again, we can see that in the single sideband region, the resultant demodulated signal is the sum of the two vectors—upper sideband and lower side-

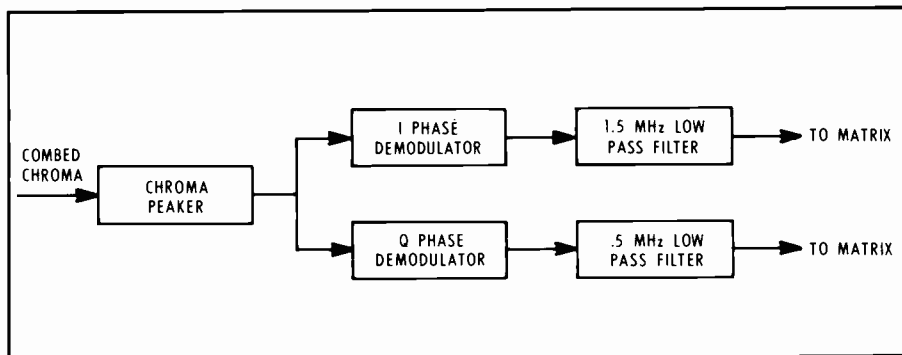


Fig. 7. Demodulator—filtering block diagram.

band. When dealing with the single sideband region, however, we only have the one vector. If proper filtering is used, we can assume that only the I component of this rotating vector exists. But since we have only one vector, the amplitude of the resultant demodulator output will be half the amplitude of the demodulator output in the double sideband region. This will give a frequency response shape similar to that shown in Fig. 3. This is one concern when designing the chroma peaker filter. If we increase the single-sideband region by 6 dB to make it approximately equal in amplitude to the double-sideband region, we can flatten the chrominance response out to 1.5 MHz.

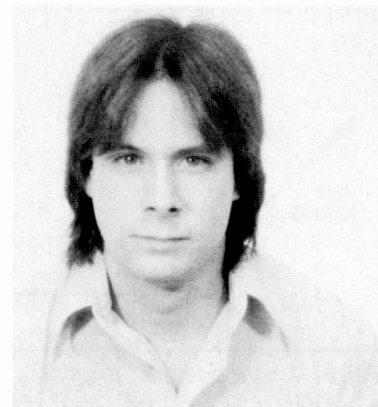
Another consideration when dealing with demodulation of wideband I signals is quadrature distortion. This is easily seen in a transition from a black-and-white section to a color section, or in a transition from one color to another. The transition from cyan to red, for example, consists of two colors that are very close to the I phase. During the transition, then, we should not see any other colors. But no filter is perfect, and any transistor circuit is inherently non-linear in one respect or another (especially demodulators). There will be extraneous colors appearing on the screen during the transition. This is known as quadrature distortion. The quadrature demodulator is demodulating a signal that is not a part of the original signal. This type of distortion will occur mainly at transitions and in higher frequencies.

When we change from an equiband system to a wideband I system, the method of dealing with quadrature distortion changes. We are using more of the higher frequencies, so there is a possibility of more quadrature distortion. To counter this effect, we must make the roll-off of the Q filter as rapid as possible without causing the group delay of the filter to increase dramatically.

Summary

The use of charge-coupled devices for creating a cost-effective comb filter has resulted in the more complete extraction of chrominance and luminance information from the NTSC-defined composite video waveform. By using a comb filter, we can increase the available amount of chrominance resolution by increasing the frequency response of the I channel in the television receiver.

At present, RCA produces two chassis that use the wideband I chrominance signal; the CTC-131 and the CTC-132. These chassis were both introduced in 1984. The increased color resolution has been demonstrated and is easily recognizable in regular network shows.



Ronald T. Keen received his BSEE from Purdue University in 1982. He then joined RCA Consumer Electronics Division, Signal Systems, where he is presently an Associate Member of the Engineering Staff. His responsibilities include comb filter ICs and applications, chrominance processing circuitry, chroma/luma ICs, external RGB interface circuitry for both linear and TTL RGB sources, and the analysis of colorimetry and colorimetry errors in the Colortrak I and Colortrak 2000 series television receivers. Contact him at:
Consumer Electronics Division
Indianapolis, Indiana
Tacnet: 422-5916

U.S. color television fundamentals—a review

The U.S. Color Television Standards represent masterfull "tradeoffs" among psychophysical effects and electronic implementation techniques.

Color is not a characteristic of an object but, rather, a characteristic of light. This realization provides the answer to the question, "What is color?" Color* may be defined as a psychophysical property of light—specifically, the combination of those characteristics of light that produces the sensations of hue, saturation, and brightness in a normal human observer. *Brightness* refers to the relative intensity of a color; *hue* refers to that attribute of color that allows separation into groups by terms such as red, green, yellow, etc. (in scientific terms, the dominant wavelength); *saturation* refers to the degree to which a color deviates from a neutral gray of the same brightness—called purity, pastel, vividness, etc.

These three characteristics—brightness, hue, and saturation—represent the total information necessary to define and or recreate a specific color stimulus. Conceptually, this definition of color is highly convenient and appropriate for an electronic color television communications system, as pointed out later.

To determine specific parameters that describe a color, three highly interrelated factors must be taken into account:

1. Spectral reflectivity of the surface being observed.
2. Spectral distribution of the ambient light illuminating the object.
3. Spectral sensitivity of the detector.

In consumer television, the detector response (except for scientific measurement purposes) consists of the spectral sensitivity of the "standard" human eye.

Thus, the product of the spectral reflectivity of the object, the spectral distribution of the ambient, and the spectral sensitivity of the detector defines those characteristics of light, called color, that generate the sensations of brightness, hue, and saturation in a human observer. The task of a television transmission system is, therefore, to interface suitable apparatus between the detector (human eye) and the source of light energy. This apparatus must transform the light electronically into a form suitable for transmission through a specified communications channel, and then actuate a light-reproducing device that will stimulate the human eye to produce a similar subjective response in the form of *perceived* color as would have occurred if the observer had been present at the scene.

Grassman's Laws

A suitable method of colorimetric measurement and specification must be available to develop a satisfactory color television system. The application of the *principles of mathematical equivalence* to the science of color-matching by a German, Herman

Grassman, in 1854 formed the background for modern tristimulus colorimetry. In essence, *Grassman's laws*** state:

1. The eye distinguishes dominant wavelength (hue), purity (saturation), and luminance (brightness).
2. The luminance (Y) of a color mixture equals the sum of the individual color luminance values:
$$Y_7 = Y_1 + Y_2 + Y_3 \dots$$
3. If color A = color B; and color C = color D; then A + C = B + D.
4. If color A = color B plus color C; then B = A - C.
5. If color A = color B; and color B = color C; then A = C.

Stated simply, when equivalent lights are linearly added to equivalent lights, as viewed by the eye as a detector, the sums are equivalent.

Trireceptor theory of vision

To understand colorimetric specification systems we must know the pertinent factors about the human eye: The primary detector for television purposes, it is sufficient for this purpose to accept the trireceptor theory of vision, which contends that the translation of radiant energy to visual stimuli is accomplished by three sets of cones and rods having individual response curves in the red, green, and blue portions of the visible spectrum such as shown in figs. 1 and 2.

*Throughout the paper, terms being defined are italicized.

**These laws represent one of the few verified facts concerning human vision from which various theories relating to the visual process are derived. The trireceptor theory of vision⁹ is one classical method used today to explain why the human eye follows Grassman's laws.

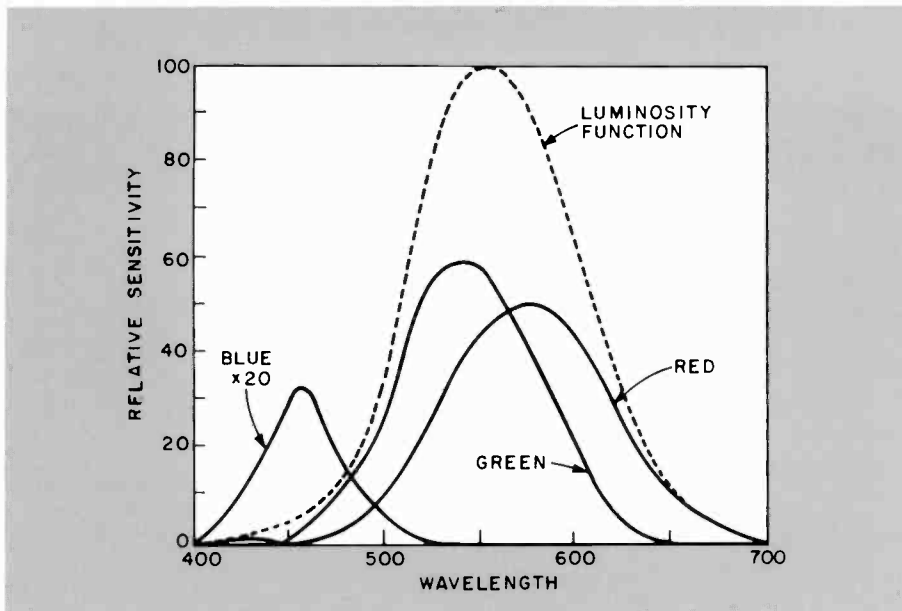


Fig. 1. Tri-receptor eye response. The sum of these response characteristics constitutes the total sensitivity, or luminosity, response curve as indicated by the dotted line (reproduced for clarity in Fig. 2). Note that the blue response curve is magnified in Fig. 1 by a factor of twenty.

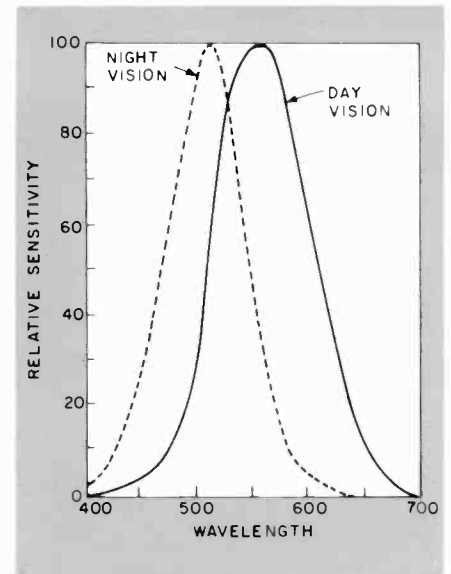


Fig. 2. Luminosity response. The responses relevant to brightness levels represented by television (daylight) viewing is determined by the cones (photopic response) as opposed to low-light response of the rods (scotopic response).

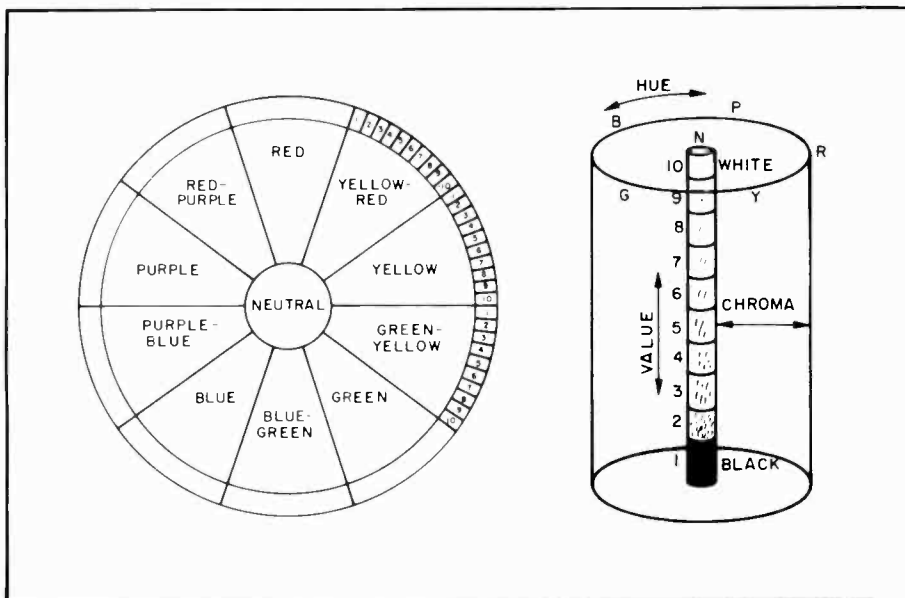


Fig. 3. Munsell color specification system. In the cylindrical Munsell color solid, various spectral hues are arranged in an equally divided circle. Saturation in this system is indicated by radial distance from the center; brightness is denoted by the height of the cylindrical solid with black at the bottom and unit, or normalized, white at the top of a ten-level cylinder.

The relative luminosity function response curve is extremely important in developing color specification and reproduction evaluation techniques; thus, it has an important role in the development of a color television transmission system. The expression, "We sometimes tend to look at the world through rose-colored glasses," perhaps should be re-stated as, "We view our sur-

roundings through a green-yellow transmission filter." Keep this in mind as we proceed to develop the electronic color television reproduction system.

The human detector evaluates the brightness, or luminosity, of an image by summing the stimuli from the three receptors, while the chromatic attributes, hue and saturation, are determined by the ratios of

the stimuli. Thus, light sources having widely different spectral distribution may give exactly the same visual color sensation as long as the amount and ratios of the total stimulation are the same.

The Munsell system

At this point, an early system of color specification that is still used for television camera performance evaluation, referred to as the *Munsell color specification system* (Fig. 3), is worthy of note. This method is used to evaluate surface reflectivity colors. Specifically calibrated paper Munsell color "chips" are available over a wide variety of colorimetric and brightness values and are still used for color television camera performance measurement and evaluation purposes. For rigorous accuracy, the spectral distribution of the ambient light, and the spectral sensitivity of the camera (detector), must be taken into account to obtain the desired colorimetric performance match.

CIE tristimulus colorimetric specification system

The contributions of Grassman, Maxwell, Ives, Munsell, Judd, and others led to the adoption, in 1931, of international color definition and measurement standards by the *Commission Internationale de L'Eclairage* (CIE). This technique, developed for color-matching purposes, does not provide

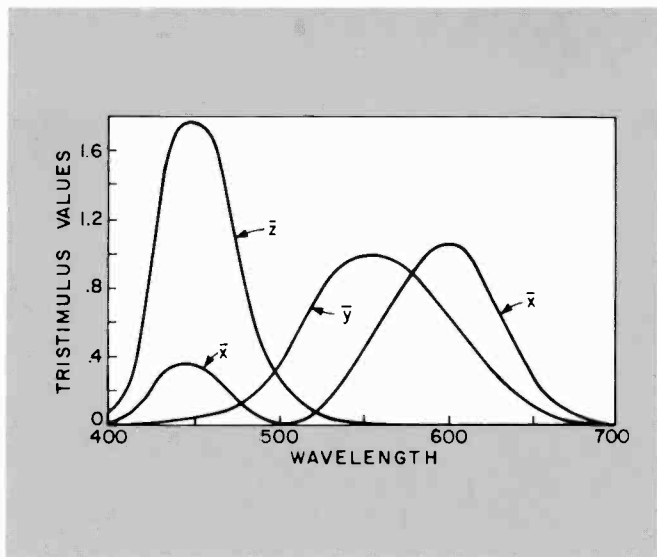


Fig. 4. CIE tristimulus curves. Note that the Y curve is the same as the standard luminosity function.

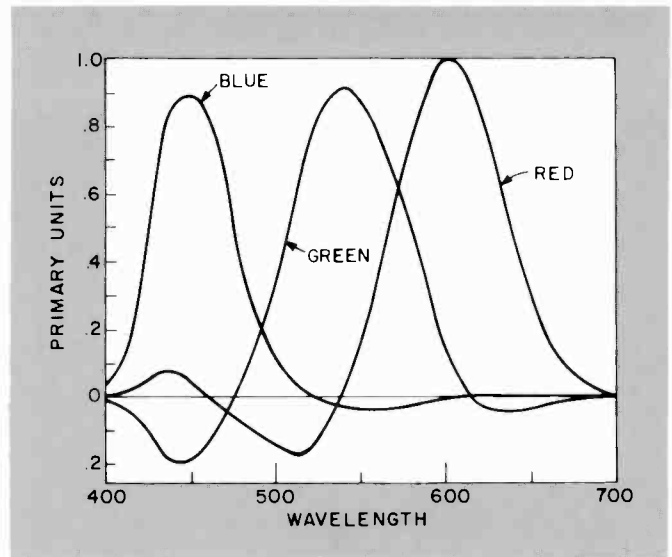


Fig. 5. NTSC color mixture primaries in the present color television system.

the information for color television systems in an ideal manner, but does serve sufficiently as a means for setting colorimetric standards and providing objective measurement of performance.

the detailed mathematical development of the CIE tristimulus colorimetric specification system is beyond the scope and intent of this paper; References 1, 2, 3, 5, 6, 7 treat the subject in depth. A brief overview of the concepts involved are given here.

Grassman's laws state that only three independent quantities are required to specify a color and that color intensities add linearly. Therefore, a color specification system can be envisioned as involving a three-dimensional color space with any set of convenient coordinates, and these coordinates may be transformed mathematically into any other set for convenient measurement or analysis. This concept of a three-dimensional color space* forms a basis for the color television colorimetric design and performance evaluation. The projection of the visible color locus, which is determined on a unit plane by a standard colorimeter technique and then transformed to the two-dimensional x, y plane, provides a method of describing the attributes of chromaticity (hue and relative saturation) independent of brightness. As will presently be seen, this concept is directly applicable to the electrical process of encoding and decoding the video sig-

nals that represent the red, green, and blue primary light energies.

A *primary light source* may be defined as one which cannot be reproduced by the summation of two other primary light sources. The reproducer in a color television system must produce light energy in the form of three primary light sources in the red, green, and blue portions of the visible spectrum, respectively. This constitutes an additive process of color mixing as opposed to the subtractive process normally encountered in paint, pigment, and dye processes where surfaces are illuminated by white light and reflect only certain portions of the spectrum of the incident energy to the eye.

Any standard system of color specification should use a set of primaries such that positive amounts of each primary could be mixed to produce any color. However, experiments have shown that certain non-spectral colors cannot be reproduced by any one choice of three imaginary, or "non-physical," primaries was made by CIE in setting up an international standard; specifically, red at 700 nanometers, green at 543.1 nanometers, and blue at 435.8 nanometers. This results in the 1931 CIE tristimulus value curves shown in Fig. 4 and designated as X , Y , and Z . *Tristimulus values* are defined as the relative amounts of the primaries that must be combined to achieve a color match with all the colors in the visible spectrum. Experiments extending over more than 200 years have shown the validity of this principle and the practicality of the "standard observer." Thus, any set of real primaries in a practical reproduction system may be expressed

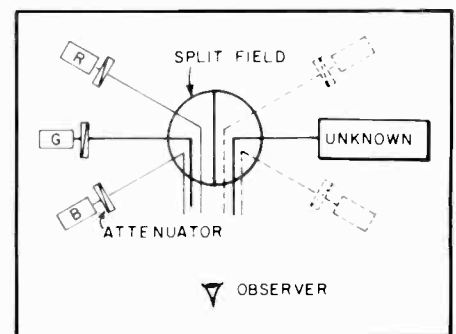


Fig. 6. Tristimulus colorimeter technique. The split-field viewer displays the light to be specified in one half of the screen, while the other half is illuminated with a mixture of the three primary light sources. Since the unknown is to be specified in terms of the three primary sources, their relative intensities are adjusted to obtain a visual match. The relative values of the three primaries are recorded and the process is repeated for all colors in the visible spectrum. Negative values for non-spectral colors are determined by adding the required amount of the appropriate primary to the unknown light to achieve a match, and is thereby recorded as a negative value.

in standardized tristimulus value form for measurement and evaluation purposes. The set of tristimulus value from for measurement and evaluation purposes. The set of tristimulus curves for the red, green, and blue primaries as specified by the NTSC for the present color television system is shown in Fig. (note the negative lobes).

The process of determining the relative tristimulus values involves a device termed a *colorimeter* (Fig. 6), which can be used

*With three orthogonal axes representing specific red, green, and blue primary light sources that may be mathematically transformed into the standardized CIE color mixture values.

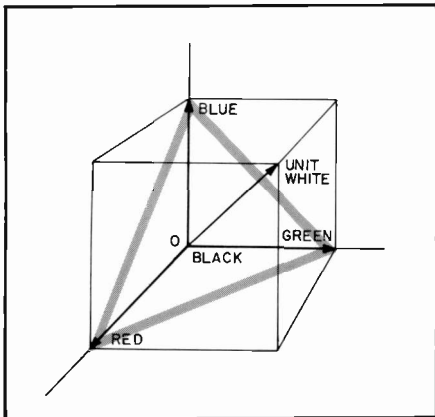


Fig. 7. Color space unit cube. Any color capable of being formed by a mixture of these three primaries may be described by coordinates located within the normalized unit cube.

to specify a light source in terms of the three primary light sources.

Thus, the tristimulus values (X, Y, Z) for any color may be determined by integrating its spectral energy distribution, $E(\lambda)$, with the standardized tristimulus values determined by a standard observer for spectrum colors using the colorimeter technique.

$$X = \int_0^{\infty} E(\lambda)X(\lambda)d\lambda$$

$$Y = \int_0^{\infty} E(\lambda)Y(\lambda)d\lambda$$

$$Z = \int_0^{\infty} E(\lambda)Z(\lambda)d\lambda$$

The three-dimensional color unit cube shown in Fig. 7 is visual representation of the mathematics—with the R, G, and B values representing the orthogonal primary color axes. Fig. 8 shows how the locus of visual colors is plotted within this space and how the unit plane is formed perpendicular to the diagonal axis of the cube, thereby representing a plane of constant brightness. If one then rotates the cube and looks directly down the Z axis, a visualization of the projection of the unit plane upon the Y, X wall of the cube is possible (see Fig. 9). Thus, the tristimulus values can be transformed to a two-dimensional set of values describing the chromaticity values (hue and saturation) independent of brightness.

The visual locus of spectrum colors, thus transformed, provides the familiar “horse-shoe” shaped CIE chromaticity diagram used extensively to describe colorimetric performance of the television system. Fig. 10 is an example of such a diagram indicating the locus of the colors reproducible by the three primaries specified by the

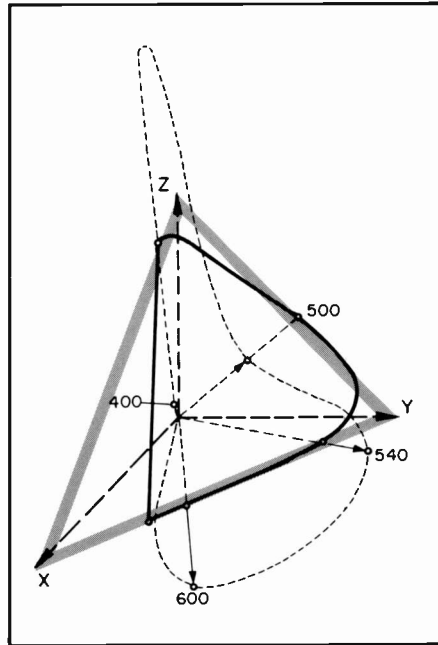


Fig. 8. Color space unit plane and spectrum locus; the unit plane (tone outline) represents constant brightness.

NTSC for color television purposes (dashed triangle). For comparison, the irregular gamut of all paints, pigment and dye processes is included.

The mathematical process of accomplishing the above transformation from tristimulus values to x, y chromaticity coordinates is as follows:

$$x = \frac{X}{X + Y + Z}$$

$$y = \frac{Y}{X + Y + Z}$$

$$z = \frac{Z}{X + Y + Z}$$

while $x + y + z = 1$.

What are the special features of the two-dimensional (x, y) CIE chromaticity color diagram?

In such diagrams (Figs. 11 and 12), points around the periphery of the visible locus indicate different hue values, while coordinates that move radially outward from the central portion of the diagram indicate increasing color saturation. Color-mixture coordinates may be determined graphically by a simple straight-line geometrical technique known as the “center-of-gravity” weighting method.

An important deficiency of this representation of chromatic attributes is that equal distances in various portions of the diagram in x, y coordinates do not produce

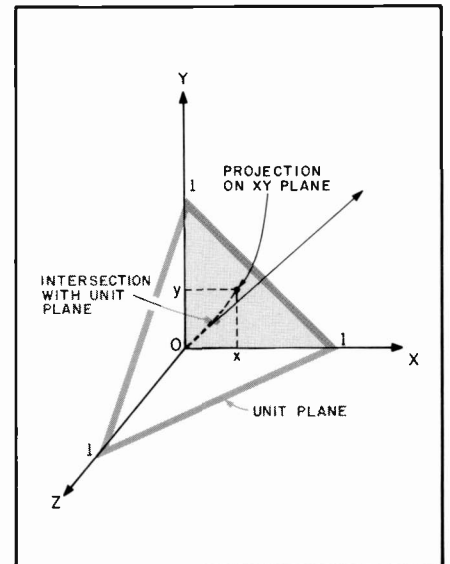


Fig. 9. Color space transformation to the X, Y plane. The intersection of the color vector and the unit plane (tone outline) can be projected into two-dimensional x, y coordinates to represent hue and saturation.

equally perceptible color differences. In fact, this type of nonlinearity varies by an amount of twenty or thirty to one. Fig. 11 is a plot of the classical Munsell colors in CIE coordinates while Fig. 12 is an indication of ellipses of equal color acuity for various portions of the diagram that points up the high order of nonlinearity of perceptual color differences relative to equal geometrical coordinates.

Different mathematical transformations

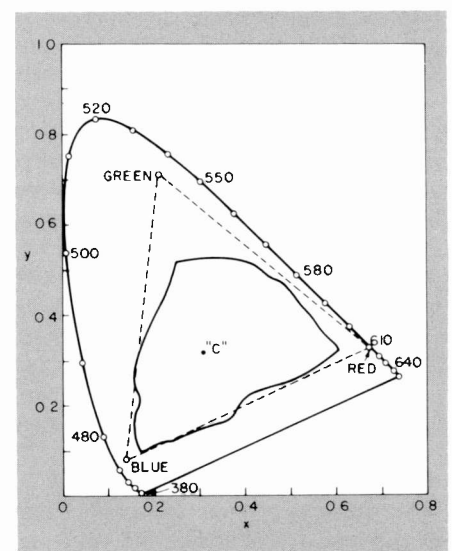


Fig. 10. CIE chromaticity diagram; NTSC color gamut (dashed triangle); and paints, pigments, and dye gamut. “C” marks the center-of-gravity of the chromaticity diagram.

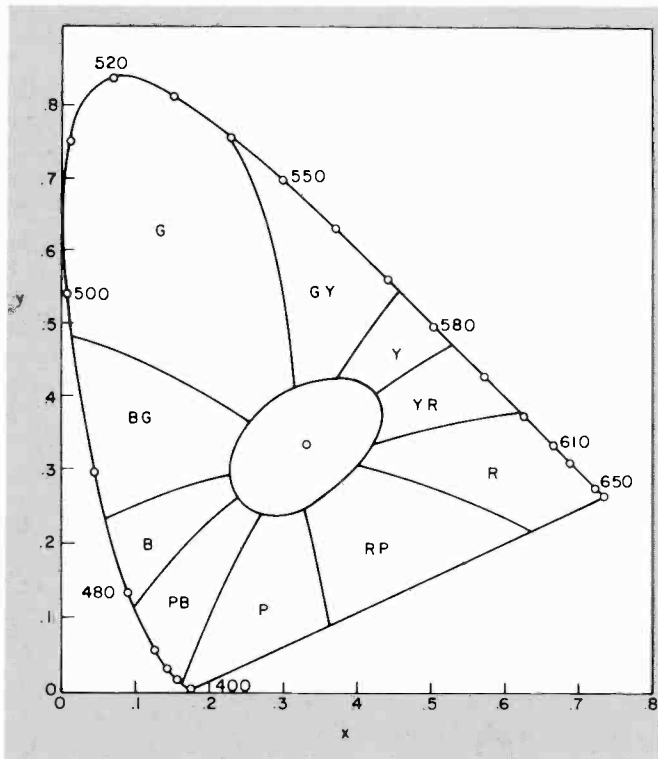


Fig. 11. Munsell colors plotted on CIE plane to represent chromatic attributes.

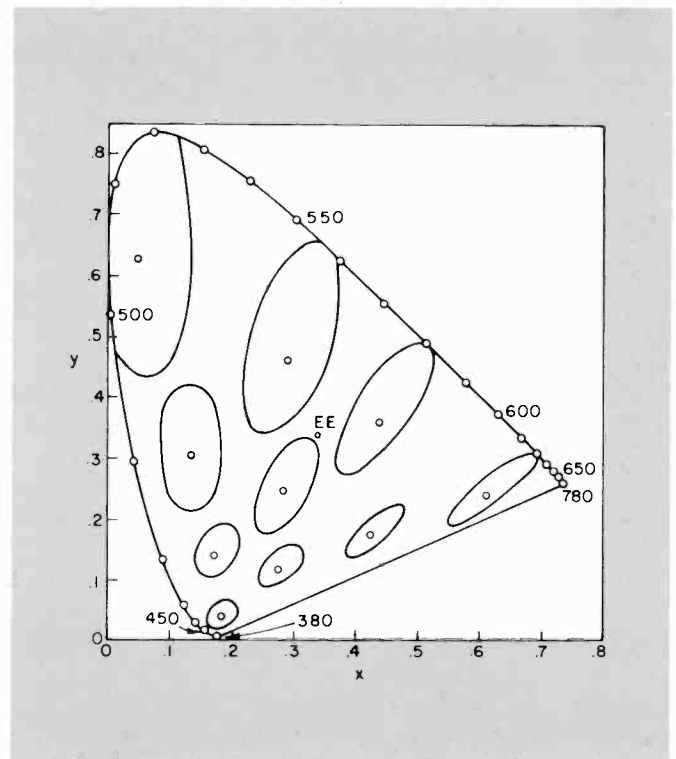


Fig. 12. Color acuity ellipses for various portions of the CIE chromaticity diagram (expanded by 100 to 1 for clarity).

have been developed, the most notable being the Eastwood modification in 1964, in attempts to provide a closer match between subjective color-difference perception and equal distances on the chromaticity diagram. Fig. 13 is an example of this transformation in terms of u, v coordinates where the relative nonlinearity is reduced to about four to one. Further transformations restore the three-dimensional factor of brightness in which the coordinates are designated as U^*, V^*, W^* . A three-dimensional vector whose absolute value represents a total color-difference sensation is often referred to as color error (C_E) and is mathematically determined by the expression:

$$C_E = \sqrt{(U_1^* - U_2^*)^2 + (V_1^* - V_2^*)^2 + (W_1^* - W_2^*)^2}$$

Various investigators have reported somewhat different variations in the perceptibility of color differences, and research in this area is continuing with the aid of computer optimization techniques.

What is "white?"

After realizing that, by definition, color depends upon the characteristics of light that create the sensations of hue, saturation, and brightness, a legitimate question might be,

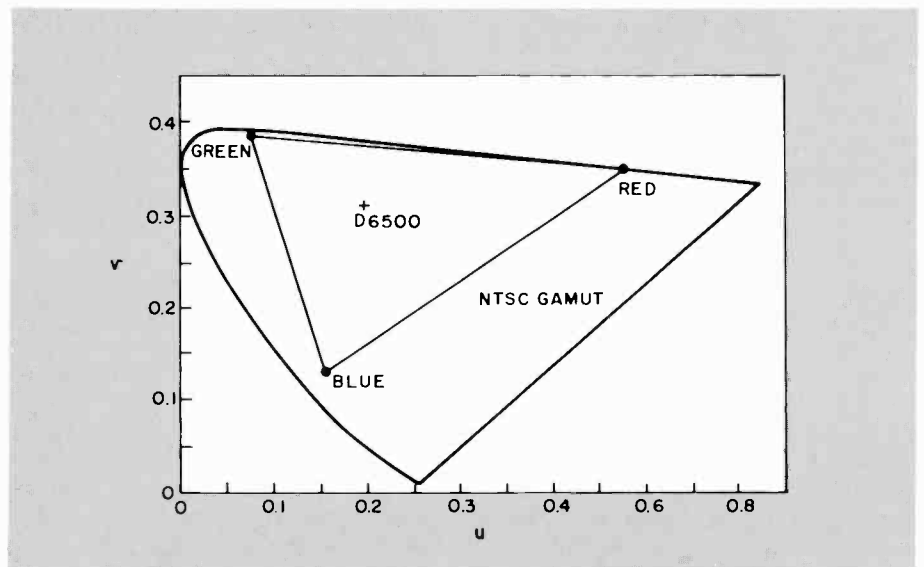


Fig. 13. Transformation of CIE diagram to u, v coordinates.

"What is white?"—defined in colorimetric terms. In normal human experience, the most nearly uniform ambient light is provided by sunlight and, in modern times, artificial sources such as incandescent and fluorescent lights. Remembering that the three interrelated factors of surface reflectivity, ambient spectral distribution, and detector response determine the perceived color of an object, one might assume that a surface that reflects all portions of a daylight ambient

equally to a standard "eye" detector would represent a reference white or gray colorimetric value. In 1931, the CIE recommended three standard reference white illuminants:

Illuminant A—incandescent lamp, 2854°K

Illuminant B—noon sunlight, 4870°K (correlated)

Illuminant C—average daylight, 6770°K (correlated)

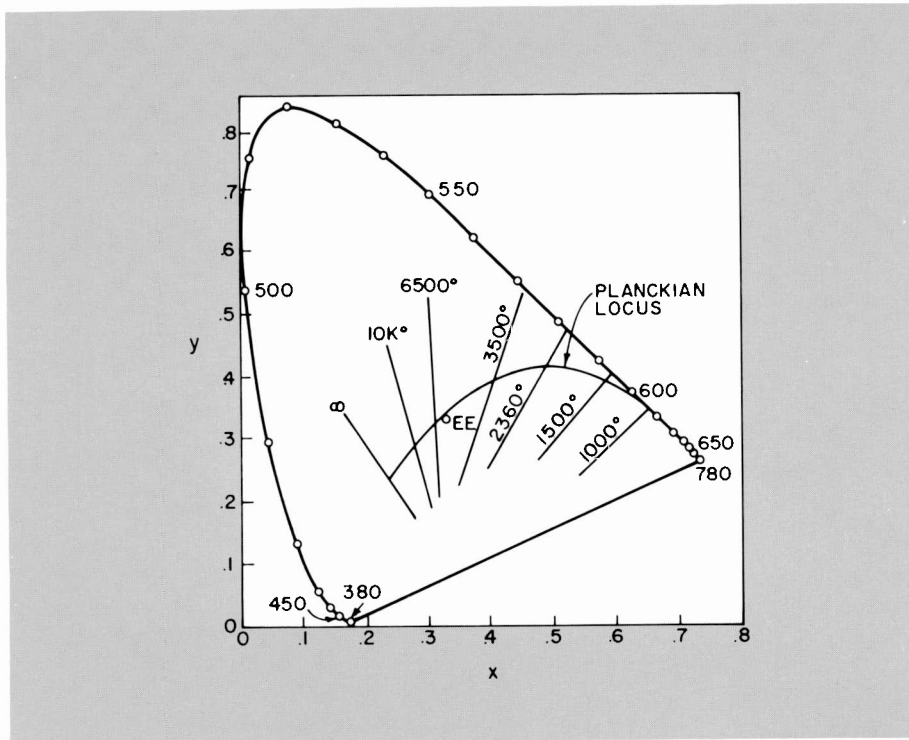


Fig. 14. Black-body locus, or Planckian locus, representation of color temperature.

Illuminant E is a hypothetical equal-energy light source whose CIE coordinates are: $x = 0.33$, $y = 0.33$.

In 1965, a correction for Illuminant C was adopted that is referred to as Illuminant D6500; 6504°K (correlated). D6500 is now accepted as the reference white for color television standards, but the difference between Illuminant C, upon which the standards were based, and D6500 is negligible for all practical purposes and must be considered only when specific computation numerical cross-checks are required.

"White" light sources may be referenced to the radiant energy emanating from a black-body radiator at any given temperature. This light follows Planck's radiation law, having a certain color characteristic according to the radiator temperature expressed in Kelvins. Thus, color temperature is a term used to describe a radiant energy source whose color matches that of a blackbody radiator at that temperature. Fig. 14 shows the black-body locus, or Planckian locus, plotted on the CIE (x , y) chromaticity diagram. A source of radiant energy that does not fall exactly on the black-body line can be described by the term, "correlated color temperature," which is the temperature of a black-body radiator that most closely matches the color coordinates of the source. The deviation of a coorelated color temperature from the

black-body curve is described in terms of minimum perceptible color difference (MPCD) units.

The color television system was based upon a white reference of Illuminant C (now D6500), and the transmission signals in the U. S. adhere to this standard. Receiver kinescope white reference practice over the years has changed in the direction of higher color temperature (typically 9300K + 17 MPCD). However, in recent years the trend is to return to D6500, which results in better color quality and less subjective colorimetric reproduction errors.

Thus, a color television display, usually a cathode ray tube, provides red, green, and blue primary light sources controlled by three electrical quantities in the form of appropriately formed electrical signals. The chromaticity coordinates of the R, G, and B primaries can be defined, and the tristimulus standardized values (X , Y , Z) for the display are the sums of the tristimulus values for each of the primaries.

A rigorous and internationally standardized system of colorimetric performance and evaluation has been established that is applicable to a practical color television system. The parameters of brightness, hue, and saturation may be directly translated into representative electrical signal implementation techniques as will be pointed out shortly.

NTSC system concepts and development

The technical basis of the NTSC color standards lies in the fundamentals of the science of colorimetry. To proceed to develop a color transmission system, we need to have a method of specifying the desired color sensation and to calculate the perceived color corresponding to a given spectral distribution of energy. The concept of hue, saturation, and brightness—coupled with the electronic technological ability to analyze the light emanating from a scene into three primary spectral color distributions—allows the communications systems engineer to recombine the specific color signal values in the proper proportions at the reproducer. Thus, the visual sensation of the color reproduction essentially corresponds to that of the original scene. The NTSC color standards define an electrical process of achieving this result within the limits of a specific communications channel.

Contrary to what might be assumed, the selection of the display (receiver) color primaries occurred first, and the color camera "taking" filter characteristics were then specified. The reasons for this relate simply to the availability at the time of suitable, and intrinsically efficient, cathodoluminescent phosphor materials to be employed in a color kinescope. The spectral distributions and dominant wavelengths of these light-emitting materials were used to determine the three systems primaries whose equivalent characteristics at the camera were obtained by appropriate dichroic filters, trimming filters, and electronic "matrixing" techniques.

The original assumption, for colorimetric reproduction fidelity reasons, was that the camera filters and the reproducer light-emitting characteristics were essentially "matched." However, over the years, the kinescope primaries have been purposely changed such as not to match the camera-standardized primary filters. This has been done primarily to obtain higher picture brightness values even though colorimetric errors are introduced. These errors can be subjectively reduced by appropriate design of the receiver decoder process, whereby subjectively critical colors (e.g., flesh color) are accurately reproduced and the major errors occur in relatively noncritical color values. This tradeoff between overall brightness and colorimetric subjective fidelity comprises design and circuit engineering that has received much attention by receiver system designers over the years.

The *basic camera function* is to convert

the spectral distribution of the scene light into tristimulus values in terms of red, green, and blue receiver primaries. The three electrical signals originating at the camera must be transmitted over the communications channel and used to control the three electron beams to make the *perceived* color at the receiver appear essentially the same as the *perceived* color at the scene. The scene to be televised is analyzed in terms of its red, green, and blue components by the three light-sensitive devices in the camera. The camera outputs consist of three signal voltages, proportional to the amounts of red, green, and blue in the scene on a point-by-point basis as determined by the scanning rates and contained within a communications-channel bandwidth of about 0-4 MHz.

The three signals representing the red, green, and blue scene information may then be transmitted over the intervening communications channel between the transmitter and the reproducer by a variety of methods. For example, three parallel and simultaneous channels might be employed, or a common channel might be time-shared at either horizontal line rate or at field rate. Neither of these approaches, however, meets the requirement of compatibility with the existing monochrome system that occupied a single 6-MHz channel allocation.

A preferred signal arrangement had to be developed that resulted in compatible operation within the existing monochrome framework and that made efficient use of the existing channel capacity. Thus, one signal (luminance) was chosen to occupy the major portion (0-4MHz) of the channel bandwidth and contained the *brightness* information as well as the detail content. A second signal (termed the *chrominance signal*) representative of the chromatic attributes of *hue* and *saturation*, was assigned to less channel width in accordance with the attributes of human vision that do not require full three-color reproduction over its entire range of resolution.

Certain important features of human color vision are exploited to package the combination of the brightness information and the color information with the 0-to-6-MHz channel allocation. First, the color acuity of the eye decreases as the size of the viewed object is decreased and thereby occupies a small part of the field of vision produce no color sensation, only that of brightness. Therefore, no color information need be transmitted in this spatial frequency range (corresponding to video frequencies above about 1.5 MHz).

Objects of a size to occupy an intermediate part of the field of view (video frequencies from about 0.5 MHz to about 1.5MHz) are perceived by a two-color vision process consisting of those colors producible by mixing only two primaries of orange and cyan. Thus, in this spatial frequency region, only orange and cyan information need be transmitted.

Large areas corresponding to video frequencies below about 0.5 MHz are seen by three-primary color vision, and full three-color information is required for satisfactory color reproduction. These system limitations do not necessarily mean that the picture quality has been reduced. Realization of these features simply allows the communications engineer to develop a color television system that does not transmit information that the eye cannot use and thereby permits a degree of compression of the required information into a specified channel.

Thus, the *principles* of "mixed-highs" and "I, Q color-acuity axis" operation were exploited. One remaining problem was to simultaneously transmit the brightness signal and the chrominance signal within the same channel limits.

Signal encoding and decoding techniques

The importance of the colorimetric concept of brightness, hue, and saturation comprising the three pieces of information necessary to analyze or re-create a specific color value becomes evident in the formation of a suitable composite color television signal format.

To provide compatibility, the total television signal must contain a monochrome signal in the conventional form such that a black-and-white receiver will function normally. For this purpose, the monochrome signal (Y) can be made to represent the desired brightness information and to include the detail signals. The additional hue and saturation information required for color is added in such a way that it is ignored by a black-and-white receiver. A color receiver detects the additional information and is designed to re-create the original red, green, and blue primary color signal values as initially generated in the color camera.

The luminance, or monochrome, signal is formed by addition of specific proportions of the red, green, and blue signals.

The "Y" signal must have voltage values representative of the brightness sensation of the human eye. Therefore, the red, green, and blue components are tailored in proportion to the standard luminosity curve for the particular values of dominant wavelength represented by the three color primaries chosen for color television. Thus, the standard luminance signal values were determined to be as follows:

$$E_Y = 0.30 E_R + 0.59 E_G + 0.11 E_B$$

The voltage outputs from the three camera tubes are adjusted to be *equal* when a scene reference *white* or neutral gray object is being scanned, regardless of the color temperature of the scene ambient. However, the colorimetric values have been determined by assuming that a reference white of D6500 will always be used at the reproducer. Thus, the color values at the reproducer will appear as if the scene had been illuminated with D6500 white light. Serious colorimetric errors result if the reproducer is allowed to vary to any large extent from a value of D6500 even though the studio reference can, and often does, legitimately use values in the order of 3250K.

Signals representing the chromaticity information (hue and saturation) may be generated by subtracting the luminance signal from the red, green, and blue signals, respectively.

This results in a new set of signals termed *color difference* signals designated as R-Y, G-Y, and B-Y. These signals are encoded in a specific manner at the transmitter, passed through the common communications channel, detected at the receiver, and individually added to the luminance signal to reproduce the original R, G, and B signals to actuate the reproducing device as indicated below:

$$\begin{aligned} E_Y + E_{R-Y} &= E_Y + E_R - E_Y = E_R \\ E_Y + E_{G-Y} &= E_Y + E_G - E_Y = E_G \\ E_Y + E_{B-Y} &= E_Y + E_B - E_Y = E_B \end{aligned}$$

In NTSC color standards, the chrominance signals (color-difference values) are encoded on a common subcarrier in the high frequency portion of the video domain by simultaneously modulating the phase of the subcarrier to represent the instantaneous hue value, and modulating the amplitude of the subcarrier relative to that of the brightness component to represent color

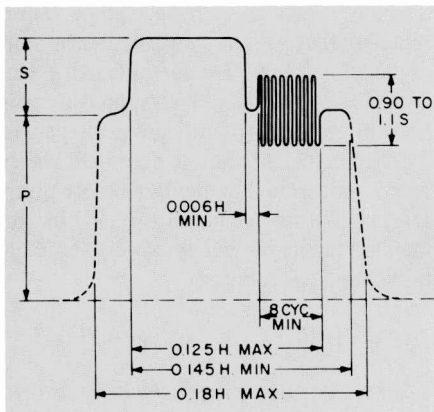


Fig. 15. Horizontal sync and color burst. The eight or nine "burst" cycles following the horizontal sync pulse allow proper relationships to be maintained through the encoding and decoding processes.

saturation. The hue and saturation information can be carried without loss of identity provided that proper timing in a phase sense is maintained between the encoding and subsequent decoding processes. This is accomplished by transmitting a reference timing signal, or *burst*, consisting of eight or nine cycles following each horizontal synchronizing pulse during the blanking interval. (See Fig. 15.) Quadrature synchronous detection is used to identify the individual color-signal components of the chrominance subcarrier. When individually recombined with the luminance signal in a linear resistive matrix, these color-signal components re-create the desired red, green, and blue signals.

At the transmitter, the color-difference signals are initially formed by linear matrix combinations of the red, green, and blue signals. These signals are band-limited: to about 0.6 MHz in the case of the color-difference signal designated as "Q", containing the green-purple color-axis information; and to about 1.5 MHz in the case of the "I" color-difference signal, representing the orange-cyan color-axis information. These two signals then are used to individually modulate the color subcarrier in two balanced modulators maintained in phase quadrature. The "sum" products are selected and linearly combined to form a composite chromaticity subcarrier whose instantaneous phase represents the hue of the scene at that moment, and whose amplitude—is a measure of saturation. This signal is then added to the luminance signal, along with the appropriate horizontal and vertical synchronizing and blanking signals to include the color-synchronizing burst. The result is the total color video signal.

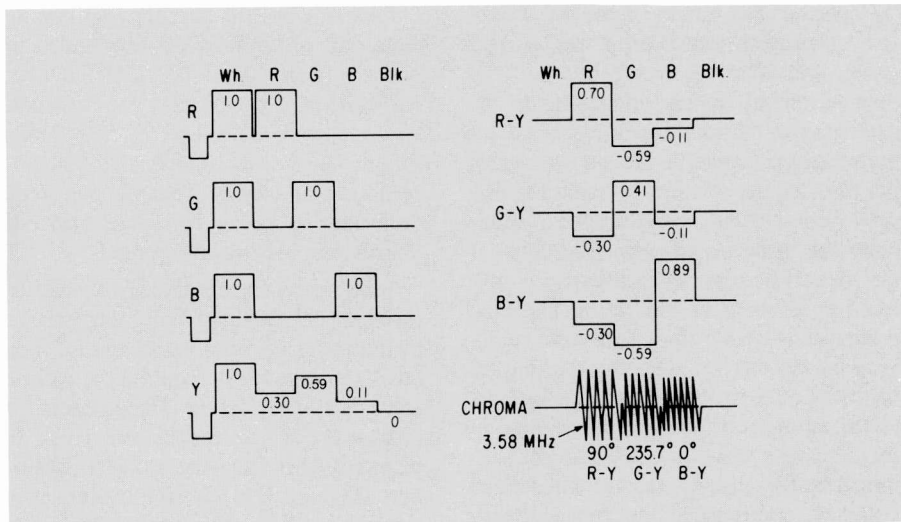


Fig. 16. Basic color signal waveforms. These signal waveform values have been normalized for a scene comprised of a white, red, green, blue, and black bar pattern. The primary color signals are shown along with the color-difference signal values required to add to the luminance signal to re-create the individual color signals. The chrominance signal component is also shown.

Symmetrical system equations

The basic process may be understood in mathematical terms by using a simplified, and historically first, form in which equal values are assigned for the R, G, and B luminance components (0.33 for each when white is normalized to a value of 1.0). Also, a *symmetrical system* of assigning 0° , 120° , and 240° phase to represent the red, blue, and green hue values, respectively, is employed, resulting in equal subcarrier amplitude values for fully saturated primary colors.

From the *symmetrical system equations*, it is easy to see that the color-difference signal values must have a positive amplitude of 0.66 for the desired color, and negative values of -0.33 for the other two primary colors. Thus, in the process of re-creating an individual primary color signal, the color-difference signals are added linearly to the "Y" signal; this reinforces the desired color signal to a value of 1.0 and cancels the luminance signal to zero for the other two colors. The same process is applied to each channel in turn.

The "prime" designation associated with each primary signal voltage value indicates that the signals are nonlinear by a specified amount to compensate for the nonlinear voltage-to-light characteristic of the reproducing kinescope. The overall system philosophy is to linearly reproduce the light input to the camera at the output of the kinescope; however, the signals in the transmission path are nonlinear with an exponent of "gamma", having a specified value of 2.2.

From the symmetrical case, a *generalized* case can be developed with two of the color-difference signals in phase quadrature and precise values for the signal voltages and the encoding and decoding angles as actually proposed by the NTSC and adopted by the FCC. *General Case I* shows that the primary color values comprising the luminance signal are not equal, but are 0.299 for red, 0.587 for green, and 0.114 for blue.

The general expressions for the three primary color-difference signals are given in *General Case II*. These same color-difference signals may also be expressed in terms of R, G, and B as indicated in *General Case III*. From these equations, nine coefficients are produced, for which values must either be assigned or calculated to specify the total system.

These coefficient values have been specified by the NTSC. The luminance primary color values have already been determined, and the receiver decoding angle representing blue was arbitrarily determined as 0° in a Cartesian coordinate system (180° from the phase of the reference burst). A difference of 90° was assigned between the signals representing blue and red. It was also decided that maximum saturation would be represented by a peak-to-peak value of subcarrier signal whose negative value would never swing "blacker-than-black" by more than -0.33 (white normalized to a value of +1.0 and black at zero).

If the coefficients of the color-difference signal values, as indicated in General Case

II, are set equal to the color-difference coefficients derived from General Case III, *nine basic equations* are formed that characterize the NTSC system. These equations may be solved for the unknowns if the *NTSC values* are inserted. (The underlined values are those specified by committee.)

Thus, the total NTSC color signal values and encoding and decoding angles are determined to form the desired luminance (brightness) and chrominance (hue and saturation) information carrying signals. A graphical representation of the mathematical process is shown in Fig. 16. Fig. 17 shows the standardized values for a composite color-bar signal. A complete statement of the *specifications of the NTSC color signal values* is included with the equations.

Encoding

In summary, the scene to be televised is analyzed in terms of its specified red, green, and blue components by the camera. The resulting three output signals are combined in linear matrices to form a luminance signal (E_Y) containing frequencies in the 0-to-4-MHz range. Two specific color-difference signals are also formed; one designated as "I" and having a bandwidth of about 1.5 MHz, and the other designated as "Q" with a bandwidth of about 0.5 MHz. The "I" signal contains the orange-cyan color hues while the "Q" signal reproduces the green-magenta range of colors. Then both the I and Q signals are present (0-to-0.5 MHz range), full three-color reproduction is available. In the frequency range from 0.5 MHz to 0.5 MHz, only the I signal exists and the preferred high-acuity orange-cyan locus of colors is reproduced. In the frequency range above 1.5 MHz, only the Y signal exists; it provides the high frequency monochrome detail information. To reproduce the preferred orange-cyan colors, the angles representing I and Q are in phase quadrature, but are rotated 33° from the B-Y and R-Y phase designations. The 33° angle was determined experimentally and specified by committee. Fig. 18 summarizes the transmitter encoding functions and signal-make-up designations.

Decoding

At the receiver, the *decoding process* is essentially the inverse of the encoding function. Fig. 19 shows two typical receiver functional diagrams. The luminance signal,

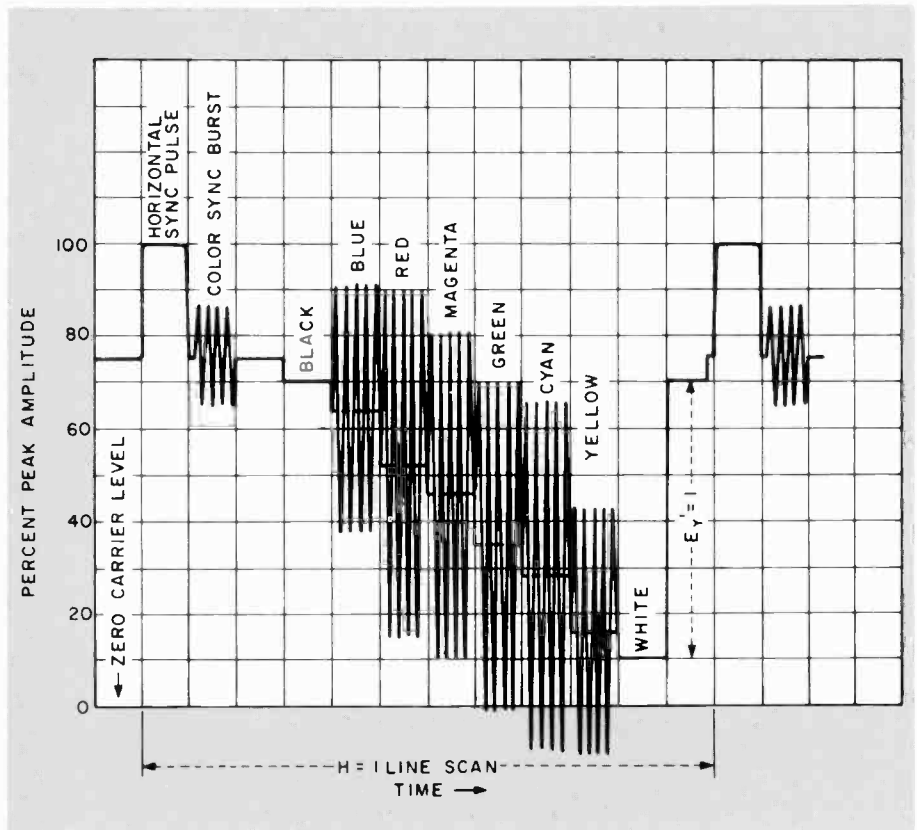


Fig. 17. Color bar standard values formed from the three primary colors and their equal-mixture complementary colors.

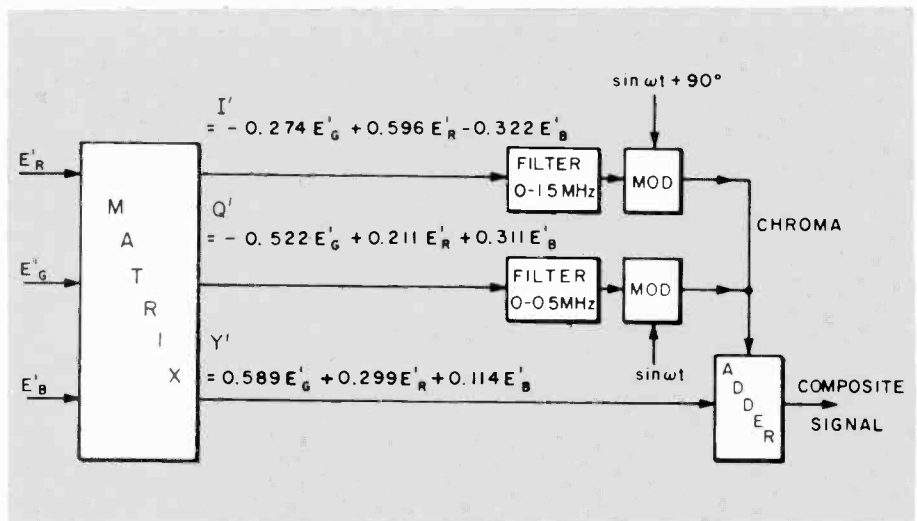


Fig. 18. NTSC encoder functions and signal make-up designations

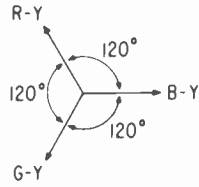
in the video domain, is fed to all three of the reproducing kinescope guns at the appropriate levels to produce a monochrome picture having a D6500 color temperature. The chrominance signal is separated by a bandpass filter and impressed upon the inputs of the synchronous demodulators. These demodulators extract the appropriate color-difference signals at the desired phase angle, as determined by a locally

generated subcarrier reference signal locked to the incoming "burst" signal.

The receiver designer is free to determine the particular decoding process. For example, the I, Q signals available, followed by the appropriate matrix, can be used to form the necessary R-Y, B-Y, and G-Y signals. On the other hand, R-Y and B-Y signals with equal bandwidth (0-to-0.5 MHz) may be decoded directly with a

NTSC System Equations

Symmetrical system equations



$$S_T = \frac{1}{3}R' + \frac{1}{3}G' + \frac{1}{3}B' + \frac{2}{3}R' \cos \omega c t + \frac{2}{3}G' \cos (\omega c t + 120^\circ) + \frac{2}{3}B' \cos (\omega c t + 240^\circ)$$

$$R' - Y' = \frac{2}{3}R' - \frac{1}{3}G' - \frac{1}{3}B'$$

$$G' - Y' = -\frac{1}{3}R' + \frac{2}{3}G' - \frac{1}{3}B'$$

$$B' - Y' = -\frac{1}{3}R' - \frac{1}{3}G' + \frac{2}{3}B'$$

$$Y' = \frac{1}{3}R' + \frac{1}{3}G' + \frac{1}{3}B'$$

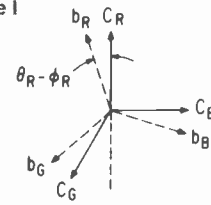
General case II DECODING ANGLES : ϕ_R, ϕ_G, ϕ_B
 DECODING GAINS : C_R, C_G, C_B

$$R' - Y' = C_R b_R R' \cos (\theta_R - \phi_R) + C_R b_G G' \cos (\theta_G - \phi_R) + C_R b_B B' \cos (\theta_B - \phi_R)$$

$$G' - Y' = C_G b_R R' \cos (\theta_R - \phi_G) + C_G b_G G' \cos (\theta_G - \phi_G) + C_G b_B B' \cos (\theta_B - \phi_G)$$

$$B' - Y' = C_B b_R R' \cos (\theta_R - \phi_B) + C_B b_G G' \cos (\theta_G - \phi_B) + C_B b_B B' \cos (\theta_B - \phi_B)$$

General case I



b = TRANSMITTER
 C = RECEIVER
 θ = TRANSMITTER
 φ = RECEIVER

$$Y' = a_R R' + a_G G' + a_B B'$$

$$C' = b_R R' \cos (\omega c t + \theta_R) + b_G G' \cos (\omega c t + \theta_G) + b_B B' \cos (\omega c t + \theta_B)$$

FOR NTSC :

$$a_R = 0.299$$

$$a_G = 0.587$$

$$a_B = 0.114$$

General case III

ALSO :

$$R' - Y' = (1 - a_R) R' - a_G G' - a_B B'$$

$$G' - Y' = -a_R R' + (1 - a_G) G' - a_B B'$$

$$B' - Y' = -a_R R' - a_G G' + (1 - a_B) B'$$

THE COEFFICIENTS ARE :

(1 - a _R)	- a _G	- a _B
- a _R	(1 - a _G)	- a _B
- a _R	- a _G	(1 - a _B)

- (1) a_R = 0.299
 a_G = 0.587
 a_B = 0.114

NTSC values specified by committee

- (2) MAXIMUM "BLACKER THAN BLACK" SWING = $\frac{1}{3}$

$$b_R = a_R + .333 = .299 + .333 = .632$$

$$b_B = a_B + .333 = .114 + .333 = .447$$

- (3) θ_B = 0°
 φ_B - φ_R = 90°

Nine basic equations

$$(1 - a_R) = C_R b_R \cos (\theta_R - \phi_R)$$

$$-a_R = C_G b_R \cos (\theta_R - \phi_G)$$

$$-a_R = C_B b_R \cos (\theta_R - \phi_B)$$

$$-a_G = C_R b_G \cos (\theta_G - \phi_R)$$

$$(1 - a_G) = C_G b_G \cos (\theta_G - \phi_G)$$

$$-a_G = C_B b_G \cos (\theta_G - \phi_B)$$

$$-a_B = C_R b_B \cos (\theta_B - \phi_R)$$

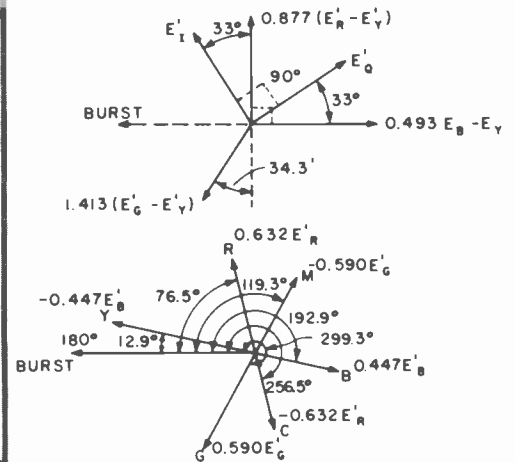
$$-a_B = C_G b_B \cos (\theta_B - \phi_G)$$

$$(1 - a_B) = C_B b_B \cos (\theta_B - \phi_B)$$

Solutions to nine basic equations for NTSC

RED	GREEN	BLUE
a _R = 0.299	a _G = 0.587	a _B = 0.114
b _R = 0.632	b _G = 0.590	b _B = 0.447
C _R = 1.1402	C _G = 0.7027	C _B = 2.0284
θ _R = 103.47°	θ _G = 240.67°	θ _B = -12.95°
φ _R = 90°	φ _G = 235.75°	φ _B = 0°

NTSC color signal specifications



$$E'_R = -0.274 E'_G + 0.596 E'_R - 0.322 E'_B$$

$$E'_G = -0.522 E'_G + 0.211 E'_R + 0.311 E'_B$$

$$\frac{E'_B - E'_Y}{2.03} = -0.545 E'_R + 0.839 E'_G$$

$$\frac{E'_R - E'_Y}{1.141} = +0.839 E'_R + 0.545 E'_G$$

$$\frac{E'_G - E'_Y}{0.703} = -0.399 E'_R - 0.900 E'_G$$

$$E'_Y = 0.589 E'_G + 0.299 E'_R + 0.114 E'_B$$

simple matrix to form G-Y. In either case, the detected color-difference signals are individually added to the luminance signal in proper proportions to re-create the specific red, green, and blue signals that actuate the kinescope display device.

The overall gain of the chrominance channel determines the reproduced color saturation (ratio of chrominance to luminance), and the overall phase adjustment of the decoding reference signal provides a control of the average hue of the reproduced scene.

Luminance—chrominance

Another reason for the choice of signal values in the NTSC system is that the eye is more responsive to spatial and temporal variations in luminance than it is to the same variations in chrominance. Therefore, the relative chrominance gain and angle values are proportioned to take advantage of this characteristic in order to reduce the visibility of random noise and interference effects introduced into the transmission path between the transmitter and the receiver. Thus, the principle of *constant luminance* is exploited to an extent that the combined brightness of random-noise variations in the red, green and blue channels appears constant in relation to the luminosity response of the average human eye. In an idealized linear system, the improvement in *visual* signal-to-noise ratio is in the 8-to-10-dB range. However, even though the system is inherently nonlinear, the brightness-cancellation process is effective at relatively low-level chromaticity signals, and the average improvement is in the order of 4 to 5 dB.

The problem remains of arranging the chrominance and luminance signals within a common channel without excessive mutual interference. Recognition that the scanning process, being equivalent to sampling, produces signal components concentrated in uniformly spaced groups across the channel width introduced the principle of *horizontal frequency interlaced* (dot interlace) operation. The color subcarrier frequency was chosen to be an odd multiple of one-half horizontal line frequency at a value of 3.579545 MHz. Thus, in an interlaced system, the phase of the subcarrier alternates in succeeding lines by 180° and four fields are required for picture completion. In addition, the chrominance subcarrier, by definition, becomes zero when no color exists and only shades of gray are to be reproduced via the luminance channel.

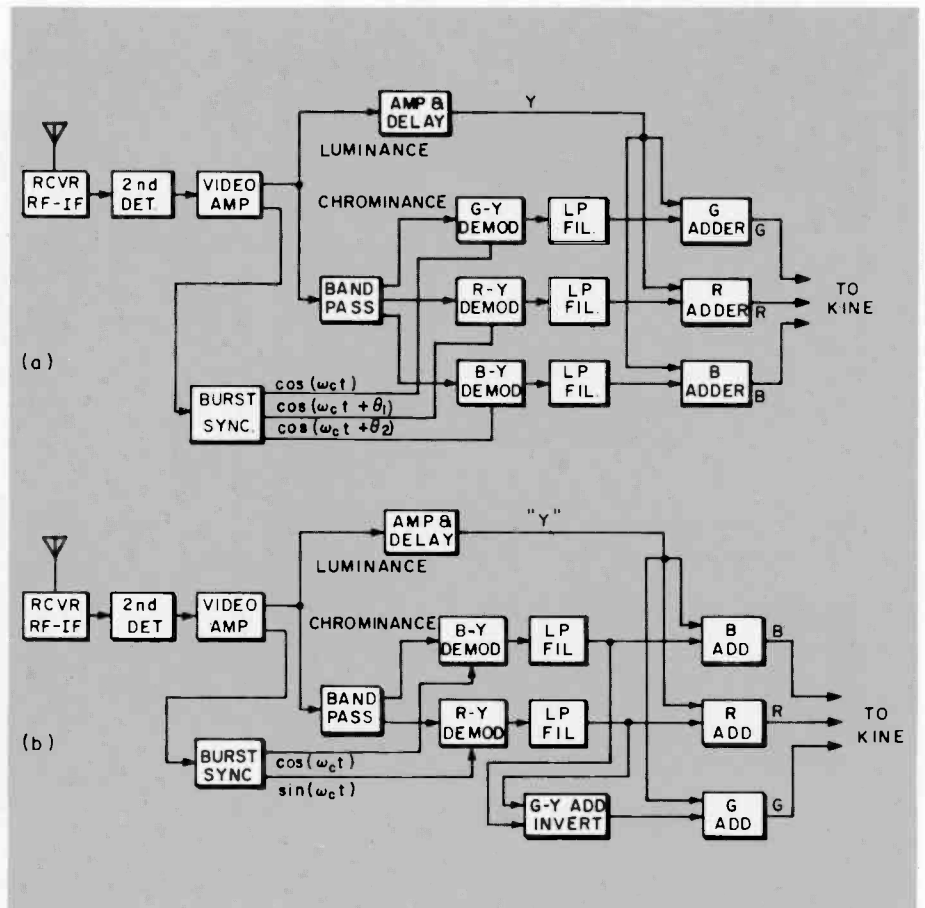


Fig. 19. NTSC receiver decoder functions. Drawing (a) shows the fundamental operation of recovering all three color difference signals; (b) is a simplification that requires only two decoders with a matrix to form the other (G-Y) color difference signal.

By the interleaved nature of the subcarrier frequency relative to the timing of the horizontal scan rate, the visibility of the subcarrier signal is reduced, and if the system were linear, would exactly cancel on alternate lines. This interleaving process, indicated in Fig. 20, makes it possible to transmit the chromaticity information in the form of a phase-and amplitude-modulated subcarrier within the same channel width as that previously occupied by the monochrome transmission alone.

Since the picture-signal-energy-distribution versus frequency is grouped into intervals having 15.734-kHz spacings (horizontal scan rate), various prime numbers can be chosen to produce odd multiples of one-half line rate. The particular choice in the vicinity of 3.6 MHz was made for two reasons. First, the high frequency resulted in a fine interference pattern having low visibility because of small spatial dimensions. Second, this value allows about 0.5 MHz of double-sideband frequency range for the color-signal sideband components allowing for the sound carrier located at

4.5 MHz. The choice of the exact frequencies is

$$f_{LINE} = \frac{4.5 \times 10^6}{286} \text{ Hz}$$

$$= 15.734.26 \text{ Hz}$$

$$f_{FIELD} = \frac{f_{LINE}}{525/2} \text{ Hz}$$

$$= 59.94 \text{ Hz}$$

$$f_{SC} = \frac{13 \times 7 \times 5}{2} \times f_{LINE}$$

$$= 3.579545 \text{ MHz}$$

This choice allows the approximate average beat of 920 kHz between the color subcarrier and the sound carrier to also be interlaced to reduce its average visibility. The sound carrier, for reasons of compatibility, remained at 5.4 MHz, and the total number of scanning lines remained at 525 lines in a two-to-one vertical interlaced system. Thus, the color subcarrier, f_{sc} , be-

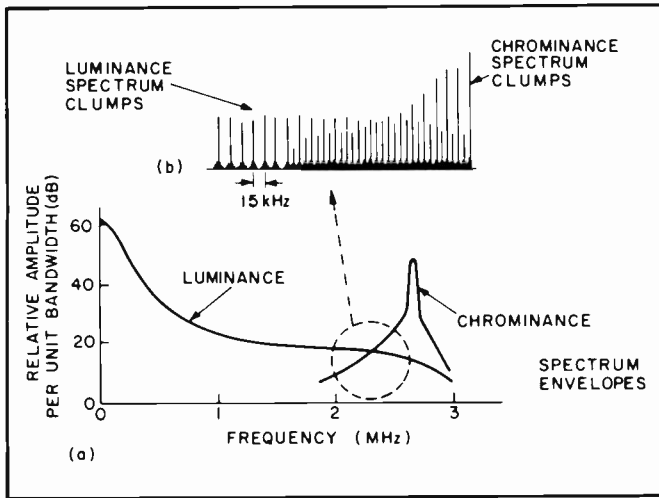


Fig. 20. Frequency-interlaced relationship of chrominance and luminance.

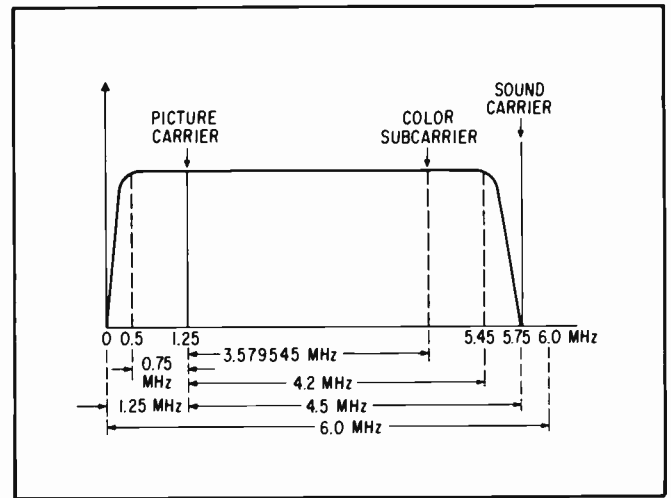


Fig. 21. Transmission channel for the NTSC color system.

came 3.579545 MHz with the horizontal scanning rate $f_{line} = 15.734$ kHz, and the vertical rate $f_{FIELD} = 59.94$ Hz. These rates, although slightly different from the black-and-white standards, fell within the previous tolerance ranges and therefore were acceptable.

The assigned communications-channel frequency relationships are shown in Fig. 21. The picture signal is handled in a vestigial-sideband manner with appropriate amplitude and phase compensation exactly as previously employed in the monochrome system with the sound signal spaced 4.5 MHz from the picture carrier. The color information is carried on a subcarrier located at 3.579545 MHz from the picture carrier. A specific color-signal phase-compensation filter introduced at the transmitter compensates for the typical characteristics of a receiver i.f. response to maintain phase and amplitude symmetry around the color subcarrier at 3.58 MHz.

Thus, the NTSC color standards provide a compatible signal with respect to the previous monochrome standards, and it follows that the numerical values describing the color signal are more precisely specified and therefore fall within previously existing tolerances. The color signal values for the complete system are regulated at $\pm 20\%$ amplitude and $\pm 10^\circ$ phase. However, the standards of good practice recommend $\pm 10\%$ amplitude and $\pm 5^\circ$ phase. The relative time delay match between the chrominance and luminance signal components is ± 50 ns. The accuracy of the 3.579545 MHz is $\pm 0.0003\%$ (approximately ± 10 cycles tolerance) with a rate of drift not to exceed one-tenth of a cycle per second. The horizontal and vertical scanning signals are, of course, derived

from the color subcarrier in order to insure the interleaving relationship.

Conclusion

In the early development period of color television, some critics quipped that NTSC

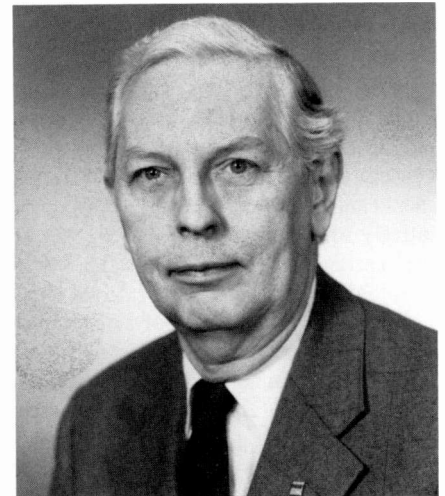
might represent, "Never The Same Color."

But this ingenious system of standards—an imaginative combination of psycho-physical and electronics characteristics—has prevailed for over twenty years and represents one of the more complex yet highly successful technological information display systems ever devised.

Dalton H. Pritchard received the BSEE degree in 1943 from Mississippi State University. He joined RCA Laboratories in 1946 as a Member of the Technical Staff at Riverhead, New York, and was engaged in communications research. In 1950 he transferred to RCA Laboratories, Princeton, N.J. There his research has involved many aspects of color television systems development, receivers, color kinescopes, transmitting encoders, cameras, and the magnetic recording of TV. This work included the planning and testing of systems and circuits proposed for adoption by the National Television System Committee (NTSC).

From 1960 to 1970, Mr. Pritchard developed video processing circuitry for color TV receivers, colorimetry and decoder matrix methods, information display techniques, and analog techniques employing CCD devices for TV applications. He also worked on SelectaVision and VideoDisc development. More recently, as a member of the Television Research Laboratory, Mr. Pritchard has been engaged in research related to high-definition TV (HDTV) systems that include applications of digital signal processing techniques.

Between 1952 and 1978, Mr. Pritchard received seven RCA Laboratories Outstanding Achievement Awards. In 1977 he received the Vladimir K. Zworykin Award for "significant contributions to color television technology." In 1981, he received the David Sarnoff Award for Outstanding Technical Achievement. Mr. Pritchard was awarded the international Eduard Rhein Prize in 1980, which was presented in Berlin in 1981. Also in 1981, he



was appointed to the New Jersey Governor's State Panel of Science Advisers. In 1983, he was elected to membership in the U.S. National Academy of Engineers (NAE).

Mr. Pritchard is the author of more than 20 technical papers and presentations. He holds 40 U.S. patents, and has several pending. He is a Fellow of the Technical Staff, RCA Laboratories, a Fellow of IEEE and SID, and a member of Sigma Xi, Tau Beta Pi, and Kappa Mu Epsilon.

Contact him at:
RCA Laboratories
Princeton, N.J.
Tacnet: 226-2205

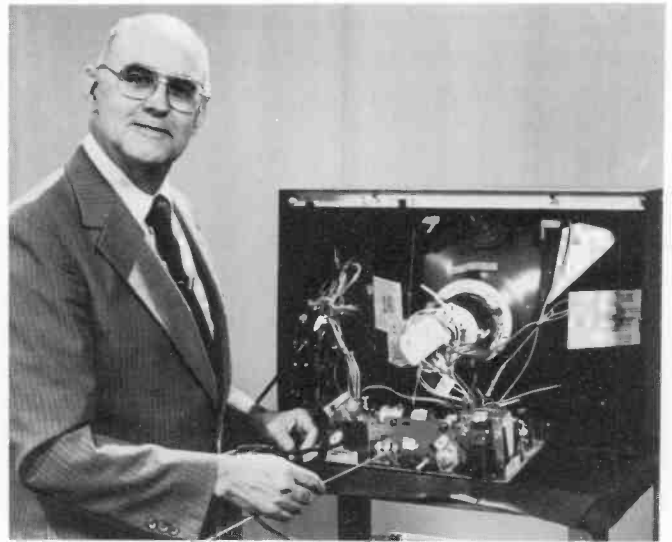
New Television Engineering Fundamentals course available from CEE

The Consumer Electronics Division Technical Excellence Committee in Indianapolis and Corporate Engineering Education (CEE) in Princeton are pleased to announce the completion of their first joint venture in course development. The result of this cooperative effort between a TEC and CEE is E60, an RCA-produced video course on the fundamentals of television engineering.

John W. Wentworth serves as video instructor for the first nine sessions of this ten-session course. Mr. Wentworth is currently active as a private consultant, but he is certainly no stranger to RCA, or to engineering education. He retired from the Broadcast Systems Division in 1982 after a 33-year career with RCA. For nine years prior to retirement he served as Manager, Broadcast Technical Training. In earlier years he served as Director of Operations for RCA Institutes, and was the founding manager of the CEE unit in the late sixties. He is also the author of an early text on the subject matter of this course: *Color Television Engineering*, published by McGraw-Hill in 1955.

In the first nine sessions of E60, Mr. Wentworth presents the concepts of standard broadcast television systems:

- Session 1:** Basic Television Principles
 - Session 2:** Transmission of the TV Signal
 - Session 3:** Basic Colorimetry
 - Session 4:** Multiplexing Techniques for Color Television
 - Session 5:** Color Television Cameras
 - Session 6:** Video Recording Principles
 - Session 7:** Electronic Subsystems for Video Recording
 - Sessions 8 and 9:** Color Receivers and Monitors I, II
- The tenth session, entitled "Survey of New Developments in Video," presents an overview of three exciting current video developments by three different RCA subject matter experts:



Multichannel TV Sound—J. J. Gibson, RCA Laboratories

Direct Broadcast Satellite—E. Lemke, Consumer Electronics

Teletext—R. J. Siracusa, RCA Laboratories

The complete course package includes the ten videotapes and a 500-page Study Guide for each course participant. The Study Guide includes statements of learning objectives, reading assignments in seven monographs included in the Study Guide, a complete video lecture outline with all visuals and text, homework, and suggested optional reading.

With RCA's enormous investment in video, participation in this course ought to be a part of the career development plans of several hundreds of RCA technical personnel.

For further details on course content, contact **Frank Burris, Tacnet 226-2971**. To schedule or order E60, call **Mary Pjura, Tacnet 226-2227**.

Perceptual analysis and simulation of color monitor displays

The human visual system is an important component of color monitor display systems. It is incorporated into the design of such systems by JND analysis and direct simulation.

RCA is developing a new line of color displays intended for use with computer systems. These displays will be used primarily for the depiction of alphanumeric characters. The creation of a new product line involves consideration of both economic and perceptual considerations. In this article we focus on the perceptual analysis of such color monitors as an aid in the design process. First we describe the application of one-dimensional just-noticeable-difference (JND) analysis to the display problem. We then discuss the two-dimensional simulation of color alphanumeric information on such displays. These two approaches complement each other and establish ranges of applicability through cross-validation.

Abstract: *This article describes the development of design aids for a product line of color alphanumeric displays. A systems study provides quantitative design criteria that include the human visual system as an element through just-noticeable-difference (JND) analysis. Also, a full-color simulation on image processing equipment makes it possible to judge proposed design subjectively.*

© 1984 RCA Corporation
Final manuscript received October 29, 1984
Reprint Re-29-6-4

Just-noticeable-difference analysis

Many image display systems can be evaluated through just-noticeable-difference (JND) analysis. The virtue of this analysis is that it converts the objective parameters that describe displays into units that quantify their perceptual impact. An example is the application of JND analysis to the determination of the number of phosphor triads needed for a television display tube.¹ Since this analysis allows the simultaneous consideration of the effects of numerous display parameters, it goes beyond the conventional design rules-of-thumb.

Just-noticeable-difference (JND) analysis refers to an experiment in which subjects viewed sequentially displayed sine-wave gratings of a given spatial frequency and were required to identify which had the greater contrast. One JND is that difference in contrast at which 75-percent accuracy of determination is achieved in a two-alternative, forced-choice experiment. Three JNDs represent a level at which about 99-percent accuracy of determination is achieved. Since the human visual system can be considered as the concatenation of a number of frequency channels of about one octave in bandwidth,² this experiment must be repeated at a number of different spatial frequencies. These results may

be displayed in a convenient graphical form, and analytical expressions are also available that accurately represent the results of such experiments.³

An arbitrary image is analyzed for the purposes of JND analysis by taking its scaled transform⁴ and integrating the resulting power spectrum over successive channels of one-octave bandwidth. Each of these permits the determination of an equivalent sine-wave contrast within that channel, and thus, a determination of the number of JNDs above threshold for that channel. The channels are assumed to act independently, so the number of JNDs within each channel are simply added to obtain a value that can be identified with the entire image. If this is done before and after the image is processed by a system, we can infer the number of JNDs of signal lost due to such processing, and thus have a measure of the quality of the image processing system. Similarly, if such an image processing system introduces artifacts that have no counterpart in the input image, we may infer a number of JNDs of such artifacts above threshold, and refer to this as the number of JNDs of "noise" introduced by the system.

An advantage of JND analysis is that it provides quantitative comparisons of the effect of the various design parameters upon

overall system performance. A disadvantage is that, at present, simplified models of the images and the display devices are used to make the computation practical.

In the present instance JND analysis is applied to the display of alphanumeric information on color display monitors, such as may be used with a variety of computer systems. We consider here a one-dimensional test image consisting of a three-pixel, on-off-on pattern and a display system having vertical phosphor stripes in a sequential red-green-blue series. The system between the input image and the display consists of an amplifier, the nonlinear voltage-to-light characteristic of the kinescope (commonly accounted for by a parameter "gamma"), the blurring due to the electron spot profiles, the misconvergence of the three electron beams, and the sampling due to the phosphor stripe structure. For our purposes, the effects due to phosphor stripe sampling are considered to be "noise."

In the analysis the effects of some display components are more easily accounted for in the spatial-frequency domain, while others are more readily analyzed in the image domain. We therefore set up a discrete version of the test image in the image domain, and transform between the image domain and spatial-frequency domain as desired through a Fast Fourier Transform (FFT) algorithm. In general, we prefer to be in that domain where system effects can be accounted for by multiplication, rather than convolution. For example, the amplifier is most readily accounted for in the spatial-frequency domain, whereas the nonlinear voltage-to-light characteristic of the kinescope can only be reasonably accounted for in the image domain. The separation of sampling artifacts from signal components, however, is most readily accomplished by convolution in the spatial-frequency domain.

A computer program has been written that incorporates these procedures. The quantities computed include the total number of JNDs lost with respect to a perfect image, the number of JNDs of noise introduced by the phosphor-stripe structure, and the number of JNDs produced at pixel frequency. The pixel frequency is defined as $1/2S$, where S is the pixel width. The number of JNDs at the pixel frequency seems to have high correlative value with respect to actual simulations of alphanumeric images. As a rule of thumb, 15 JNDs at the pixel frequency are needed to produce recognizable characters. This can also be related to studies of the legibility of

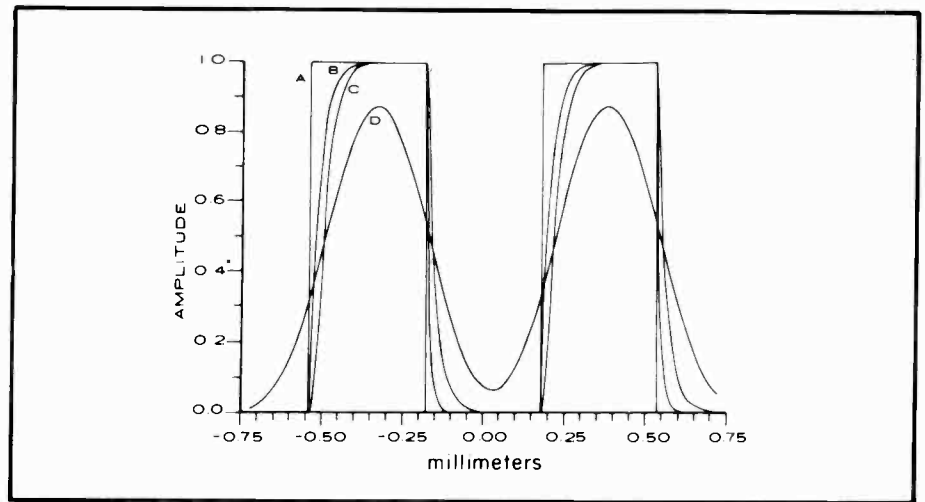


Fig. 1. The form of the image at various stages of processing: (a) the input image, (b) after amplification, (c) after kinescope gamma, and (d) after smoothing by the electron spot (assumed to be Gaussian in form).

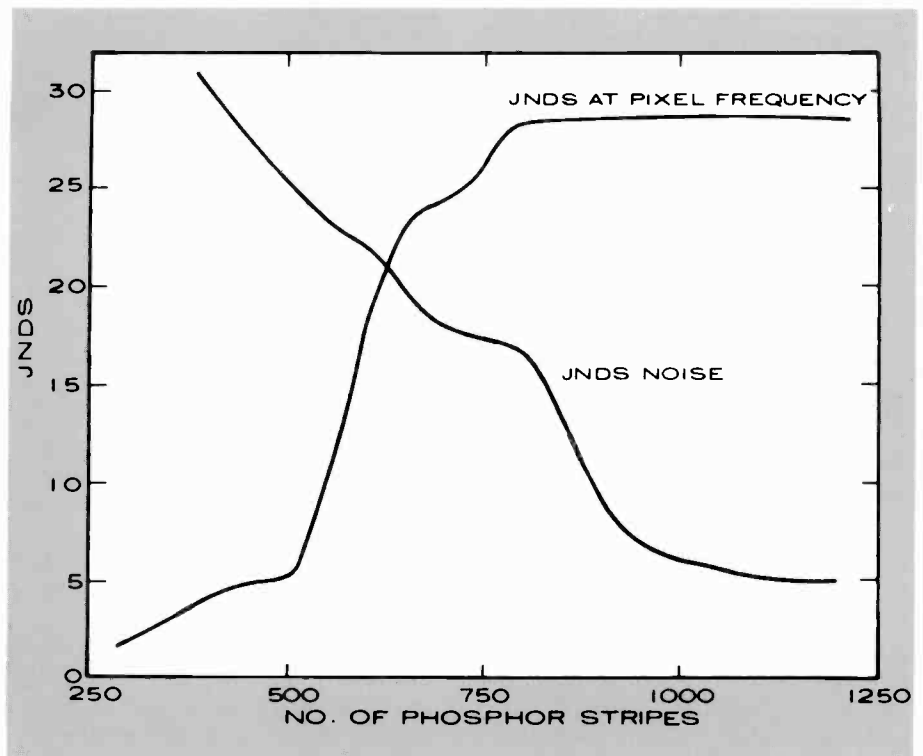


Fig. 2. Just-noticeable-difference (JND) results as a function of the number of phosphor strips on the display.

newsprint, and to previous display design practices.

This computational tool has been applied to a number of proposed color display monitors. In particular, we consider in some detail a proposed monitor for which the diagonal size of the display is about nine inches. This corresponds to a display width of 166 millimeters. The test image is shown in Fig. 1a. In Fig. 2 we show the results of an investigation of the

effects of the density of phosphor stripes on image quality. Other parameters of the display system were kept fixed for this investigation. A single-pole amplifier was assumed, with a 3-dB bandwidth of 18 MHz. The nonlinear voltage-to-light characteristic was determined by a power law with gamma of 2.7. The full width of the electron spot at the 5-percent level was taken as 0.5 millimeters. The misconvergence and coma were taken as zero, approxi-

mating conditions near the center of the display. Figure 1b shows the image shape after being processed by the amplifier, while Fig. 1c exhibits the additional effect introduced by gamma. Finally, the electron spot introduces an additional smoothing effect leading to the result shown in Fig. 1d. These curves are produced automatically in conjunction with a graphical aids package.

Finally, the image is sampled by the phosphor-stripe structure. The result of sampling can be characterized by the number of JNDs of signal at pixel frequency in the sampled image, along with the JNDs of noise introduced (the visibility of the sampling structure). In Fig. 2, these quantities have been plotted against the number of phosphor stripes. In this case, the Nyquist frequency corresponds to about 480 phosphor stripes. The present JND analysis indicates a very poor result at this sampling frequency. This has been previously indicated in the context of displays for consumer television.¹ However, at about 1.5 times the Nyquist frequency (720 phosphor stripes) nearly the full signal quality has been achieved, though significant levels of sampling noise remain. Finally, at about 2.0 times the Nyquist frequency (960 phosphor stripes) very adequate levels of both signal and noise have been achieved. The quantitative predictions illustrated in Fig. 2 are verified by the following discussion of the simulations.

Simulation of alphanumeric characters on color monitors

The JND analysis described in the previous section assumes a one-dimensional pattern. In order to verify the JND model in the case of color alphanumeric displays, and also to aid in the design process, we have performed a full two-dimensional simulation of such displays.

A digital image-processing-based facility has been developed that simulates the display of alphanumeric information on color monitors. The monitor's performance can then be determined quickly through inspection of the simulated images. The display engineer can see the results of trading off one display characteristic against another, and can determine where the most gain in performance is to be found.

Since both the image processor and the presentation monitor have limiting resolutions that are not fine enough to represent the simulated characters at their normal size without introducing artifacts, the characters are magnified by a factor of 50. At

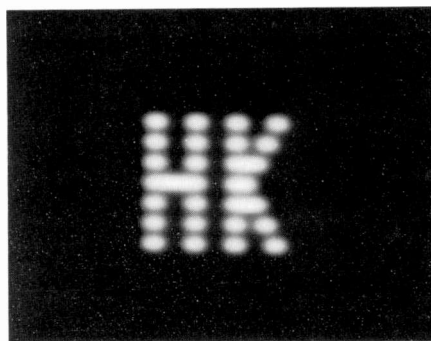


Fig. 3. Simulated characters without phosphor sampling.

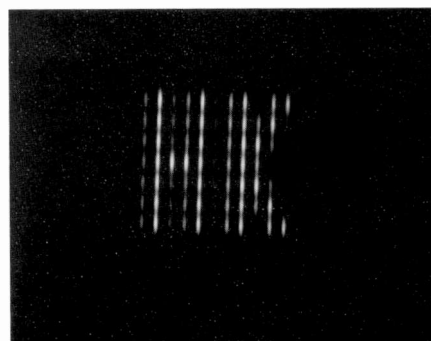


Fig. 5. Sampled characters - $F_n = 1/2 \times$ Nyquist frequency.

this magnification, the resolution of the image processing system does not influence the conclusions of the simulations. Increasing the size of the simulated characters is valid if the characters are viewed at 50 times the normal viewing distance, since the relevant parameter for the human visual system is not the absolute size of an image, but rather the size of an image as it is formed on the retina. Therefore, by increasing the viewing distance by the same factor that the image is magnified, the retinal size of the image is unchanged.

The simulations are performed on a mini-computer with an attached image processor. Program development and image processor control is performed by the mini-computer, while the image processor performs all the filtering, manipulation, and sampling of the images. The image processor is capable of simultaneously displaying three RGB images with $512 \times 512 \times 24$ bits of resolution. The selection of the best display specifications is simplified by displaying several images side-by-side.

We can presently simulate the following monitor parameters:

- Arbitrarily shaped fonts
- Finite-bandwidth RC amplifiers
- The kinescope's voltage-to-light output characteristic (gamma)

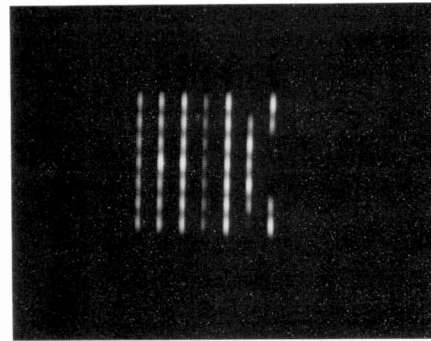


Fig. 4. Sampled characters $F_n =$ Nyquist frequency.

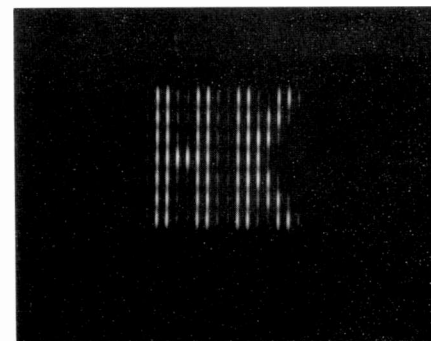


Fig. 6. Sampled characters - $F_n = 2 \times$ Nyquist frequency.

- Gaussian-shaped electron spots
- Electron-spot misconvergence
- Line phosphor-stripe sampling.

The simulation allows the display engineer to see the effect that each monitor parameter has on the alphanumeric characters, thereby giving additional insight into the appropriate design trade-offs. This is an important capability, because it aids in the verification of the design process.

As an example of the system capabilities, we have simulated the effects that varying the number of phosphor stripes on a monitor will have on alphanumeric characters. We have assumed that the characters will be displayed as a single color, in which case the other two colored phosphor stripes are not shown. Also, we have chosen the relative phase between the phosphor stripes and the characters so that there will be maximum aliasing. This is a worst-case performance criterion.

The following display characteristics are assumed:

1. Pixel size = 0.36 mm.
2. Single-pole RC amplifier response with an 18-MHz bandwidth at the -3 dB point.

3. Light output is proportional to applied voltage raised to the 2.7 power (i.e., gamma equals 2.7).
4. Gaussian-shaped electron spots with a full width of 0.5 mm at the 5-percent points.
5. Line phosphor stripes with a duty cycle of 75 percent.

Figure 3 shows the appearance of the characters after passing through the previously defined system, but without phosphor sampling. Figures 4, 5, and 6 are sampled versions of the characters, with varying phosphor pitch. If we define the Nyquist frequency F_N such that we have one phosphor triad per pixel, then $F_N = 1, 1.5,$ and 2 for Figs. 4, 5, and 6, respectively. (Note that the character "H" is three pixels wide.)

These resulting images can be compared to the JND analysis⁵ described earlier. This analysis defines a measure of monitor performance that is based on the properties of the human visual system. The three cases simulated here correspond directly with the JND analysis depicted in Fig. 2, with the number of phosphor stripes equal to 480 stripes-per-picture-width ($F_N = 1$), 720 stripes-per-picture-width ($F_N = 1.5$), and 960 stripes-per-picture-width ($F_N = 2$). The JND analysis gives the following results:

F_N	JNDs at	
	Pixel Frequency	JNDs of Noise
1	5	25.5
1.5	25	17.5
2	26.6	5.8

For this example, the JND analysis assumes a one-dimensional test pattern consisting of three pixels, with the first and last pixel at unit amplitude, and the center pixel at zero amplitude (that is, the upper portion of the character "H"). The pixel frequency is then defined as $1/2S$, where S is the width of a single pixel in degrees of visual angle. The JNDs at pixel frequency indicated the visibility of the test pattern is an on-off-on sequence. The JNDs of noise, in this case, measure the interference of the phosphor—stripe structure on the visibility of the test pattern.

Summary

A useful and flexible tool has been developed that permits JND analysis of the one-dimensional images characteristic of alphanumeric displays. The investigation described in the first section is illustrative of many similar types of studies that may



Authors, left to right: Klopfenstein, Carlson, Pica.

Ralph W. Klopfenstein received the B.S. degree in Electrical Engineering from the University of Washington in 1944. He received the M.S. and Ph.D. degrees in Applied Mathematics from Iowa State University in 1951 and 1954, respectively. He joined the RCA Victor Division in Camden, N.J. as an Electrical Engineer in 1948 and worked on the development of high-power filters and transmitting antennas for VHF and UHF television applications. Since 1953 he has been engaged in research at RCA Laboratories, where he is a Fellow of the Technical Staff.

In 1957, Dr. Klopfenstein was named Head, Mathematical Services. Since 1963 he has been engaged in research related to the application of mathematics, with a principal interest in developing algorithms for the numerical solution of differential equations.

Dr. Klopfenstein is a member of the American Mathematical Society, Association for Computing Machinery, IEEE, Mathematical Association of America, Society for Industrial and Applied Mathematics, and Sigma Xi, and a Fellow of the Institute of Mathematics and Its Applications. He received an RCA Laboratories Outstanding Achievement Award in both 1968 and 1969.

Contact him at:
RCA Laboratories
Princeton, N.J.
Tacnet: 226-2982

Albert P. Pica received a B.S. degree from the City College of the City University of New York in 1974, and an M.S. degree from Rutgers University in 1976, both in Physics. Mr. Pica joined RCA Laboratories in 1977 as a Research Associate, and was promoted to Member of the Technical Staff in 1981. He has worked on human visual perception and digital image processing, and contributed to the development of the digital scanning capacitance microscope (DSCM). The work in visual perception helped find the appropriate parameters for a just-noticeable-difference model of human perception. This model was used for guidance in the design of displays for high-definition TV and alphanumeric displays.

Recently, Mr. Pica has been engaged in digital image processing; specifically, he has built a simulation system that will aid in the design of color alphanumeric displays. This facility allows the user to see the effects of bandwidth, kinescope gamma, and coma on alphanumeric characters.

In 1983, Mr. Pica received an RCA Laboratories Outstanding Achievement Award. He is a member of the Optical Society of America, the American Physical Society, the Association for Computing Machinery, and the IEEE. Contact him at:
RCA Laboratories
Princeton, N.J.
Tacnet: 226-2859

Curtis R. Carlson is a Tau Beta Pi graduate of Worcester Polytechnic Institute, where he received the B.S. degree in Physics in 1967. He received his M.S. and Ph.D. degrees from Rutgers University in 1969 and 1973, respectively. In 1973 Dr. Carlson joined RCA Laboratories as a Member of the Technical Staff. His research has centered on processing in both human and machine visual systems. In 1981 he was named Head, Image Quality and Human Perception Research, and in 1983 he joined the Advanced Video Systems Research Laboratory as Head, Advanced Image Processing Research. In 1984 he was appointed Director of Information Systems Research, where he is responsible for research in artificial intelligence and home information systems.

Dr. Carlson is a member of the IEEE, Sigma Xi, SMPTE, SPIE, ARVO, and OSA. He is a member of the SMPTE Vision Committee on High Definition Television, and was a Special Editor of an issue of the *SID Proceedings* on "Recent Advances in Visual Information Processing." He received an RCA Laboratories Outstanding Achievement Award in 1979 and again in 1983. Dr. Carlson has published or presented over 40 papers in the fields of image quality, image coding, and human perception research. Contact him at:
RCA Laboratories
Princeton, N.J.
Tacnet: 226-2436

be carried out to obtain quantitative measures of the interplay of the design parameters pertinent to color display monitors. One such example is the trade-off possible between spot size and misconvergence. Additionally, the digital image processing facility just described permits the two-dimensional simulation of color, alphanumeric information on such displays. An example corresponding to phosphor stripe sampling

was simulated and a comparison made to a JND analysis of the same images.

References

1. C. R. Carlson, "Application of Psychophysics to the Evaluation of Imaging Systems," *Proc. 1982 Inter. Display Research Conf.*, Cherry Hill, N.J., pp. 1-15, (1982).
2. M. B. Sacks, J. Nachmias, and J. G. Robinson, "Spatial Frequency Channels in Human Vision," *J. Opt. Soc. Am.*, 61, pp. 1176-1192 (1971).
3. C. R. Carlson, and R. W. Cohen, "A Simple Psychophysical Model for Predicting the Visibility of Displayed Information," *Proceedings of the SID*, 21, pp. 229-246 (1980).
4. C. R. Carlson, R. W. Klopfenstein, and C. H. Anderson, "Spatially Inhomogeneous Scaled Transforms in Vision and Pattern Recognition," *Optics Letters*, 6, pp. 386-388 (1981).
5. C. R. Carlson and R. W. Cohen, "Visibility of Displayed Information," *Tech. Report to the Office of Naval Research*, Cont. No. N00014-74-C-0184, (July, 1978).

Consumer Electronics Library

Where can a CE engineer:

Find general information about television systems?

Locate industry standards that apply to a new method he or she is using?

Find examples of conic sections used in parametric geometry?

In the Consumer Electronics Engineering Library. The book and periodicals collection is strong in the subject areas of electronics, computer science, mathematics, mechanical and electrical engineering, radio and television engineering, and telecommunications. The library maintains a subscription to the VSMF microfilm system, which includes manufacturers' catalogs, industry standards, and military documents.

The collection is augmented by information made available through library networks and computerized information retrieval. The CE library is a

member of the RCA Technical Library Network and the OCLC library network of shared resources. Information from articles in technical journals can be located by entering specific words, phrases, titles, or authors into the library computer. The librarian has access to over 250 different subject databases, including the RCA Technical Abstracts database. Copies of pertinent articles can be obtained through the inter-library loan network.

Centrally located in Building 6 of the Indianapolis Sherman Drive facility, the CE Engineering Library serves a community of approximately 400 engineers. It is a dynamic resource, constantly being updated with state-of-the-art information.

For more information, contact **Susan M. Tamer**, Administrator of Library Services, at:
(317) 267-5925
Tacnet: 422-5925

If you are not able to find the information you need at your local library, your librarian will be able to get it for you from another site. Just ask.

Pyramid methods in image processing

The image pyramid offers a flexible, convenient multiresolution format that mirrors the multiple scales of processing in the human visual system.

Digital image processing is being used in many domains today. In image enhancement, for example, a variety of methods now exist for removing image degradations and emphasizing important image information, and in computer graphics, digital images can be generated, modified, and combined for a wide variety of visual effects. In data compression, images may be efficiently stored and transmitted if translated into a compact digital code. In machine vision, automatic inspection systems and robots can make simple decisions based on the digitized input from a television camera.

But digital image processing is still in a developing state. In all of the areas just mentioned, many important problems remain to be solved. Perhaps this is most obvious in the case of machine vision: we still do not know how to build machines

that can perform most of the routine visual tasks that humans do effortlessly.

It is becoming increasingly clear that the format used to represent image data can be as critical in image processing as the algorithms applied to the data. A digital image is initially encoded as an array of pixel intensities, but this raw format is not suited to most tasks. Alternatively, an image may be represented by its Fourier transform, with operations applied to the transform coefficients rather than to the original pixel values. This is appropriate for some data compression and image enhancement tasks, but inappropriate for others. The transform representation is particularly unsuited for machine vision and computer graphics, where the spatial location of pattern elements is critical.

Recently there has been a great deal of interest in representations that retain spatial localization as well as localization in the spatial—frequency domain. This is achieved by decomposing the image into a set of spatial frequency bandpass component images. Individual samples of a component image represent image pattern information that is appropriately localized, while the bandpassed image as a whole represents information about a particular fineness of detail or scale. There is evidence that the human visual system uses such a representation,¹ and multiresolution schemes are becoming increasingly popular in machine vision and in image processing in general.

The importance of analyzing images at many scales arises from the nature of

images themselves. Scenes in the world contain objects of many sizes, and these objects contain features of many sizes. Moreover, objects can be at various distances from the viewer. As a result, any analysis procedure that is applied only at a single scale may miss information at other scales. The solution is to carry out analyses at all scales simultaneously.

Convolution is the basic operation of most image analysis systems, and convolution with large weighting functions is a notoriously expensive computation. In a multiresolution system one wishes to perform convolutions with kernels of many sizes, ranging from very small to very large, and the computational problems appear forbidding. Therefore one of the main problems in working with multiresolution representations is to develop fast and efficient techniques.

Members of the Advanced Image Processing Research Group have been actively involved in the development of multiresolution techniques for some time. Most of the work revolves around a representation known as a "pyramid," which is versatile, convenient, and efficient to use. We have applied pyramid-based methods to some fundamental problems in image analysis, data compression, and image manipulation.

Image pyramids

The task of detecting a target pattern that may appear at any scale can be approached in several ways. Two of these, which involve only simple convolutions, are illus-

Abstract: *The data structure used to represent image information can be critical to the successful completion of an image processing task. One structure that has attracted considerable attention is the image pyramid. This consists of a set of lowpass or bandpass copies of an image, each representing pattern information of a different scale. Here we describe a variety of pyramid methods that we have developed for image data compression, enhancement, analysis and graphics.*

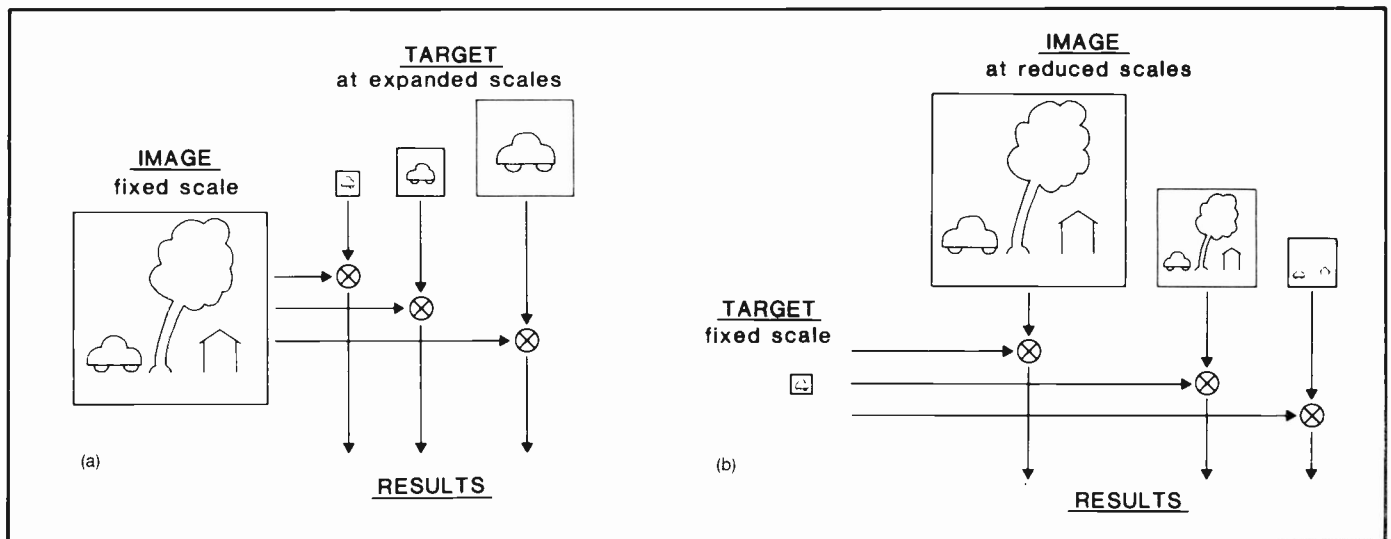


Fig. 1. Two methods of searching for a target pattern over many scales. In the first approach, (a), copies of the target pattern are constructed at several expanded scales, and each is convolved with the original image. In the second approach, (b), a single copy of the target is convolved with

copies of the image reduced in scale. The target should be just large enough to resolve critical details. The two approaches should give equivalent results, but the second is more efficient by the fourth power of the scale factor (image convolutions are represented by 'O').

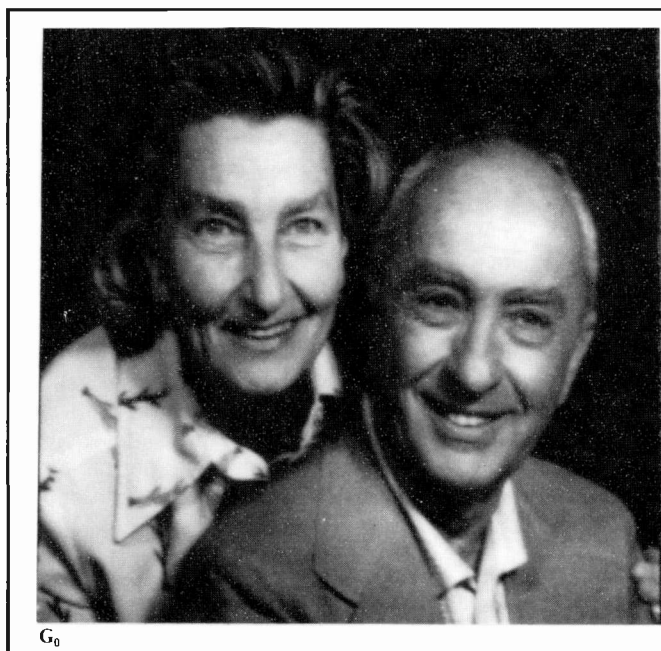
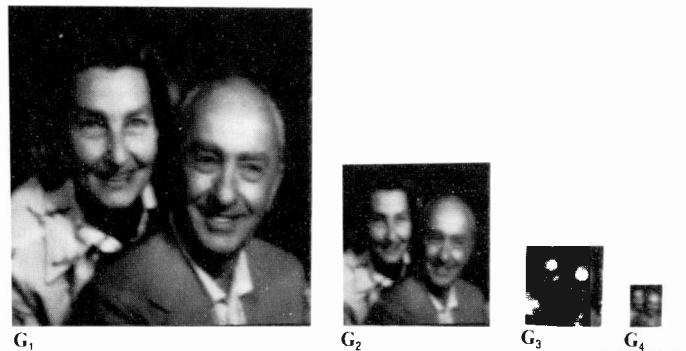


Fig. 2a. The Gaussian pyramid. The original image, G_0 , is repeatedly filtered and subsampled to generate the sequence of reduced resolution image G_1 , G_2 , etc. These comprise a set of lowpass-filtered copies of the original image in which the bandwidth decreases in one-octave steps.



trated in Fig. 1. Several copies of the pattern can be constructed at increasing scales, then each is convolved with the image. Alternatively, a pattern of fixed size can be convolved with several copies of the image represented at correspondingly reduced resolutions. The two approaches yield equivalent results, provided critical information in the target pattern is adequately represented. However, the second approach is much more efficient: a given convolution with the target pattern expanded in scale by a factor s will require s^4 more arithmetic operations than the corresponding

convolution with the image reduced in scale by a factor of s . This can be substantial for scale factors in the range 2 to 32, a commonly used range in image analysis.

The image pyramid is a data structure designed to support efficient scaled convolution through reduced image representation. It consists of a sequence of copies of an original image in which both sample density and resolution are decreased in regular steps. An example is shown in Fig. 2a. These reduced resolution levels of the pyramid are themselves obtained through a highly efficient iterative algorithm. The

bottom, or zero level of the pyramid, G_0 , is equal to the original image. This is lowpass-filtered and subsampled by a factor of two to obtain the next pyramid level, G_1 . G_1 is then filtered in the same way and subsampled to obtain G_2 . Further repetitions of the filter/subsample steps generate the remaining pyramid levels. To be precise, the levels of the pyramid are obtained iteratively as follows. For $0 < l < N$:

$$G_l(i,j) = \sum_{m,n} w(m,n) G_{l-1}(2i+m, 2j+n) \quad (1)$$

However, it is convenient to refer to this



Fig. 2b. Levels of the Gaussian pyramid expanded to the size of the original image. The effects of lowpass filtering are now clearly apparent.

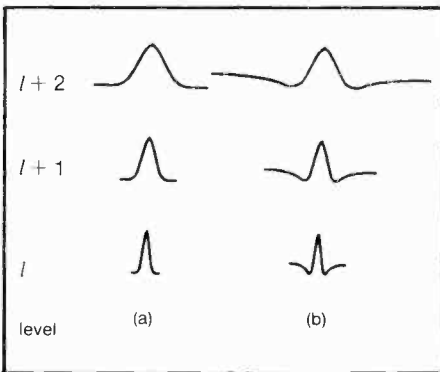


Fig. 3. Equivalent weighting functions. The process of constructing the Gaussian (lowpass) pyramid is equivalent to convolving the original image with a set of Gaussian-like weighting functions, then subsampling, as shown in (a). The weighting functions double in size with each increase in l . The corresponding weighting functions for the Laplacian pyramid resemble the difference of two Gaussians, as shown in (b).

process as a standard REDUCE operation, and simply write

$$G_l = \text{REDUCE} [G_{l-1}].$$

We call the weighting function $w(m,n)$ the "generating kernel." For reasons of computational efficiency this should be small and separable. A five-tap filter was used to generate the pyramid in Fig. 2a.

Pyramid construction is equivalent to convolving the original image with a set of Gaussian-like weighting functions. These "equivalent weighting functions" for three successive pyramid levels are shown in Fig. 3a. Note that the functions double in width with each level. The convolution acts as a lowpass filter with the band limit

reduced correspondingly by one octave with each level. Because of this resemblance to the Gaussian density function we refer to the pyramid of lowpass images as the "Gaussian pyramid."

Bandpass, rather than lowpass, images are required for many purposes. These may be obtained by subtracting each Gaussian (lowpass) pyramid level from the next-lower level in the pyramid. Because these levels differ in their sample density it is necessary to interpolate new sample values between those in a given level before that level is subtracted from the next-lower level. Interpolation can be achieved by reversing the REDUCE process. We call this an EXPAND operation. Let $G_{l,k}$ be the image obtained by expanding G_l k times. Then $G_{l,k} = \text{EXPAND} [G_{l,k-1}]$ or, to be precise, $G_{l,0} = G_l$, and for $k > 0$,

$$G_{l,k}(i,j) = 4 \sum_{mm} G_{l,k-1} \left(\frac{2i+m}{2}, \frac{2j+n}{2} \right) \quad (2)$$

Here only terms for which $(2i+m)/2$ and $(2j+n)/2$ are integers contribute to the sum. The expand operation doubles the size of the image with each iteration, so that $G_{l,1}$ is the size of $G_{l,1}$, and $G_{l,l}$ is the same size as that of the original image. Examples of expanded Gaussian pyramid levels are shown in Fig. 2b.

The levels of the bandpass pyramid, L_0, L_1, \dots, L_N , may now be specified in terms of the lowpass pyramid levels as follows:

$$L_l = G_l - \text{EXPAND} [G_{l+1}] \quad (3)$$

$$= G_l - G_{l+1,1}.$$

The first four levels are shown in Fig. 4a. Just as the value of each node in the

Gaussian pyramid could have been obtained directly by convolving a Gaussian-like equivalent weighting function with the original image, each value of this bandpass pyramid could be obtained by convolving a difference of two Gaussians with the original image. These functions closely resemble the Laplacian operators commonly used in image processing (Fig. 3b). For this reason we refer to the bandpass pyramid as a "Laplacian pyramid."

An important property of the Laplacian pyramid is that it is a complete image representation: the steps used to construct the pyramid may be reversed to recover the original image exactly. The top pyramid level, L_N , is first expanded and added to L_{N-1} to form G_{N-1} ; then this array is expanded and added to L_{N-2} to recover G_{N-2} , and so on. Alternatively, we may write

$$G_0 = \sum L_{ll} \quad (4)$$

The pyramid has been introduced here as a data structure for supporting scaled image analysis. The same structure is well suited for a variety of other image processing tasks. Applications in data compression and graphics, as well as in image analysis, will be described in the following sections. It can be shown that the pyramid-building procedures described here have significant advantages over other approaches to scaled analysis in terms of both computation cost and complexity. The pyramid levels are obtained with fewer steps through repeated REDUCE and EXPAND operations than is possible with the standard FFT. Furthermore, direct convolution with large equivalent weighting functions requires 20- to 30-bit arithmetic to maintain the same ac-

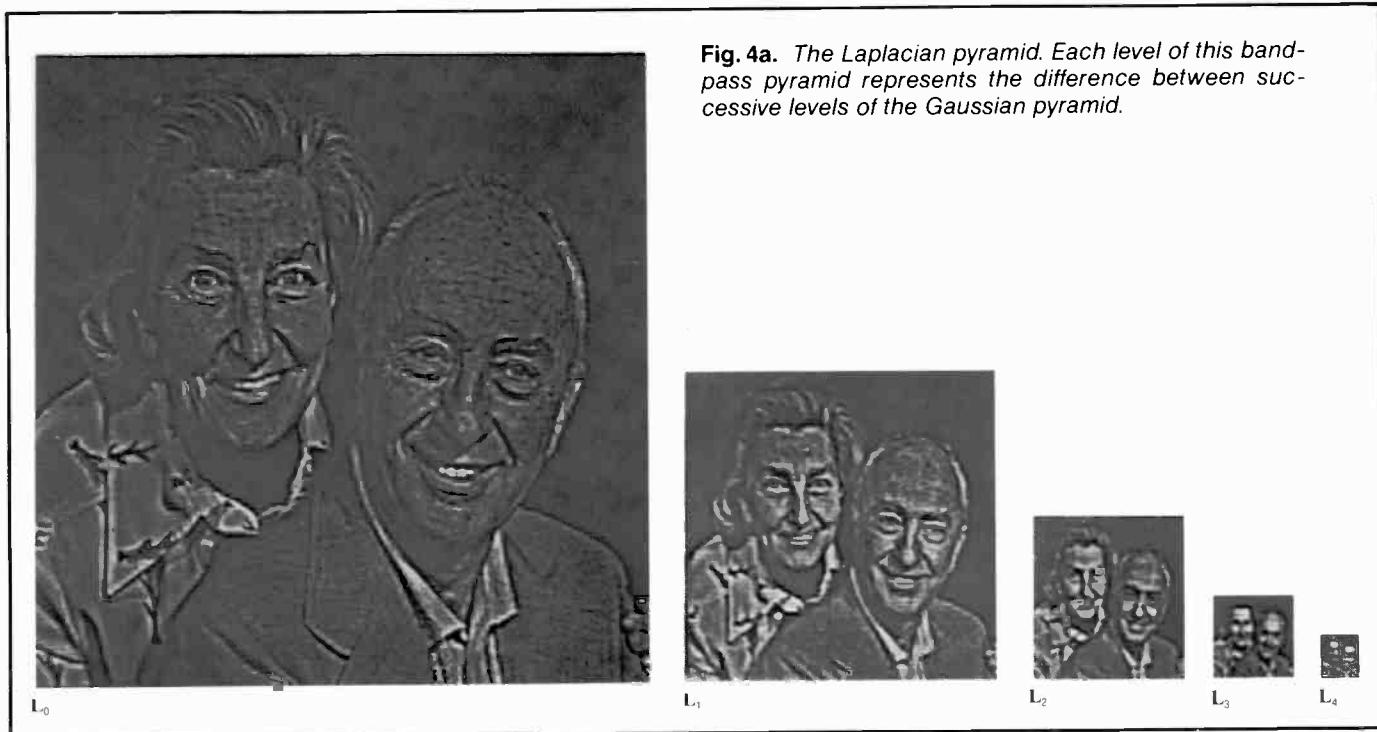


Fig. 4a. *The Laplacian pyramid. Each level of this band-pass pyramid represents the difference between successive levels of the Gaussian pyramid.*



Fig. 4b. *Levels of the Laplacian pyramid expanded to the size of the original image. Note that edge and bar features are enhanced and segregated by size.*

curacy as the cascade of convolutions with the small generating kernel using just 8-bit arithmetic.

A compact code

The Laplacian pyramid has been described as a data structure composed of bandpass copies of an image that is well suited for scaled-image analysis. But the pyramid may also be viewed as an image transformation, or code. The pyramid nodes are then considered code elements, and the equivalent weighting functions are sampling functions that give node values when convolved with the image. Since the original image can be

exactly reconstructed from its pyramid representation (Eq. 4), the pyramid code is complete.

There are two reasons for transforming an image from one representation to another: the transformation may isolate critical components of the image pattern so they are more directly accessible to analysis, or the transformation may place the data in a more compact form so that they can be stored and transmitted more efficiently. The Laplacian pyramid serves both of these objectives. As a bandpass filter, pyramid construction tends to enhance image features, such as edges, which are important for interpretation. These features

are segregated by scale in the various pyramid levels, as shown in Fig. 4. As with the Fourier transform, pyramid code elements represent pattern components that are restricted in the spatial-frequency domain. But unlike the Fourier transform, pyramid code elements are also restricted to local regions in the spatial domain. Spatial as well as spatial-frequency localization can be critical in the analysis of images that contain multiple objects so that code elements will tend to represent characteristics of single objects rather than confound the characteristics of many objects.

The pyramid representation also permits data compression.³ Although it has one



(a)



(b)



(c)

Fig. 5. Pyramid data compression. The original image represented at 8 bits per pixel is shown in (a). The node values of the Laplacian pyramid representation of this image were quantized to obtain effective data rates of 1 b/p and $\frac{1}{2}$ b/p. Reconstructed images (b) and (c) show relatively little degradation.

third more sample elements than the original image, the values of these samples tend to be near zero, and therefore can be represented with a small number of bits. Further data compression can be obtained through quantization: the number of distinct values taken by samples is reduced by binning the existing values. This results in some degradation when the image is reconstructed, but if the quantization bins are carefully chosen, the degradation will not be detectable by human observers and will not affect the performance of analysis algorithms.

Figure 5 illustrates an application of the pyramid to data compression for image transmission. The original image is shown in Fig. 5a. A Laplacian pyramid representation was constructed for this image, then the values were quantized to reduce the effective data rate to just one bit per pixel, then to one-half bit per pixel. Images reconstructed from the quantized data are shown in Figs. 5b and 5c. Humans tend to be more sensitive to errors in low-frequency image components than in high-frequency components. Thus in pyramid compression, nodes at level zero can be quantized more coarsely than those in higher levels. This is fortuitous for compression since three-quarters of the pyramid samples are in the zero level.

Data compression through quantization may also be important in image analysis to reduce the number of bits of precision carried in arithmetic operations. For example, in a study of pyramid-based image motion analysis it was found that data could be reduced to just three bits per sample without noticeably degrading the computed flow field.⁴

These examples suggest that the pyramid is a particularly effective way of representing image information both for transmission and analysis. Salient information is enhanced for analysis, and to the extent that quantization does not degrade analysis, the representation is both compact and robust.

Image analysis

Pyramid methods may be applied to analysis in several ways. Three of these will be outlined here. The first concerns pattern matching and has already been mentioned: to locate a particular target pattern that may occur at any scale within an image, the pattern is convolved with each level of the image pyramid. All levels of the pyramid combined contain just one third more nodes than there are pixels in the original image. Thus the cost of searching for a pattern at many scales is just one third more than that of searching the original image alone.

The complexity of the patterns that may be found in this way is limited by the fact that not all image scales are represented in the pyramid. As defined here, pyramid levels differ in scale by powers of two, or by octave steps in the frequency domain. Power-of-two steps are adequate when the patterns to be located are simple, but complex patterns require a closer match between the scale of the pattern as defined in the target array, and the scale of the pattern as it appears in the image. Variants on the pyramid can easily be defined with squareroot-of-two and smaller steps. However, these not only have more levels, but many more samples, and the computational

cost of image processing based on such pyramids is correspondingly increased.

A second class of operations concerns the estimation of integrated properties within local image regions. For example, a texture may often be characterized by local density or energy measures. Reliable estimates of image motion also require the integration of point estimates of displacement within regions of uniform motion. In such cases early analysis can often be formulated as a three-stage sequence of standard operations. First, an appropriate pattern is convolved with the image (or images, in the case of motion analysis). This selects a particular pattern attribute to be examined in the remaining two stages. Second, a nonlinear intensity transformation is performed on each sample value. Operations may include a simple threshold to detect the presence of the target pattern, a power function to be used in computing texture energy measures, or the product of corresponding samples in two images used in forming correlation measures for motion analysis. Finally the transformed sample values are integrated within local windows to obtain the desired local property measures.

Pattern scale is an important parameter of both the convolution and integration stages. Pyramid-based processing may be employed at each of these stages to facilitate scale selection and to support efficient computation. A flow diagram for this three-stage analysis is given in Fig. 6. Analysis begins with the construction of the pyramid representation of the image. A feature pattern is then convolved with each level of the pyramid (Stage 1), and the resulting correlation values may be passed through

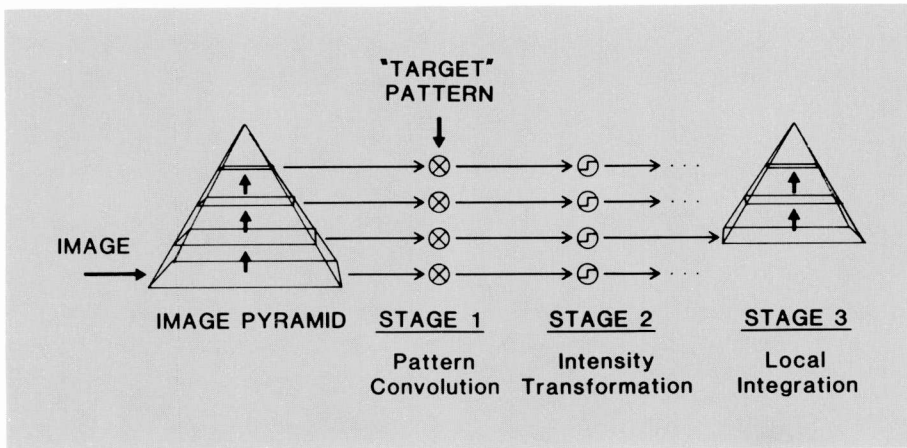


Fig. 6. Efficient procedure for computing integrated image properties at many scales. Each level of the image pyramid is convolved with a pattern to enhance an elementary image characteristic, step 1. Sample values in the filtered image may then be passed through a nonlinear transformation, such as a threshold or power function, step 2. Finally, a new "integration" pyramid is built on each of the processed image pyramid levels, step 3. Node values then represent an average image characteristic integrated within a Gaussian-like window.

a nonlinear intensity transformation (Stage 2). Finally, each filtered and transformed image becomes the bottom level of a new Gaussian pyramid. Pyramid construction has the effect of integrating the input values within a set of Gaussian-like windows of many scales (Stage 3).

As an example, integrated property estimates have been used to locate the boundary between the two textured regions of Fig. 7a. The upper and lower halves of this image show two pieces of wood with differently oriented grain. The right half of the image is covered by a shadow. The boundary between the shaded and unshaded regions is the most prominent feature in the image, and its location can be detected quite easily as the maximum of the gradient of the image intensity (Fig. 7b). However, a simple edge-detecting operation such as this gradient-based procedure cannot be used to locate the boundary between the two pieces of wood. Instead it would isolate the line patterns that make up the wood grain.

The texture boundary can be found through the three-step process as follows: A Laplacian pyramid is constructed for the original texture. The vertical grain is then enhanced by convolving the image with a horizontal gradient operator (Stage 1). Each pyramid node value is then squared, (Stage 2) and a new integration pyramid is constructed for each level of the filtered image pyramid (Stage 3). In this way energy measures are obtained within windows of various sizes. Figure 7c shows level 2 of the integration pyramid for level L_0 of the filtered-image pyramid.

Note that texture differences in the original image have been converted into differences in gray level. Finally, a simple gradient-based edge-detection technique can be used to locate the boundary between image regions, Fig. 7d. (Pyramid levels have been expanded to the size of the original image to facilitate comparison.)

A third class of analysis operations concerns fast coarse-fine search techniques. Suppose we need to locate precisely a large complex pattern within an image. Rather than attempt to convolve the full pattern with the image, the search begins by convolving a reduced-resolution pattern with a reduced-resolution copy of the image. This serves to roughly locate possible occurrences of the target pattern with a minimum of computation. Next, higher-resolution copies of the pattern and image can be used to refine the position estimates through a second convolution. Computation is kept to a minimum by restricting the search to neighborhoods of the points identified at the coarser resolution. The search may proceed through several stages of increased resolution and position refinement. The savings in computation that may be obtained through coarse-fine search can be very substantial, particularly when size and orientation of the target pattern and its position are not known.

Image enhancement

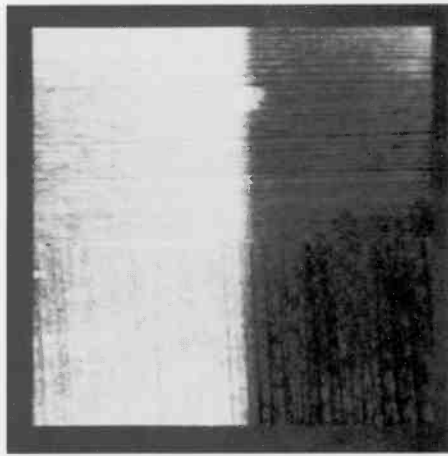
Thus far we have described how pyramid methods may be applied to data compression and image analysis. But there are other areas of image science where these

methods have proved to be useful. For example, a method we call multi-resolution coring may be used to reduce random noise in an image while sharpening details of the image itself.⁵ The image is first decomposed into its Laplacian pyramid (bandpass) representation. The samples in each level are then passed through a coring function where small values (which include most of the noise) are set to zero, while larger values (which include prominent image features) are retained, or "peaked." The final enhanced image is then obtained by summing the levels of the processed pyramid. This technique is illustrated in Fig. 8. Figure 8a is the original image to which random noise has been added, and Fig. 8b shows the image enhanced through multiresolution coring.⁶

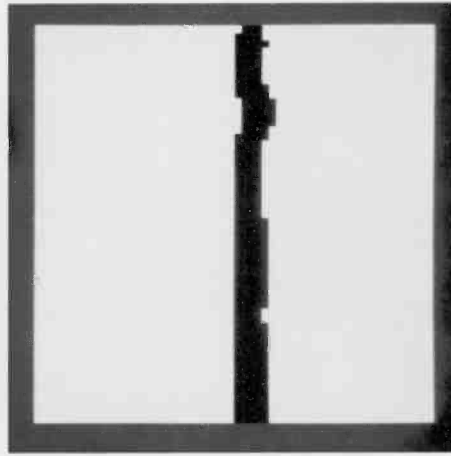
We have recently developed a pyramid-based method for creating photographic images with extended depth of field. We begin with two or more images focused at different distances and combine them in a way that retains the sharp regions of each. As an example, Figs. 9a and 9b show two pictures of a circuit board taken with the camera focused at two different depth-planes. We wish to construct a composite image in which all the components and the board surface are in focus. Let LA and LB be Laplacian pyramids for the two original images in our example. The low-frequency levels of these pyramids should be almost identical because the low spatial-frequency image components are only slightly affected by changes in focus. But changes in focus will affect node values in the pyramid levels where high-spatial-frequency information is encoded. However, corresponding nodes in the two pyramids will generally represent the same feature of the scene and will differ primarily in attenuation due to blur. The node with the largest amplitude will be in the image that is most nearly in focus. Thus, "in focus" image components can be selected node-by-node in the pyramid rather than region-by-region in the original images. A pyramid LC is constructed for the composite image by setting each node equal to the corresponding node in LA or LB that has the larger absolute value:

$$\begin{aligned} & \text{If } |LA_i(i,j)| > |LB_i(i,j)|, \\ & \text{then } LC_i(i,j) = LA_i(i,j) \\ & \text{otherwise, } LC_i(i,j) = LB_i(i,j) \end{aligned} \quad (7)$$

The composite image is then obtained simply by expanding and adding the levels of LC . Figure 9c shows an extended depth-of-field image obtained in this way.



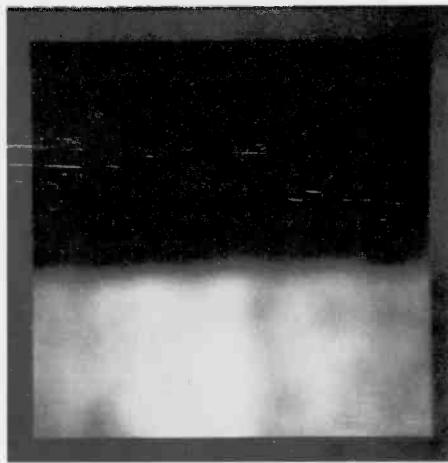
(a)



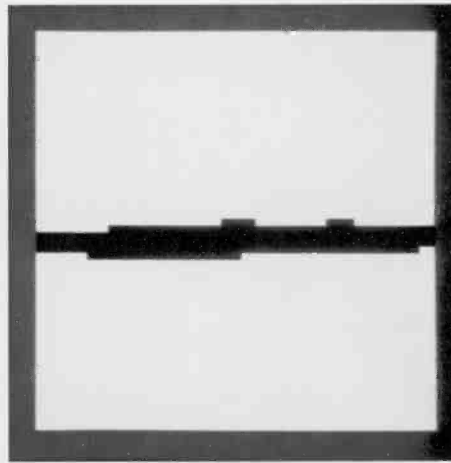
(b)



(a)



(c)



(d)



(b)

Fig. 7. Texture boundary detection using energy measures. The original image, (a), contains two pieces of wood with differently oriented grain separated by a horizontal boundary. The right half of this image is in a shadow, so an attempt to locate edges based on image intensity would isolate the boundary of the shadow region, (b). In order to detect the boundary between the pieces of wood in this image we first convolve each level of its Laplacian pyramid with a pattern that enhances vertical features. At level L_1 , this matches the scale of the texture grain on the lower half of the image. The nodes at this level are squared and integrated (by constructing an additional pyramid) to give the energy image in (c). Finally, an intensity edge-detector applied to the energy image yields the desired texture boundary.

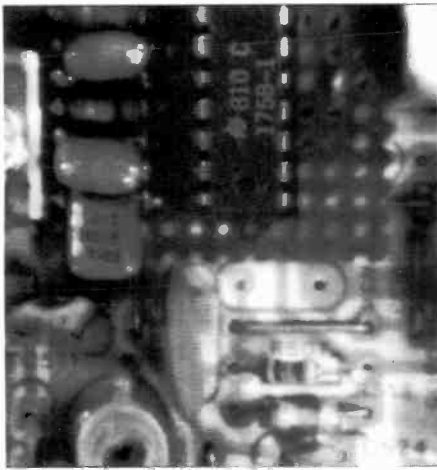
A related application of pyramids concerns the construction of image mosaics. This is a common task in certain scientific fields and in advertising. The objective is to join a number of images smoothly into a larger mosaic so that segment boundaries are not visible. As an example, suppose we wish to join the left half of Fig. 10a with the right half of Fig. 10b. The most direct method for combining the images is to catenate the left portion of Fig. 10a with the right portion of Fig. 10b. The result, shown in Fig. 10c, is a mosaic in which the boundary is clearly visible as a sharp (though generally low-contrast) step in gray level.

An alternative approach is to join image components smoothly by averaging pixel values within a transition zone centered on the join line. The width of the transition zone is then a critical parameter. If it is too narrow, the transition will still be visible as a somewhat blurred step. If it is too wide, features from both images will be visible within the transition zone as in a photographic double exposure. The blurred-edge effect is due to a mismatch of low frequencies along the mosaic boundary, while the double-exposure effect is due to a mismatch in high frequencies. In general, there is no choice of transition zone width that can avoid both defects.

Fig. 8. Multiresolution coring. Part (a) shows an image to which noise has been added to simulate transmission degradation. The Laplacian pyramid was constructed for this noisy image, and node values at each level were "cored." As a result, much of the noise is removed while prominent features of the original image are retained in the reconstructed image, (b).

This dilemma can be resolved if each image is first decomposed into a set of spatial-frequency bands. Then a bandpass mosaic can be constructed in each band by use of a transition zone that is comparable in width to the wavelengths represented in the band. The final mosaic is then obtained by summing the component band-pass mosaics.

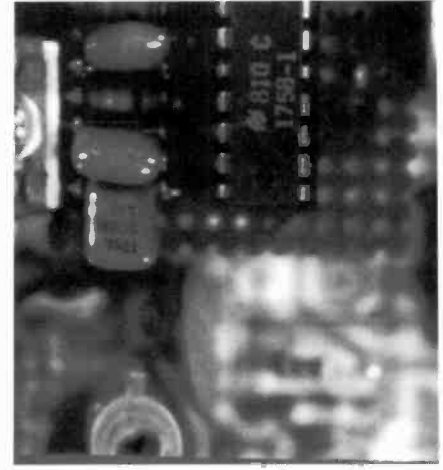
The computational steps in this "multiresolution splining" procedure are quite simple when pyramid methods are used.⁶ To begin, Laplacian pyramids LA and LB are constructed for the two original images. These decompose the images into the required spatial-frequency bands. Let P be the



(a)

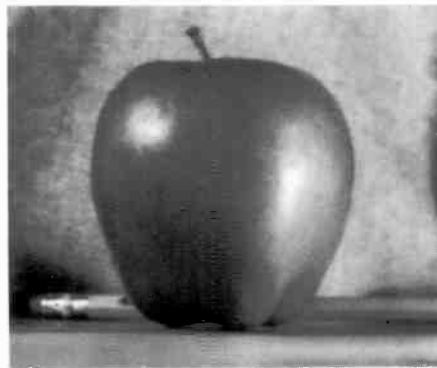


(b)



(c)

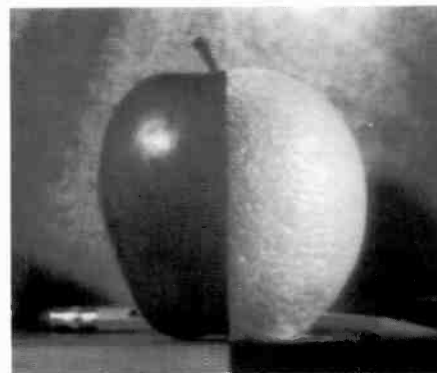
Fig. 9. Multifocus composite image. The original images with limited depth of field are shown in (a) and (b). These are combined digitally to give the image with an extended depth of field in (c).



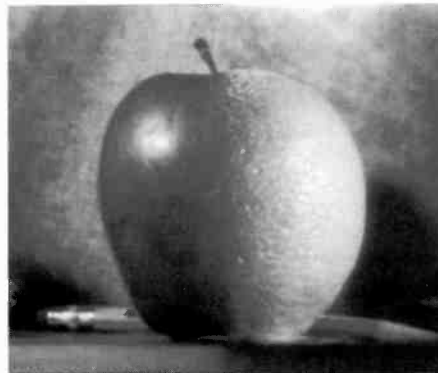
(a)



(b)



(c)



(d)

Fig. 10. Image mosaics. The left half of image (a) is catinated with the right half of image (b) to give the mosaic in (c). Note that the boundary between regions is clearly visible. The mosaic in (d) was obtained by combining images separately in each spatial frequency band of their pyramid representations then expanding and summing these bandpass mosaics.

locus of image points that fall on the boundary line, and let R be the region to the left of P that is to be taken from the left image. Then the pyramid LC for the composite image is defined as:

If the sample is in R , then

$$LC_l(i,j) = LA_l(i,j)$$

If the sample is in P , then

$$LC_l(i,j) = LB_l(i,j),$$

Otherwise,

$$LC_l = LC_l(i,j) \quad (8)$$

The levels of LC are then expanded and

summed to yield the final mosaic, Fig. 10d. Note that it is not necessary to average node values within an extended transition zone since this blending occurs automatically as part of the reconstruction process.

Conclusions

The pyramid offers a useful image representation for a number of tasks. It is efficient to compute; indeed pyramid filtering is faster than the equivalent filtering done with a fast Fourier transform. The information is also available in a format that is convenient to use, since the nodes in each level represent information that is localized in both space and spatial frequency.

We have discussed a number of examples in which the pyramid has proven to be valuable. Substantial data compression (similar to that obtainable with transform methods) can be achieved by pyramid encoding combined with quantization and entropy coding. Tasks such as texture analysis can be done rapidly and simultaneously at all scales. Several different images can be combined to form a seamless mosaic, or several images of the same scene with different planes of focus can be combined to form a single sharply focused image.

Because the pyramid is useful in so many tasks, we believe that it can bring some conceptual unification to the problems of representing and manipulating low-level visual information. It offers a flexible, convenient multiresolution format that matches the multiple scales found in the visual scenes and mirrors the multiple scales of processing in the human visual system.

References

1. H. Wilson and J. Bergen, "A four mechanism model for threshold spacial vision", *Vision Research*, Vol. 19, pp.19-31, 1979.

2. C. Anderson, "An alternative to the Burt pyramid algorithm", memo in preparation.
3. P. Burt and E. Adelson, "The Laplacian Pyramid as a Compact Image Code," *IEEE Transactions on Communication*, COM-31, pp. 532-540, 1983a.

4. P. Burt, X. Xu and C. Yen, "Multi-Resolution Flow-Through Motion Analysis," RCA Technical Report, PRRL-84-TR-009, 1984.
5. J. Ogden and E. Adelson, "Computer Simulations of

Oriented Multiple Spatial Frequency Band Coring," in preparation, 1984.

6. P. Burt and E. Adelson, "A Multiresolution Spline with Application to Image Mosaics," *ACM Transactions on Graphics*, Vol. 2, pp. 217-236, 1983b.



Authors, left to right: Bergen, Anderson, Adelson, Burt.



Joan Ogden received a B.S. in Mathematics from the University of Illinois, Champaign-Urbana in 1970, and a Ph.D. in Physics from the University of Maryland in 1977. Coming to the Princeton Plasma Physics laboratory as a Post-Doctoral research associate, she continued her work in nuclear fusion, specializing in plasma theory and simulation. In 1980, she started her own consulting company, working on a variety of applied physics problems. In December 1982, she began working with the Advanced Image Processing Research Group, and has recently joined RCA as a part-time Member of the Technical Staff. Her research interests at RCA include applications of the pyramid algorithm to problems of noise reduction, data compression, and texture generation.

Contact her at:
RCA Laboratories
Princeton, N.J.

Edward H. Adelson received a B.A. degree, summa cum laude, in Physics and Philosophy from Yale University in 1974, and a Ph.D. degree in Experimental Psychology from the University of Michigan in 1979. His dissertation dealt with temporal properties of the photoreceptors in the human eye. From 1979 to 1981 Dr. Adelson did research on human motion perception and on digital image processing as a Postdoctoral Fellow at New York University. Dr. Adelson joined RCA Laboratories in 1981 as a Member of the Technical Staff. As part of the Advanced Image Processing Research group in the Advanced Video Systems Research Laboratory, he has been involved in developing models of the human visual system, as well as image-processing algorithms for image enhancement and data compression.

Dr. Adelson has published a dozen papers on vision and image processing, and has made numerous conference presentations. His awards include the Optical Society of America's Adolph Lomb medal (1984), and an RCA Laboratories Outstanding Achievement Award (1983). He is a member of the Association for Research in Vision and Ophthalmology, the Optical Society of America, and Phi Beta Kappa.

Contact him at:
RCA Laboratories
Princeton, N.J.
Tacnet: 226-3036

Peter J. Burt received the B.A. degree in Physics from Harvard University in 1968, and the M.S. degree from the University of Massachusetts, Amherst, in 1974 and 1976, respectively. From 1968 to 1972 he conducted research in sonar, particularly in acoustic imaging devices, at the U.S. Navy Underwater Systems Center, New London, Conn. and in London, England. As a Postdoctoral Fellow, he has studied both natural vision and computer image under-

standing at New York University (1976-1978), Bell Laboratories (1978-1979), and the University of Maryland (1979-1980). He was a member of the engineering faculty at Rensselaer Polytechnic Institute from 1980 to 1983. In 1983 he joined RCA David Sarnoff Research Center as a Member of the Technical Staff, and in 1984 he became head of the Advanced Image Processing Group.

Contact him at:
RCA Laboratories
Princeton, N.J.
Tacnet: 226-2451

Charles H. Anderson received B.S. degree in Physics at the California Institute of Technology in 1957, and a Ph. D. from Harvard University in 1962. Dr. Anderson joined the staff of RCA Laboratories, Princeton, NJ, in 1963. His work has involved studies of the optical and microwave properties of rare-earth ions in solids. These studies have produced an optically-pumped microwave maser and a new spectrometer for acoustic radiation in the 10-to 300-GHz range. In 1971 he was awarded an RCA fellowship to do research at Oxford University for a year, and in 1972 became a Fellow of the American Physical Society. Upon returning to RCA, he became involved in new television displays. Between 1973 and 1978 he was a leader of a subgroup developing electron-beam guides for flat-panel television displays. In March 1977 he was appointed a Fellow of the Technical Staff of RCA Laboratories.

From August 1978 through December 1982 he was head of the Applied Mathematical and Physical Sciences group. In January 1983 he returned full time to research as a member of the Vision Group, while maintaining a role as a task force leader in studies of the stylus/disc interface. In January 1984 he spent 5 weeks as a Regents Lecturer at the invitation of the Physics Department of UCLA. This was

did research into and developed a model of the structure of the primate visual system from the retina to the striate cortex. Research was also done on the Hopfield model of associative memory.

Contact him at:
RCA Laboratories
Princeton, N.J.
Tacnet: 226-2901

James R. Bergen received the B.A. degree in Mathematics and Psychology from the University of California, Berkeley, in 1975, and the Ph.D. in Biophysics and Theoretical Biology from the University of Chicago in 1981. His work concerns the quantitative analysis of information processing in the human visual system. At the University of Chicago he was involved in the development of a model of the spatial and temporal processing that occurs in the early stages of the system. From 1981 to 1982 he was with Bell Laboratories, Murray Hill, N.J. His work concentrates on the effect of visual system structure on the extraction of information from a visual image. His current work includes basic studies of visual perception as well as perceptual considerations for design of imaging systems.

Contact him at:
RCA Laboratories
Princeton, N.J.
Tacnet: 226-3003

Real-time dynamic range compression of electronic images

Developed at Automated Systems, Burlington, this technique is expected to find application in autonomous processors for pattern recognition and display systems.

A common problem with IR imaging systems using CRTs for displays is that the dynamic range of the thermal images far exceeds that of the display system. The dynamic range of typical TV display systems is about 40 dB (100 : 1), whereas the dynamic range of typical IR scenes can be 10 to 100 times greater. The dynamic range capability of the Schottky Barrier IR focal plane array (FPA) sensor, for which a real-time processor has been developed,¹ is greater than 10,000 : 1. If the dynamic range of the video signal from the IR FPA sensor is simply linearly attenuated to fit the dynamic range capability of the display system, then some scene detail is attenuated below the contrast threshold of the observer and is lost.

The basic approach used for design of the real-time processor is shown in Fig. 1. It consists of cascading a two-dimensional high-pass filter with a histogram equalizer. The use of the high-pass filter is based upon the ability of the eye to spatially

integrate energy from pixels comprising large objects. Therefore, these large objects can be compressed relative to small objects. However, when the high-amplitude, low-frequency content of an IR image is removed by linear filtering, the image still is not suitable for display because it contains high-amplitude residual "spikes" corresponding to edge transitions of large objects. However, since these spikes originate from edges of large objects, they occur rather rarely in the processed image. A histogram of the pixel amplitudes would show low probability for large edge spikes.

The histogram equalizer shown in Fig. 1 has a two-fold purpose:

1. Compression of large-object edge spikes that are residual from the high-pass filter operation.

2. Expansion of image detail at levels at which detail is concentrated.

Histogram equalization has been shown by others to yield excellent expansion of image detail within the constraints of limited dynamic range.² However, since it operates on the basis of probability of occurrence, a small object within a given field-of-view can ordinarily be de-emphasized if its detail lies at an infrequently occurring level. This limitation can be minimized by preceding the histogram process with a high-pass filter, as shown in Fig. 1. Thus, the high-pass filter and histogram equalizer complement each other to provide a powerful processor design approach.

Performance of this dynamic range compressor is determined by the content of the image and by key design parameters such as

Abstract: *For both human display and automatic interpretation of electronic imagery, there is a need to appropriately compress the very large dynamic range of high-quality sensors. A real-time processor for use with IR sensors has been designed and successfully demonstrated.*

©1984 RCA Corporation
Final manuscript received September 14, 1984
Reprint Re-29-6-6

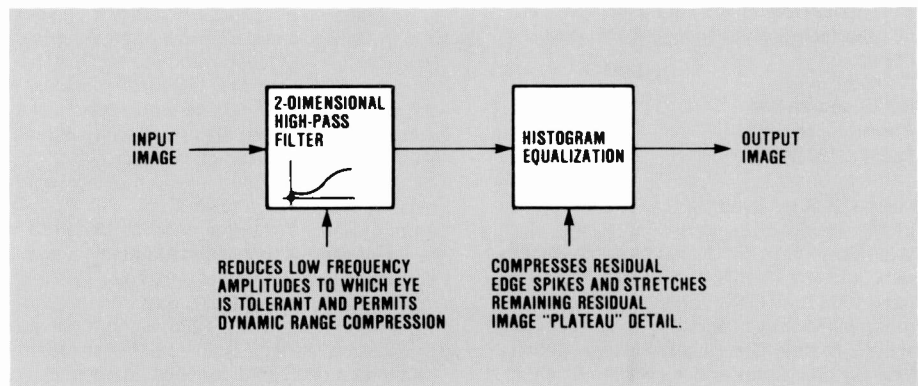


Fig. 1. Real-time image processor concept.

the high-pass filter peaking ratio and the number of image quantization levels used in the histogram equalizer.

With a 10 : 1 high-pass filter peaking ratio and eight levels of histogram quantization, a compression range on the order of 80:1 has been demonstrated with typical IR images.

Two-dimensional high-pass filter

A wide variety of two-dimensional high-pass linear filters can be designed. The type chosen for establishing the feasibility of the real-time processor described in this paper is depicted in Fig. 2. It contains delay lines to provide a 3×3 -element kernel of two-dimensional sample points. The short delays were implemented with L-C elements, and the long (1-H) delays were implemented with CCD shift registers.

The step and frequency responses are also shown in Fig. 2. The peaking level compared to the DC response is defined as the peaking ratio, and can be expressed as:

$$\text{Peaking Ratio} = 1 + \frac{4a}{b} \quad (1)$$

In the setup of the processor, this ratio can be adjusted for a compromise between the suppression of DC response and the residual undershoots and overshoots at image edges. Optimization of this adjustment depends on image content and on the histogram equalizer parameters.

The magnitude of the frequency response of the filter in the horizontal direction for a single-element delay (T) is:

$$H(\omega) = b + 2a(1 - \cos \omega T) \quad (2)$$

This filter has a linear phase function corresponding to the delay period.

Histogram equalization processor

Design principles

Histogram equalization processing of an image statistically compresses the image by attenuating those gray level ranges with in it that occur infrequently, while stretching those that occur frequently. This fully utilizes the output dynamic range. Histogram equalization is a type of non-linear point-to-point mapping of pixel gray levels such that the histogram (or probability density function, for continuous signals) of the gray levels of the processed image is uniform.²

Since all gray levels of the processed

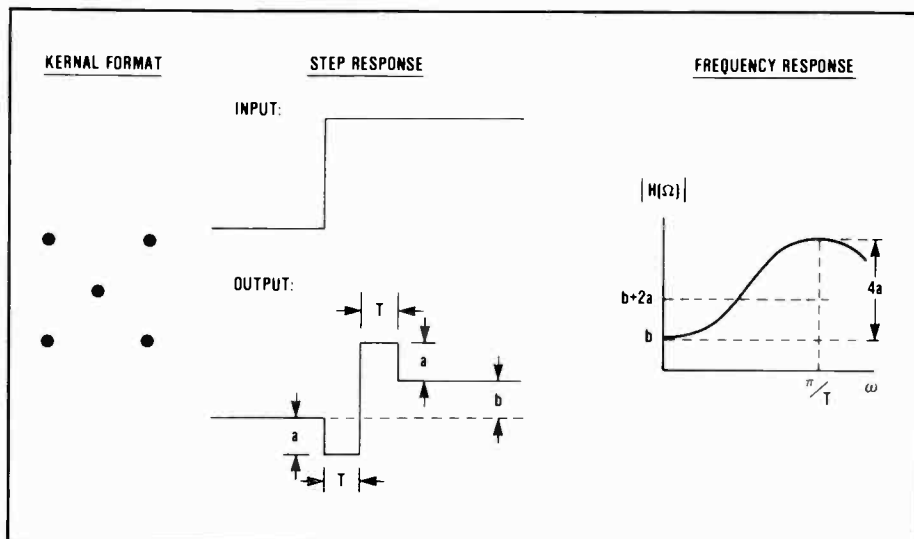


Fig. 2. Two-dimensional high-pass filter.

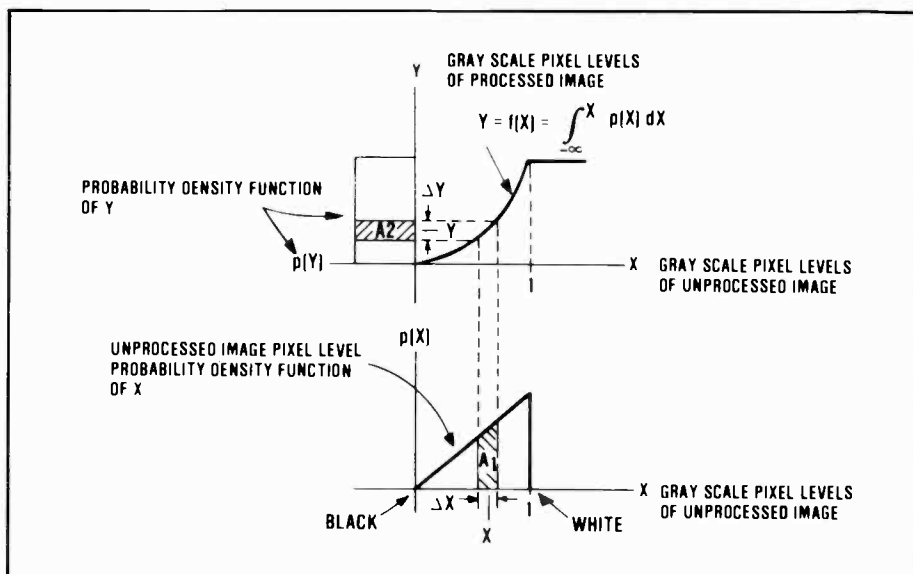


Fig. 3. Transformation between unprocessed and processed pixel levels.

image are equi-probable, each has a minimum associated probability and a maximum associated information content because

$$\text{INFO} = \log_2 \frac{1}{p(\text{GRAY LEVEL})} \text{ bits} \quad (3)$$

The required non-linear transformation between the unprocessed image pixel gray level x , and the processed image gray level y can be derived by referring to Fig. 3. In the unprocessed image, as often as pixel levels occur in the range ΔX , the pixel levels of the processed image will be found in the range ΔY . Area A_1 is therefore equal to A_2

$$A_1 = A_2 \quad (4)$$

but

$$A_1 = p(X) \Delta X$$

$$A_2 = p(Y) \Delta Y$$

and in the limit

$$p(Y) \Delta Y = p(X) \Delta X \quad (5)$$

$$p(Y) dY = p(X) dX$$

If we demand that the probability density of the processed image pixel levels be constant, then

$$p(Y) = 1 \quad (6)$$

and (3) becomes

$$dY = p(X) dX \quad (7)$$

or

$$Y = f(X) = \int_{-\alpha}^x p(X) dX \quad (8)$$

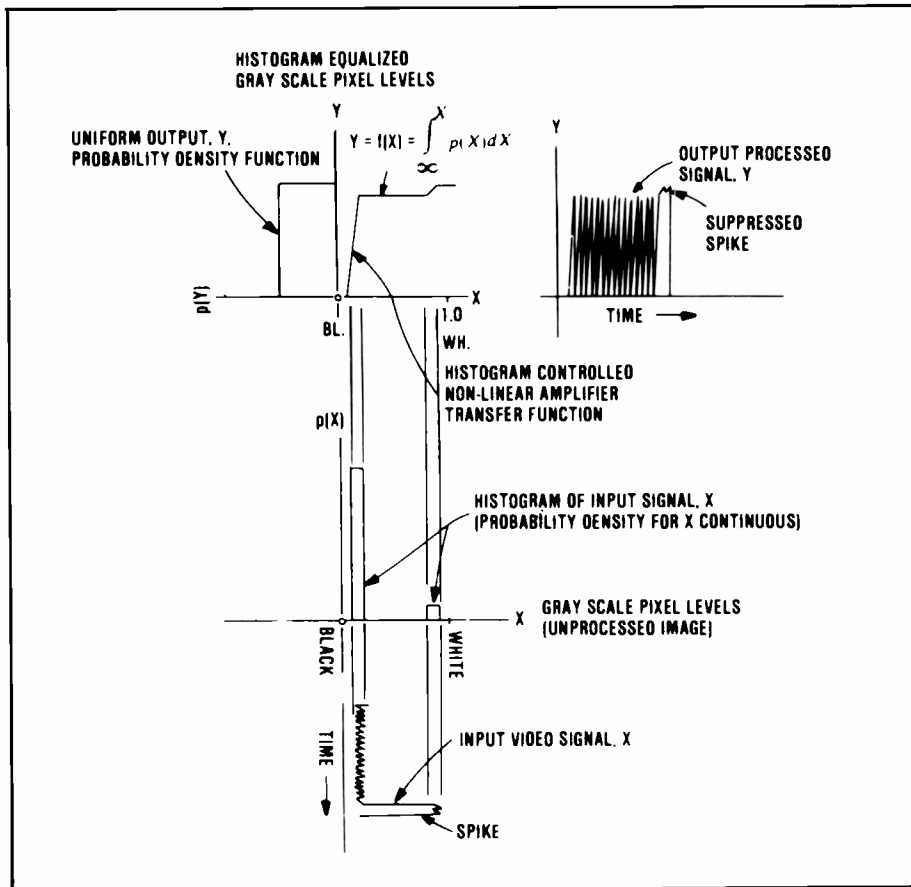


Fig. 4. Example of histogram equalization processing.

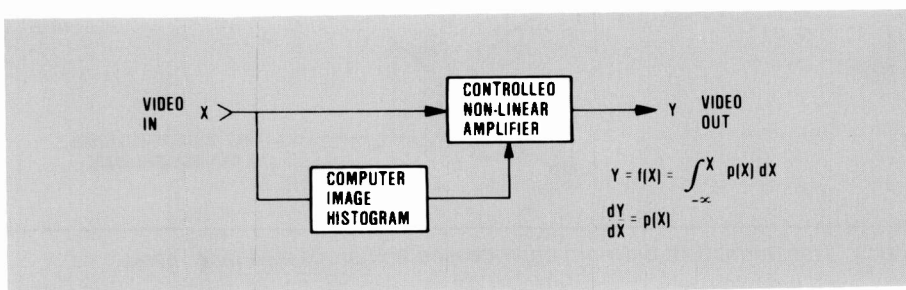


Fig. 5. Block diagram for the real-time histogram equalization processor.

From Eq. (8) the non-linear transformation between X and Y that gives a uniform probability density for the processed image is the cumulative distribution function of X .

Figure 4 is an example of histogram equalization processing. The input signal X is drawn to have approximately the probability density function shown. Examination of this figure reveals the following:

- High transfer gain between X and Y occurs in those ranges of X that have high probability;
- Low transfer gain between X and Y occurs in those ranges of X that have low probability.

In other words, pixel-length ranges that stretched, while those that occur infrequently will be compressed. If certain ranges of input pixel-levels do not occur at all, they will be completely eliminated from the output.

Hardware Implementation

The histogram equalization processor³ consists essentially of a non-linear amplifier through which the input pixel amplitudes are passed in order to generate the output pixel amplitudes. In order for the output-pixel amplitudes to be equally probable, the non-linearity of the amplifier must be controlled by the image histogram. Specif-

ically, the transfer function must be the cumulative distribution function of the image histogram (probability density function for continuous variables). A block diagram for the histogram equalization processor is shown in Fig. 5.

Since the output Y is related to the input X by

$$Y = \int_{-\infty}^X p(X) dX \quad (9)$$

then,

$$\frac{dY}{dX} = p(X) \quad (10)$$

Equation (10) can be interpreted as stating that the incremental transfer gain at any input pixel-level is equal to the probability of finding the pixel level at that particular level.

The IR histogram equalization processor implemented approximates Equation (10) by establishing eight amplitude bands and setting the band incremental gain proportional to the duration of the video signal within the band. A larger number of bands approximates Equation (10) more closely, and increases the dynamic range compression capability, but with increased circuit complexity. Signals are integrated for a frame time to generate the pixel probability density functions. In the present frame, the non-linearity of the amplifier is controlled by the probability density function determined from the previous frame, while the probability density function for the next frame is being generated. Since there is only a single-frame lag, the computation is a very accurate, real-time estimate of the image histogram.

The histogram-controlled non-linear amplifier uses level-clamped emitter followers driving operational transconductance amplifiers (OTA). As the input video linearly traverses upward through each band, the associated OTA supplies output current proportional to its transconductance, which is set by the corresponding probability density function voltage. Summation of all of these currents in the output transimpedance amplifier results in an output voltage that approximates the cumulative density function as required.

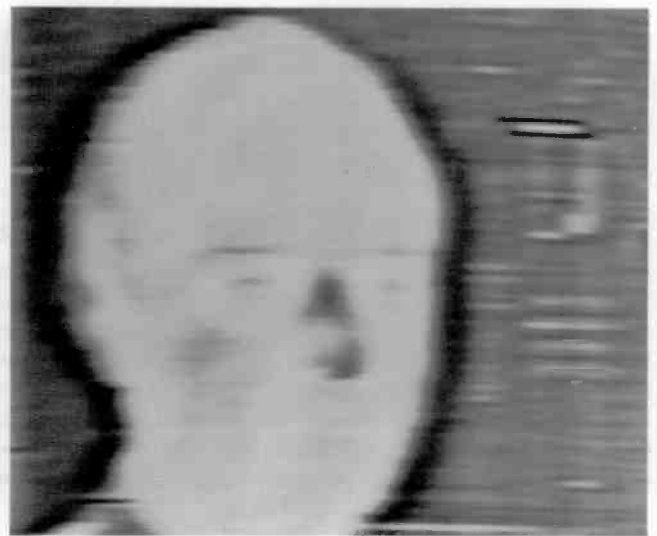
Performance

The ratio of image compression achievable is a function of the scene content, the high-pass filter peaking ratio, and the number of histogram equalizer quantization-levels.

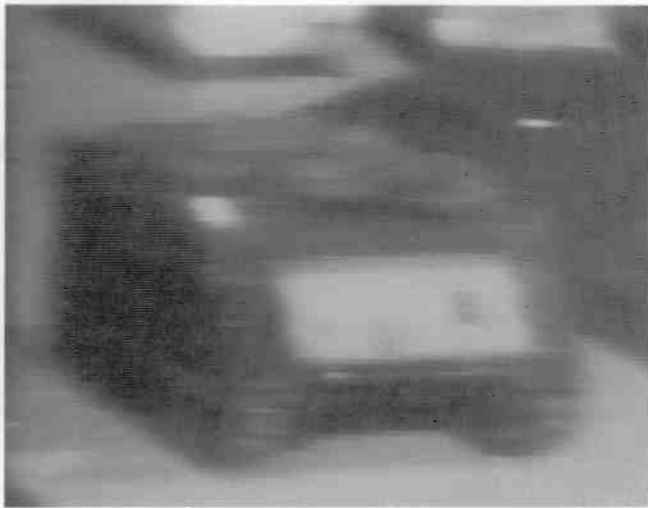
Usually, IR-imagery has a highly non-uniform gray-scale histogram, the signal



(a)



(b)



(c)



(d)

Fig. 6. Images from an IR CCD camera.

typically being characterized by low amplitude video information riding on high-level DC plateaus. In this instance, if the compression ratio is defined as

Compression ratio =

Output peak-to-peak signal as a percentage of processor output voltage range

Input peak-to-peak signal as of a percentage of processor input voltage range

then the compression ratio can approach the product of the filter peaking ratio and histogram quantization levels. The processor was implemented with a filter peaking ratio of ten and with eight histogram quantization levels. This provides a combined image-compression ratio of 80.

Figure 6 shows two IR images from an IR CCD camera (using a 64×128 Schottky barrier focal plane array sensor) processed with this real time circuit. Enhanced image detail is evident in the pro-



Donald Dion received his BSEE from the University of Maine, and became associated with RCA in 1951. His experience includes work

as an inductive component design engineer, and logic design on automatic test equipment. From 1963 to 1984 Don worked in the Electro-Optical group, where his work included statistical analysis of the low contrast performance of television image tubes, circuit design on IR and high resolution TV cameras for ground and airborne applications, and implementation of techniques for detecting standing bowling pins by digitally processing the sensing TV camera output. Recently, in the IR field, he has been involved with IR focal plane arrays, where his work has centered on performance analysis, sampling effects, and techniques to enhance performance. He has five U.S. Patents.

Contact him at:
RCA Automated Systems
Burlington, Mass
Tacnet: 326-5055

cessed images. Note, in the example of the facial image, that not only are facial features enhanced but an IR differential temperature source (to the right of the face) at room temperature is also greatly enhanced. In the example of the tank image, relatively small differential temperature detail in both the tank and surrounding terrain are highly enhanced.

The test results obtained thus far have established the basic feasibility of the real-time processing technique described in this paper. In the future, performance improvements are anticipated through optimization of the number of quantization levels and of the weighting factors and peaking ratio

used in the high-pass filter. This processor is expected to find application in display systems and in autonomous processors for pattern recognition.

Acknowledgements

Michael Cantella is a former RCA Senior Engineering Scientist. The authors wish to express their appreciation to their coworkers at RCA Corporation for sponsorship of this effort and for design and fabrication of the IR camera instrumentation used in the test. They are particularly grateful to Dr. Harvey Waldman, RCA Laboratories for

his processor computer simulation, which enabled effective optimization of hardware parameters.

References

1. W.F. Kosonocky, H.G. Erhardt, G.M. Meary, F.V. Shallcross, H.A. Elabd, M.J. Cantella, J. Klein, L.H. Skochnik, B.R. Capone, R.W. Taylor, W. Ewing, F.D. Shepherd, S.A. Roosild, "Advances in Platinum-Silicide Schottky-Barrier IR-CCD Image Sensors," *SPIE*, Vol. 225, IR-Image Sensor Technol. (1980), pp. 69-71.
2. R.C. Gonzalez and Paul Wintz, "Digital Image Processing," Addison-Wesley, 1977.
3. M.J. Cantella and D.F. Dion, "A Real-Time Histogram Equalization Processor for Dynamic Range Compression of IR Images," *Proc. IEEE NAECON*, May 1984.

September issue of *RCA Review* available

RCA Review is a technical journal published quarterly by RCA Laboratories in conjunction with the subsidiaries and divisions of RCA Corporation. A one-year subscription to *RCA Review* costs \$12.00, and back issues are \$5.00 (employees get a 20 percent discount); reprints of individual papers are generally available from the authors.

Contents, September 1984

Adherence of Phosphor Screens

S. Larach and J. E. McGowan

Operating Mechanism of the One-Piece Cathode

K. T. Chiang and J. J. Maley

A Contour Deformation Model of Capacitance

VideoDisc Signal Pickup

P. D. Southgate

Some Applications of z-Transforms and State Variables to Feedback Shift Registers

Harry Urkowitz

Image Formation in Contact-Printed PMMA Resist Sublayers

L. K. White and D. Meyerhofer

An Analytical Study of the Winding Harmonics of a Saddle Deflection Coil

Basab B. Dasgupta

Extending the Content and Expanding the Usefulness of the Simple Gaussian Lens Equations—Part 3-B

L. T. Sachtleben

Development of multispectral detector technology

RCA is developing all-solid-state sensor technology aimed toward the next generation of Earth resources instruments.

Since the advent of the artificial earth satellite, considerable interest has developed in the remote sensing of the Earth's surface and its resources. An early impetus for this work came from a need to identify acceptable landing sites for the lunar landing program. Not enough was known about the lunar surface structure. Techniques for determining that structure from lunar orbit had to be verified. To do this, desert sites whose geological surface features were thought to be similar to the lunar surface were selected. Optical instrumentation installed in Earth satellites, and the data processing techniques to be used on data obtained from these instruments, could now be tested against known ground structures. Out of this work came an appreciation for the wealth of geologic information available from orbiting optical platforms. The Earth observation program soon broadened to include test sites for agriculture, geography, geology, forestry and mineral resources, hydrology and water resources, oceanography and marine resources, and urban and regional studies.

Abstract: *High-performance, high-density visible and shortwave infrared sensor technology is being developed. Linear arrays currently under development will provide future Earth resources instruments with unprecedented operational flexibility and significantly improved performance.*

© 1984 RCA Corporation
Final manuscript received October 30, 1984
Reprint Re-29-6-7

With the utility of remote sensing satellites demonstrated, an operational system was initiated in the early 1970s. The first Landsat satellites provided radiometrically accurate (calibrated) imagery of the Earth, but in a limited number of visible wavelength spectral channels. Today, the state-of-the-art spaceborne instrument is the Thematic Mapper (TM). This instrument views the Earth's surface in the visible, near-infrared (near-IR), shortwave-IR (SWIR), and thermal-IR (TIR) spectral regions. The visible, near-IR and shortwave-IR spectral channels provide data on the reflectivity of features and vegetation on the Earth's surface. Due to the absolute calibration of the instrument, this data may be used to identify mineral deposits, assess land usage, and predict crop yields, to name just a few applications. As an example of spectral classification, Fig. 2 shows the TM spectral bands 1 through 6 against the reflectance data of sandstone, shale, and green vegetation. Since each spectral channel of the instrument is coregistered spatially, a determination of the ground covering (e.g., sandstone vs. shale) may easily be determined by comparing TM image data to catalogued reflectance data such as that shown in Fig. 2.

The next generation instrument

The TM produces image data employing the 'whiskbroom' scanning principle and a small number of discrete detectors (approximately 30 detectors in each wavelength).

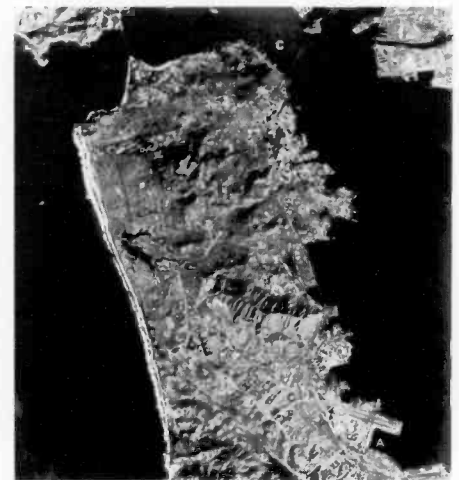


Fig. 1. LANDSAT image of San Francisco.

The whiskbroom approach calls for an oscillating mirror to 'paint' each detector's field-of-view across the entire spacecraft field-of-view (crosstrack). A next generation instrument concept, the Multispectral Linear Array (MLA) shown in Fig. 3, calls for up to 12,000 detectors in each of four visible and near-IR bands, and two SWIR bands (1 to 2.5 μm). The role of the scanning mirror (Fig. 4) is eliminated by this 'pushbroom' scanning approach, since the full field-of-view may be simultaneously acquired with the 12,000 detectors with comparable or better spatial resolution (Fig. 5). With the pushbroom approach, the only scan motion is the forward motion of the spacecraft, with each detector integrating the reflected light from the

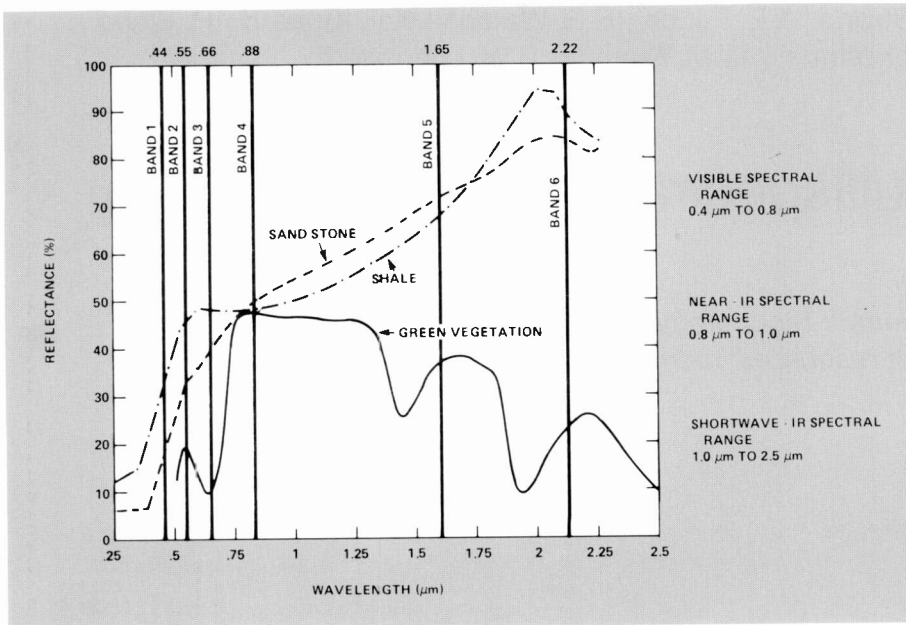


Fig. 2. Spectral reflectances of two rock types and typical green vegetation.

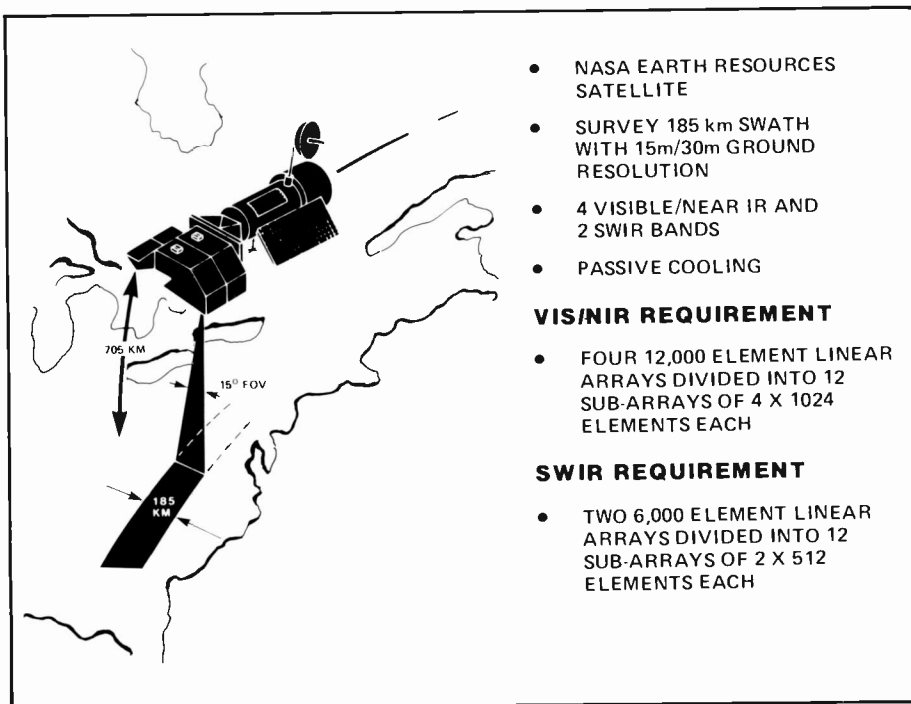


Fig. 3. Multispectral linear array instrument concept.

Earth's surface for the entire line time. This approach thereby provides a 12,000/30, or 400-fold, increase in the dwell time of each detector footprint on the ground. This increase in the dwell time corresponds to an increase in signal intensity, which may be used to simultaneously provide improved signal-to-noise performance, higher spatial resolution, and higher spectral resolution. It is toward this promise of improved system performance that RCA has been funded by NASA God-

dard Space Flight Center to develop new, state-of-the-art focal plane technology.

RCA development efforts

The sensor research at RCA is organized into two programs: VIS/NIR, with four sensor lines covering the visible and near-infrared portion of the spectrum, and SWIR, with two lines of sensors for detection in the shortwave infrared. In the MLA system, all six cross-track sensor lines would

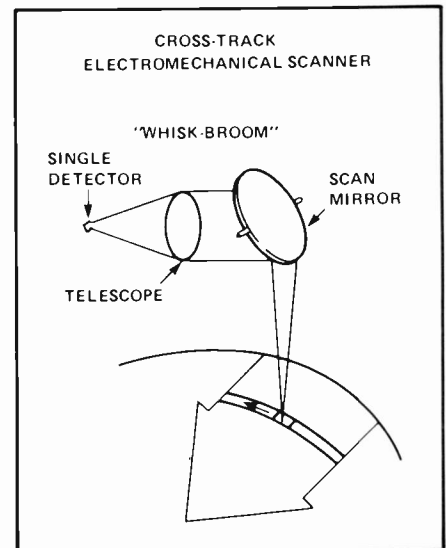


Fig. 4. Whiskbroom electromechanical scanner principle.

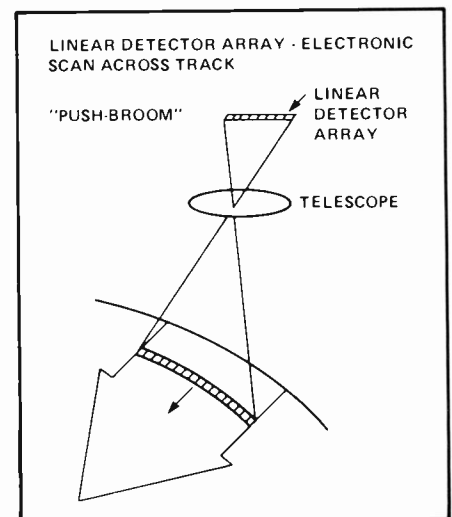


Fig. 5. Pushbroom electronic scanner principle.

be simultaneously exposed to the optical input image, with their integration time and readout rate dependent on the forward velocity of the satellite.

To provide the capability to increase the length of the sensor lines to a larger number of pixels (detectors) than can be practically manufactured on a single integrated circuit chip, both the VIS/NIR and SWIR devices have been designed to be edge-butable, with no more than a two-pixel loss at each joint. The VIS/NIR device is a frame-transfer charge-coupled device (CCD) imager using silicon photocapacitors as the sensor elements. The SWIR device is an interline CCD structure using Schottky-barrier, palladium-silicide diode sensor elements.

The current effort involves the devel-

opment of VIS/NIR and SWIR devices, along with bandpass filters, and precision micro-packaging techniques. The development work is being conducted at four RCA locations: the Advanced Technology Laboratories (prime contractors), the David Sarnoff Research Center, the New Products Division, and the Missile and Surface Radar Division Hybrid Laboratory. Each has a significant portion of the development work.

Visible and near-infrared sensor

Visible imager technology

Over the past ten years, rapid strides have been made in applying CCD technology to electronic imaging, first as line arrays and later as raster area structures. Full TV imaging capabilities competitive with camera tubes have been widely reported by US and Japanese electronic companies. Noteworthy progress has been made not only in providing a significant increase in the number of small-area pixels (e.g., $15 \times 15 \mu\text{m}$) in the raster (typically 400 or more horizontal elements and 500 vertical elements, with interlace operation), but also in reducing the charge transfer loss, ϵ , to less than or equal to 10^{-5} per transfer, which allows several thousand transfers to be made without significant modulation transfer function (MTF) degradation.

Sensitivity has been improved by increasing the sensing area of the raster to nearly 100 percent, and by reducing the attenuation of the input light transmitted through the structural layers of the device. Loss of resolution because of carrier diffusion has been reduced by limiting the active substrate region by fully depleting either a thin substrate or an epitaxial layer. Image blooming in regions of input overloads has been controlled by a variety of structural additions or modifications. Low-light imaging has been improved by reducing the input capacitance of the on-chip amplifier to approximately 0.03 pF, and improvements in output signal processing have made it possible to produce useful images with an image charge in the range of 100 electrons per pixel.

At RCA, our work on the NASA VIS/NIR sensor builds directly on the CCD technology of the SID403 imager. This device, which is currently offered in two of our camera product lines, is a 512×403 -pixel frame transfer TV imager with a $16\text{-}\mu\text{m}$ horizontal pitch (see G.W. Hughes' article in this issue).

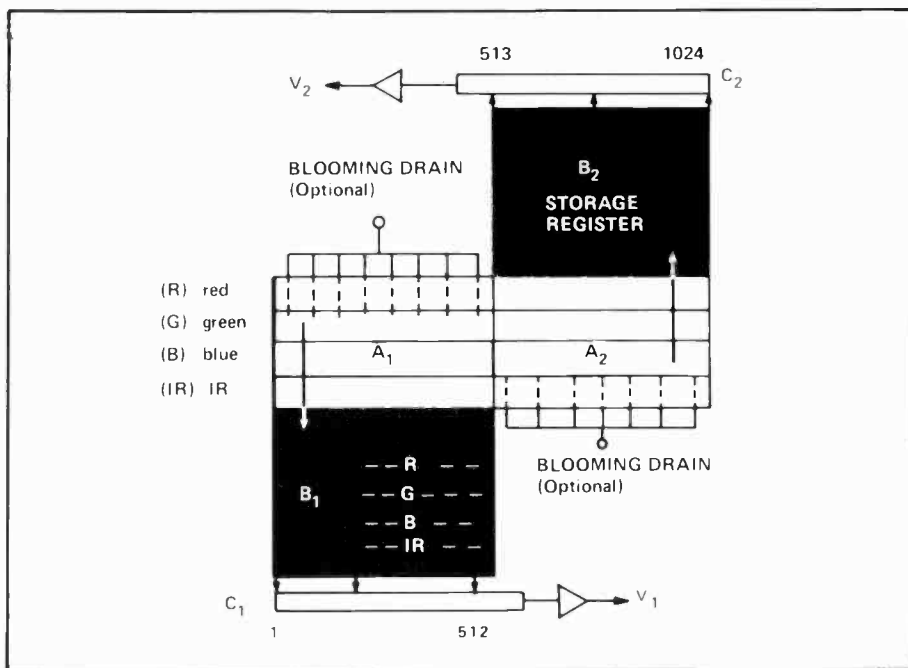


Fig. 6. VIS/NIR four-band sensor architecture.

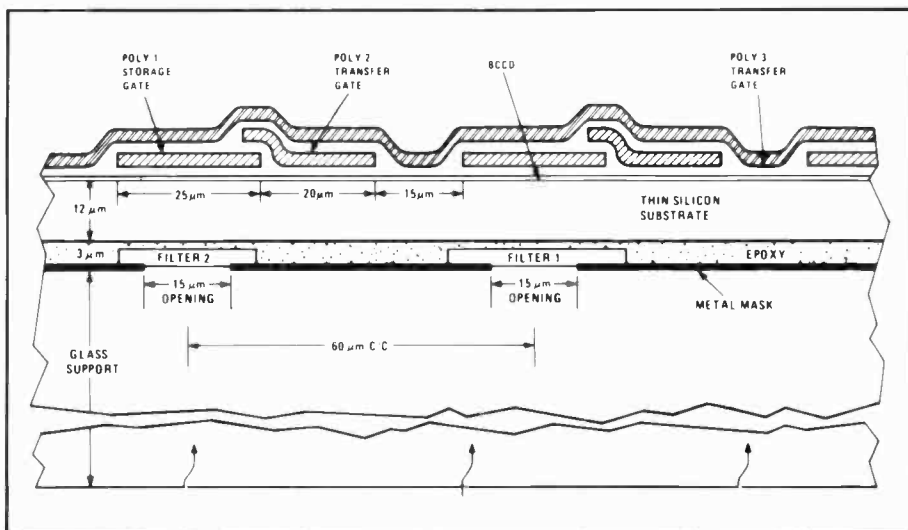


Fig. 7. VIS/NIR device/Filter cross-section.

Chip description

The VIS/NIR imager is a three-phase, buried-channel, frame-transfer CCD structure. It consists of two identical structures (Fig. 6), each containing four parallel sensor lines 512 pixels long, a five-line storage register, and an output register feeding a floating diffusion output amplifier. A cross-section of the imaging register is shown in Fig. 7. The pixel width of $15 \mu\text{m}$ is defined by either a channel stop or a blooming drain structure. The pixel length of $60 \mu\text{m}$ consists of the three polysilicon gates. The optical exposure takes place through a $15\text{-}\mu\text{m}$ opening in an opaque metal mask. The passband of incident irradiation illum-

inating each of the four sensor lines is defined by a set of interference filters covering the slot openings. The metal mask and filters are deposited on a glass substrate that is laminated by an epoxy layer to the fully-processed CCD structure. Maximum photosensitivity can only be obtained by treating the surface of both the glass and silicon substrates with anti-reflection coatings. In addition, selective treatment of the silicon adjacent to the illuminated surface is required.

The two edges of this imager that will be butted against adjacent imagers must be free of bus bars and bonding pads, a requirement that complicates the connec-

Table I. Four-band visible sensor design

Number of pixels	4 x 1024
Pixel size	15mm x 15 μ m
Peak quantum efficiency	80%
Optical integration time	1-40 msec
Noise floor	50e rms
Dark current (25°C)	2nA/ μ m ²
MTF at Nyquist frequency	760% @ 600 nm

Table II. Dual-band SWIR sensor design

Number of detectors	2 x 512
Detector size	30 μ m x 30 μ m
Fill-factor	80%
Optical integration time	2-40 msec
Noise floor	200e rms
Dark current (120K)	4nA/cm ²
MTF at Nyquist frequency	65%

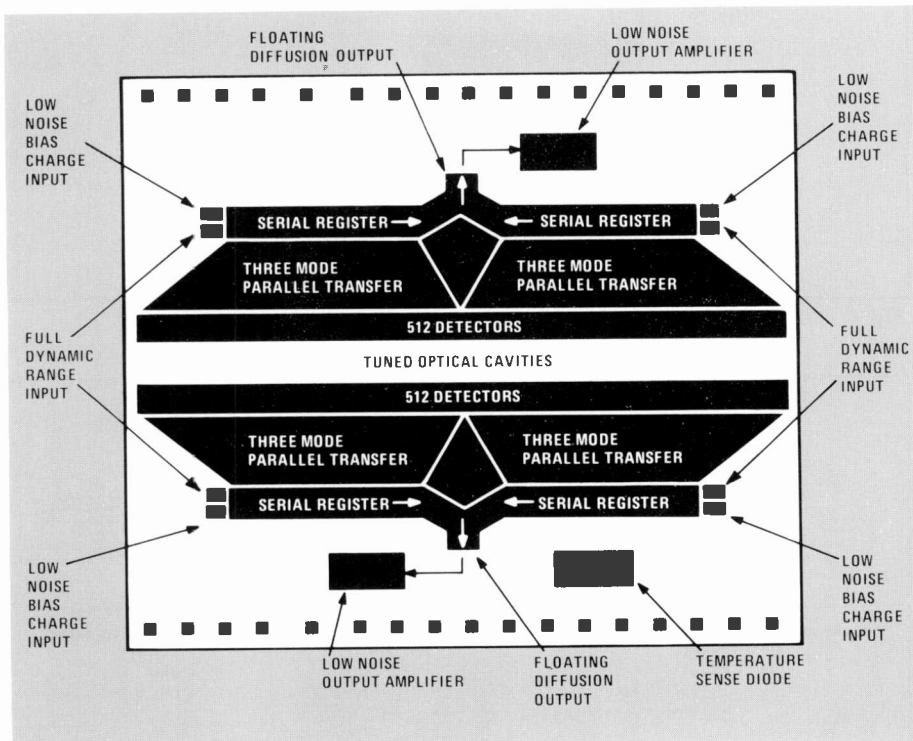


Fig. 8. SWIR dualband sensor architecture.

tions to the CCD gates. By splitting the device into two sections, access to the gates is provided along one side of the storage register and along the bottom of the output register. For the image register, metal bus bars are run across the top of the structure, contacting the polysilicon gates through openings in the appropriate layers of the silicon and silicon dioxide stack. This contact geometry is feasible for rear-illuminated devices, since the presence of opaque material covering the top of the gate structure does not affect its photosensitivity. Table 1 provides an overview of the VIS/NIR device characteristics. The device architecture and design take full advantage of the merits of RCA's thin silicon technology to meet the requirements of this demanding application.

Shortwave infrared (SWIR) sensor

Schottky barrier IRCCD technology

In parallel with the development of the visible pushbroom sensor, RCA is making a major effort to develop a dual-band pushbroom sensor responsive in the shortwave infrared band (1-3 μ m). The SWIR sensor uses the Schottky barrier (SB) infrared-charge-coupled device (IRCCD) technology for two linear arrays of 512 detectors each. A major advantage of the IRCCD technology is that these monolithic sensor arrays are fabricated employing conventional, high-yield, silicon integrated circuit processing techniques. It is thus possible to construct blemish-free line arrays with high-density designs and large numbers of elements. In addition, SB focal plane arrays have considerably higher photoresponse uniformity than other focal plane array (FPA) detector technologies (typical rms nonuniformity is below 2 percent). The SB has another attractive attribute: its inherent anti-blooming control.

Two Schottky barrier technologies have been developed by RCA: platinum silicide

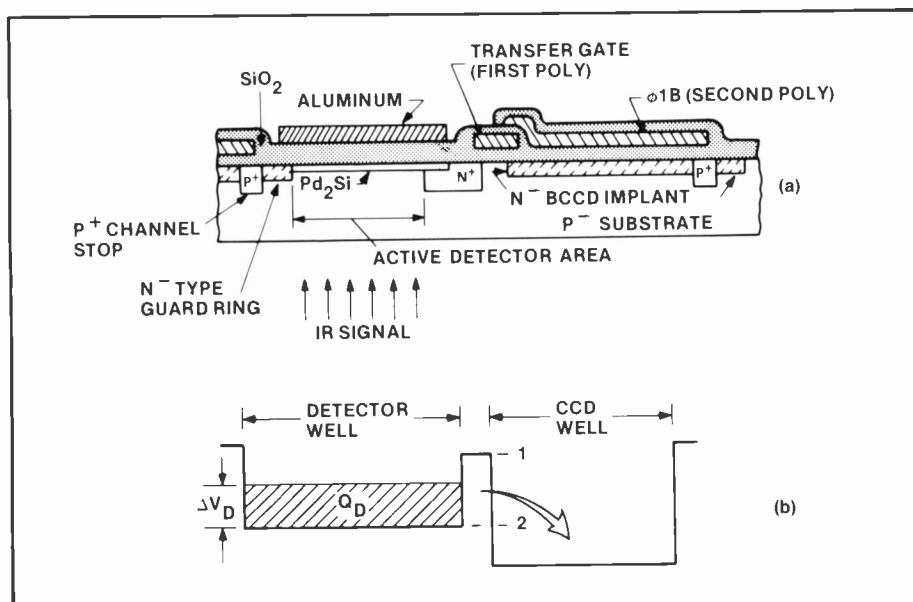


Fig. 9. Schottky barrier IRCCD cross-section.

(PtSi) IRCCDs, which have received the most attention to date, and the palladium silicide (PdSi) IRCCD technology. The PtSi devices operate between 1 and 6 μm and require cooling to 80 K. Although the PtSi devices have higher quantum efficiencies than their PdSi counterparts, PdSi devices are preferred for SWIR satellite-borne applications because their higher operating temperature of 125 K is compatible with current satellite passive cooling technology.

SWIR device description

The SWIR dual-band sensor (Fig. 8) consists of two linear arrays of Schottky barrier detectors, coupled via parallel transfer registers to serial CCD multiplexers. Each linear array and associated output multiplexer may be controlled independently. This chip layout permits butting multiple arrays to produce long linear focal planes with a loss of only two detectors at each seam. To accomplish this two-pixel seam loss the output register is placed at the center of the CCD and multiplexes the left and right sides of the CCD to the output.

The cross-section of the PdSi detector is illustrated in Fig. 9. The SWIR radiation is incident on the detector through a single-layer anti-reflection (AR) coating and the silicon substrate. The IR radiation is absorbed in a thin, 20-200 \AA PdSi film. The single-layer AR coating results in a 30-percent increase in optical absorbance at the tuning wavelength. Optical absorbance in the PdSi film is maximized by the effect of an optical cavity placed above the detector. This optical cavity is composed of a dielectric layer and an aluminum mirror. The proper choice of the dielectric layer thickness and index of refraction is essential for maximum quantum efficiency. The detector elements were designed at a 30- μm center-to-center spacing, consistent with MLA system requirements. This 30- μm pitch is coupled with a fill-factor requirement of 80 percent active area per 30 \times 30 μm detector. Because of the high-density design, innovative isolation techniques had to be developed.

The operating cycle of the device starts with the integration of photon energy (proportional to the scene) for essentially the full line time (4 ms for this application). The energy absorbed in the detectors produces a proportionate number of electrons, which are rapidly transferred to the serial CCD register at the end of the line time. The detector is then reset, and the charge (e^-) is clocked through the CCD to a floating diffusion output. This output technique

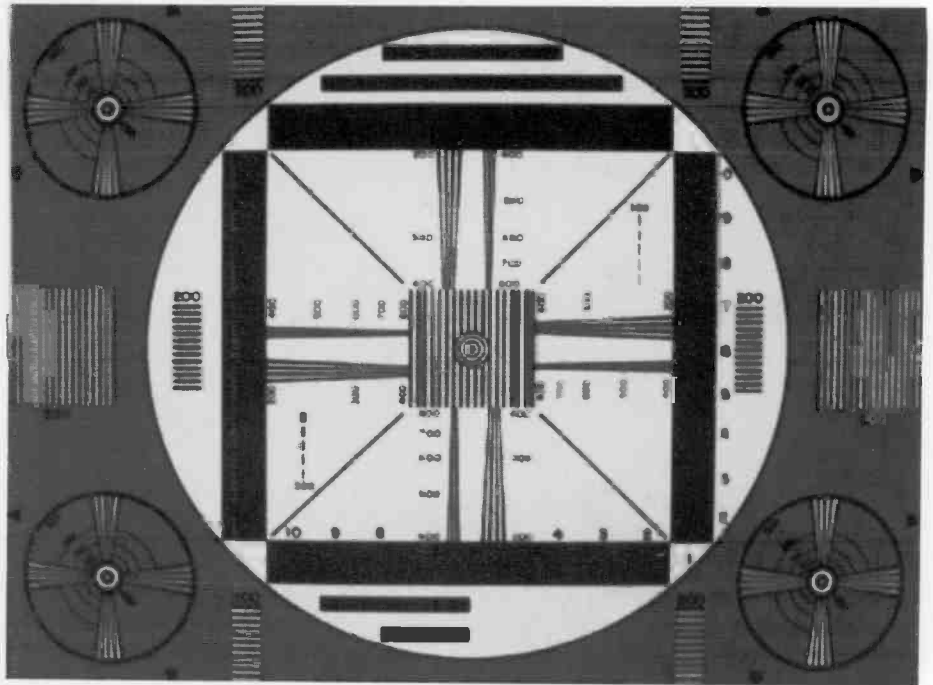


Fig. 10. Developmental SWIR test pattern imagery.

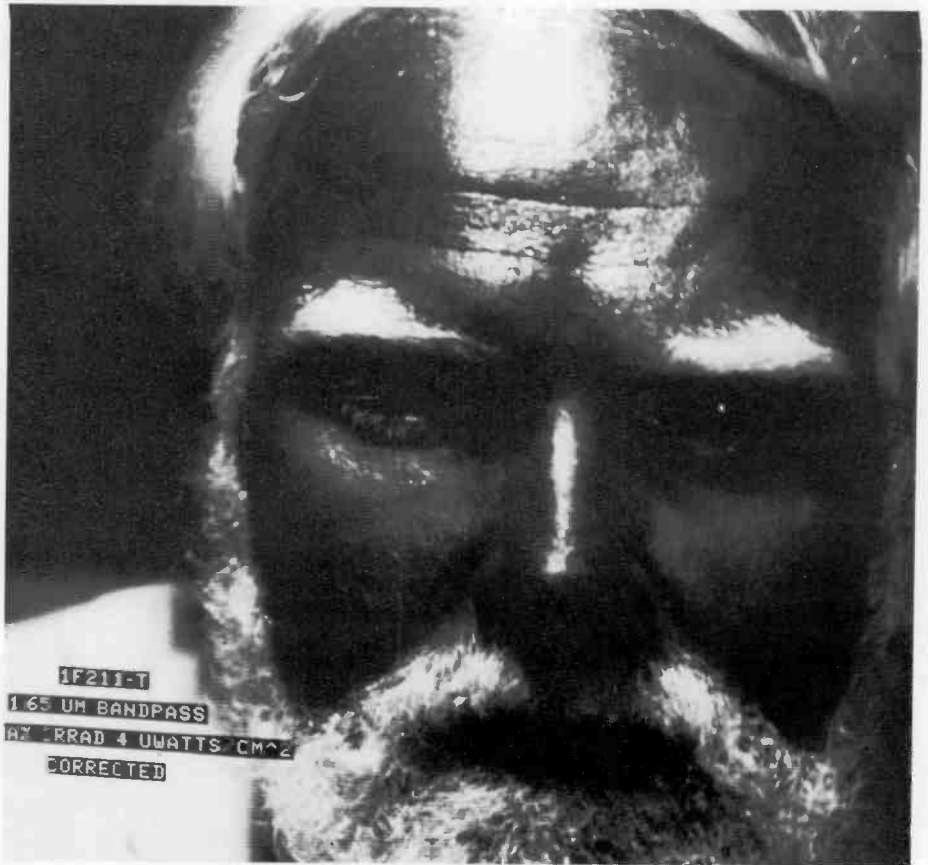


Fig. 11. Developmental SWIR imagery.

converts the electron charge to a proportional voltage, which is then amplified to produce usable video. Table 2 provides a summary of the SWIR device operating characteristics.

By using a mechanical scanning device it is possible to sweep out test images. Figure 10 shows a standard TV test pattern imaged by a first generation SWIR device. The SWIR device images in the

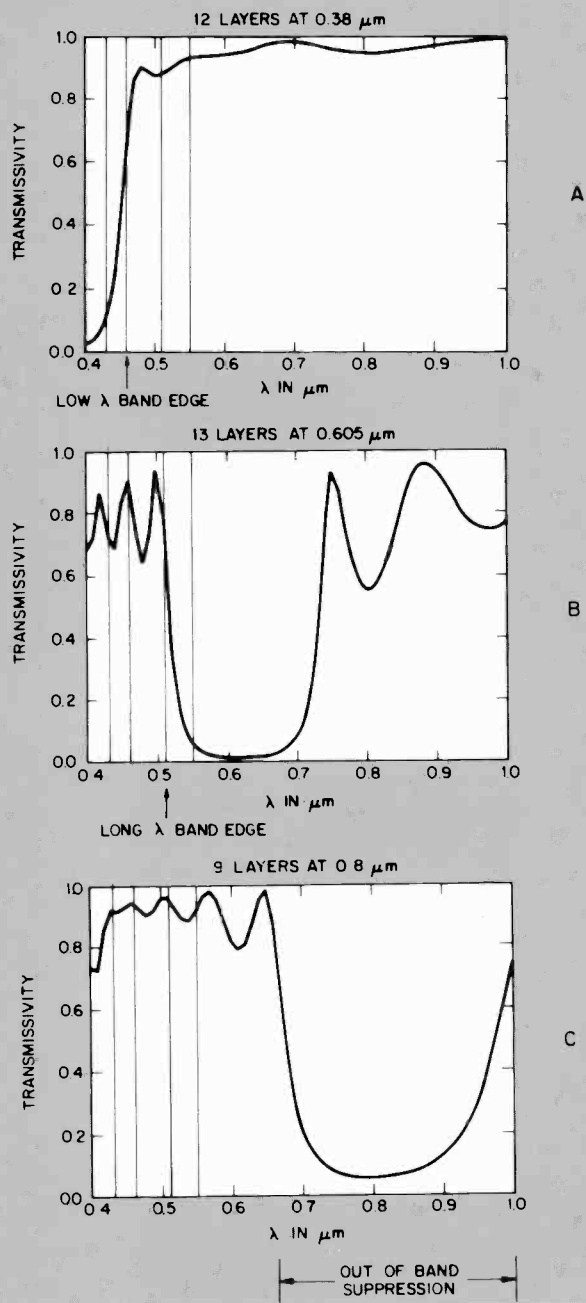


Fig. 12. Interference filter transmissivity versus wavelength for filter "building blocks."

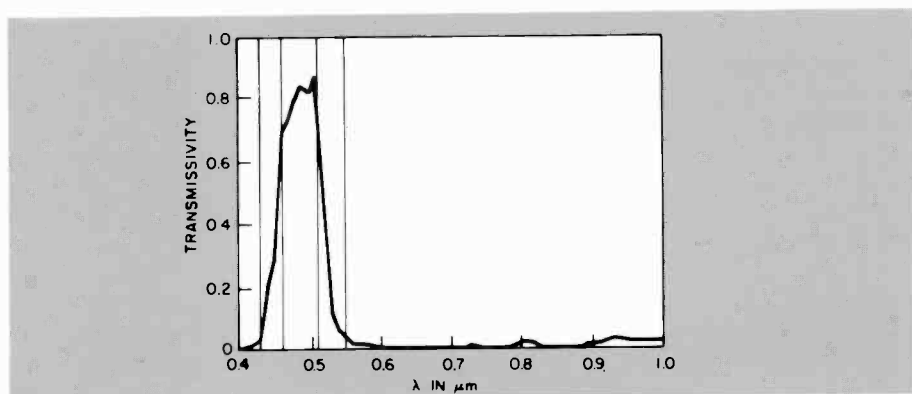


Fig. 13. Completed interference filter design For TM band I.

horizontal direction and is scanned vertically 512 times. Figure 11 is a shortwave infrared image of ATL's Gary Krause (in the SWIR skin is not reflective, but hair is highly reflective). As can be seen by these images, very good uniformity is attained, there is no blooming, and there are few blemishes from this early sample device.

Filter technology development

Integral to the MLA sensor development is the development of tightly spaced, multiband spectral filters. The VIS/NIR thin-silicon device is laminated to a glass supporting substrate upon which four spectral bandpass filters have been placed. The band-to-band, along-track spacing is only 60 μm . The SWIR device will require a two-band filter with 300- μm spacing. As part of the NASA VIS/NIR contract, RCA has been funded to produce dielectric VIS/NIR filters having the TM specifications.

An existing catalog of $\frac{1}{2}$ alternating high and low index-of-refraction stacks (from 1 to 20 layers thick between 0.40 and 1.0 μm) is used as a starting point to determine the number of layers required to obtain a desired slope for each side of a wide bandpass filter. The position of the filter is adjusted by changing the thickness of the layers. This is done by successively altering the wavelength at which the layers are calculated. Additional layers are added to match stacks to the substrate and to each other. Figure 12a illustrates a 12-layer stack at 0.38 μm . Figure 12b is a 13-layer stack at 0.605 μm . When the two are superimposed, we obtain a bandpass filter for our blue design. However, we see that the transmission increases markedly beyond about 0.68 μm . If we need further blocking we must add stacks, which will transmit in the filter region and reject anything past 0.68 μm . Adding an additional stack (Fig. 12c) at 0.8 μm will then lower the transmissivity out to about 0.9 μm . Further addition of stacks enables us to obtain blocking to a desired wavelength on both sides of a filter.

All these techniques provide the starting point from which a design is obtained. An RCA-developed computer program entitled "Synthesis and Monitoring of Optical Interference Coatings" is used to complete the design. Many iterations are made to minimize the number of layers required, to use primarily $\frac{1}{4}$ wavelength layers for ease of monitoring, and to satisfy the final specifications. Where difficulties in direction arise, an RCA-developed optimization program can be used for guidance.

The filter design obtained, such as the one shown in Fig. 13, has high in-band transmissivity and band-edge sharpness that meet the specifications. Suppression of the out-of-band transmissivity is achieved by increasing the number of layers in the successive design iterations that have been made for each of the four filters. The final VIS/NIR filters require between 37 and 40 layers of alternating low-index cryolite and high-index ZnS for each filter. There are thus over 150 evaporated layers on each four-band filter plate. The thickness of the filter stacks varies from 3.2 μm for band 4 to 4.1 μm for band 2. The high out-of-band rejection is further assured by anti-reflection coatings on all optical entrance surfaces, and a "black chrome" opaque filter deposited on the glass (15 μm openings for each filter stack).

Packaging technology

The packaging concept for an MLA focal plane is shown in Fig. 14. Both the VIS/NIR and SWIR chips are precisely mounted to their respective hybrid substrates, and are backside-illuminated through a filter window and baffled aperture. The metal interconnections on the hybrid substrates consist of two levels of metal fabricated with thick-film materials. An output buffer amplifier and miniature bypass capacitors are placed in close proximity to the chips on the hybrid to reduce noise pickup. The chip-to-hybrid connections are provided by wire bonds. The substrate temperature is controlled by conduction through the package cover to a cold surface. Since the SWIR focal plane must be cooled to cryogenic temperatures, it is this packaging approach that has been studied most closely.

For the SWIR focal plane, the primary packaging goals are precision and stability over the 200 K temperature range between the room temperature assembly environment and the cryogenic operating temperature of the precision-mounted infrared imagers. Pixel alignment of $\pm 5 \mu\text{m}$ for colinearity and $\pm 5 \mu\text{m}$ for coplanarity are required. To minimize distortion of the focal plane due to thermal expansion mismatch between the silicon chips and the hybrid substrate, the focal plane assembly is designed with a novel polysilicon hybrid substrate. The substrate incorporates an aperture slit covered by a silicon filter window that has an anti-reflection coating. After the aligned devices have been attached to the substrate with a thermally-conducting epoxy, the package is completed by the addition of a polysilicon cover. Using sil-

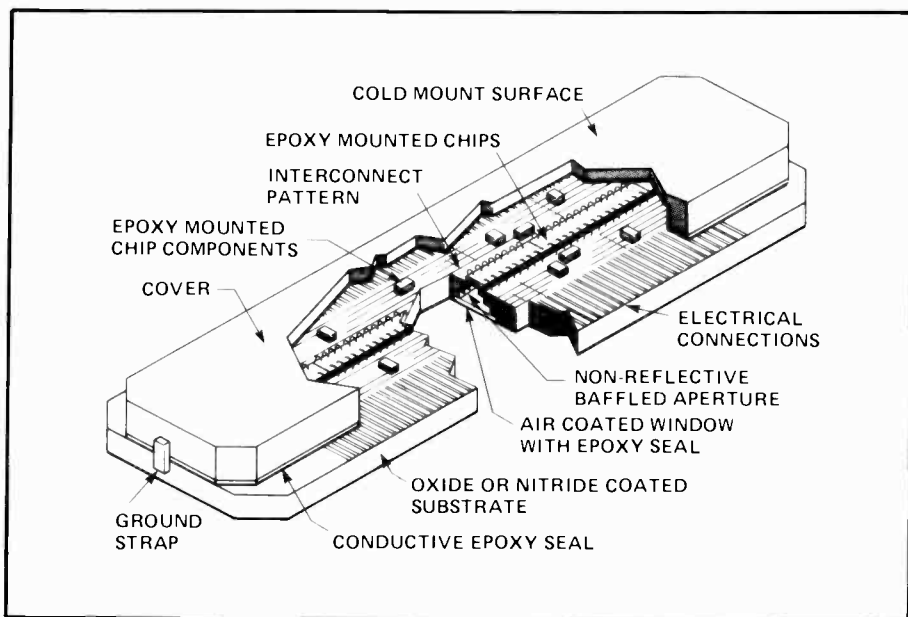


Fig. 14. MLA focal plane packaging design.

icon for all major components reduces thermal distortion and provides a light-weight, rigid package with 120 K thermal conductivity equal to that of silver.

For the VIS/NIR focal plane, the major components are made of beryllia, a more conventional material. This is possible because the VIS/NIR chips operate at room temperature and have a correspondingly smaller range of temperature over which the focal plane must remain aligned and stable.

Both the packages and the devices have been designed to facilitate butting with a two-pixel loss at the seams. The buttable edges of the devices incorporate special structures to minimize deleterious effects due to edge definition. Special mechanical/optical butting and alignment equipment incorporating precision optical flats have been developed to assure precise alignment. Devices are positioned by stepper motor translation stages with a 0.4- μm step size. Alignment verification is performed with optical techniques built around a laser profilometer built for ATL by RCA Zurich Laboratories.

Conclusion

RCA is building a five-chip VIS/NIR and a five-chip SWIR focal plane for NASA Goddard as a proof-of-concept demonstration of the MLA technology. These focal planes will be delivered during the Summer of 1985. The VIS/NIR focal plane will thus have 5000 detectors in each of four spectral bands. The SWIR focal plane will have 2500 detectors in each of two bands.

These focal planes will represent a significant addition to RCA's accomplishments in the field of electro-optics.

Acknowledgement

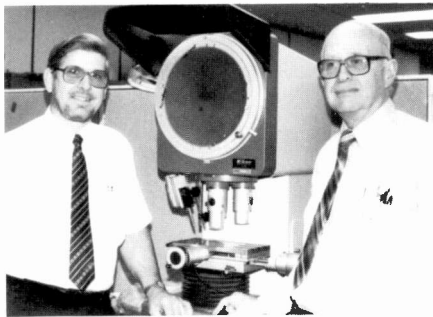
The authors wish to acknowledge the contributions of MLA management and other design and processing engineers. At ATL, the development work is conducted in the Device Technology Laboratory managed by F.B. Warren. Contributions to the development work were made by ATL's A. Boonard, P.J. Coyle, M.S. Crouthamel, S. Goldfarb and G.E. Krause. The work at RCA Laboratories is managed by G.W. Hughes and B.J. Korenjak. At the RCA Laboratories W.F. Kosonocky, F.V. Shallcross, A.D. Cope, G.M. Meray, T.S. Villani, R. Miller and J.J. O'Neill contributed to the development work. At the New Products Division, E.D. Savoye and T.W. Edwards provided excellent CCD processing services. At the Moorestown Hybrid Laboratories, R.R. Bigler and D. O'Malley Flood are performing the hybrid substrate development.

References

1. K.J. Ando, "The NASA MLA program," *Digest*, Vol. II: 1983 International Geoscience and Remote Sensing Symposium, pp. 5.1-5.6, San Francisco, CA. (Aug. 1983).
2. P.K. Weimer and A.D. Cope, "Image Sensors for Television and Related Applications," *Advances in Image Pickup and Display*, Vol. 6, Academic Press Inc. (1983).
3. W.F. Kosonocky and H. Elabd, "Infrared Monolithic

Silicon Imagers with Schottky-Barrier Detectors." IEEE South Conf., Orlando, FL, January 17, 1984.

4. J.R. Tower et al. "Visible and Shortwave Infrared Sensors for Remote Sensing Instruments." IGARSS Conference, Strasbourg, France, Sept. 1984.



Authors: Longsderff (left) and Kramer.

John Tower received the BSEE and MSEE degrees from the University of Pennsylvania in 1976 and 1980, respectively. Since joining RCA Advanced Technology Laboratories in 1976, he has been involved in the design of signal processing and imaging CCDs. He designed a number of CCD correlators for spread spectrum matched filtering in both NMOS and CMOS process technologies. During 1980 and 1981 he worked at RCA Laboratories on the development of time-delay-and-integration CCD imagers for electronic mail applications.

Mr Tower has been a Unit Manager in the ATL Device Technology Laboratory since 1981. He is the Program manager of the NASA VIS/NIR and SWIR programs. Contact him at:

**Advanced Technology Laboratories
Moorestown, N.J.
Tacnet: 222-3883**

Ken Kinnard received his BS in Mathematics and Physics from Northeastern University, Boston, MA, and has done graduate study at Northeastern and MIT in communications engineering. He is a Principal Member of the Engineering Staff. Since joining RCA in 1975 he has worked on millimeter wave imaging systems. He has developed systems employing TV tracking of aircraft as an adjunct to radar tracking. He developed techniques for calibration of instrumentation radars employing star positions, and a number of concepts for MX security using TV and infrared sensors. He was responsible for a computer controlled TV system for monitoring boarder crossings of illegal aliens (recently installed in El Paso, TX). He is presently responsible for electro-optic system analysis for the NASA contracts, and other system opportunities.

Contact him at:
**Advanced Technology Laboratories
Moorestown, N.J.
Tacnet: 222-4930**

Brian McCarthy received the BS and MS degrees in Electrical Engineering in 1978 and 1981, respectively, from Villanova University. He joined RCA Advanced Technology Laboratories in 1978, and has worked on



Authors, left to right: back row; Tower, Kinnard, Strong. Front row; Watson, McCarthy, Pellon.



Authors, left to right: standing; Elabd, Moldovan, Levine. Seated: Hoffman.

various aspects of infrared charge-coupled devices. He has been responsible for the electronic design, system integration, and field testing of an IR fence surveillance system and a laboratory prototype shortwave IR system for NASA. He also worked at RCA Laboratories on process development and testing for shortwave sensors.

He is presently pursuing a PhD degree in Systems Engineering at the University of Pennsylvania. Contact him at:
**Advanced Technology Laboratories
Moorestown, N.J.
Tacnet: 222-4543**

Tom Strong received the BS degree in Electrical Engineering in 1980 from Widener University, Chester, PA. Since joining RCA Advanced Technology Laboratories in 1980, he has been responsible for computer

software in support of millimeter wave and infrared imaging system development. He has also written radiometric software for evaluating the performance of CCDs. He has been responsible for the design and layout of the SWIR and VIS/NIR hybrids.

Mr. Strong is presently pursuing the MSEE degree at the University of Pennsylvania. Contact him at:
**Advanced Technology Laboratories
Moorestown, N.J.
Tacnet: 222-2950**

Ed Watson received the BS degree in Mechanical Engineering in 1981 from the Catholic University of America, Washington, DC. Since joining RCA Advanced Technology Laboratories in 1981, he has been involved in the design and implementation of precision hybrid alignment equipment for butting and assembly of CCD sensor arrays for the SWIR

and VIS/NIR programs. He has also worked on the design of optical disk recorders, including the study of concepts for a high capacity optical disk buffer system.

Mr. Watson is presently pursuing a Masters degree in Mechanical Engineering at Drexel University.

Contact him at:

**Advanced Technology Laboratories
Moorestown, N.J.
Tacnet: 222-2438**

Leo Pellon received the BSEE degree in 1981 from Manhattan College. He joined RCA Princeton Laboratories in 1981, where he worked on the testing and evaluation of Schottky barrier IRCCDs for two years. He transferred to the Advanced Technology Laboratories in 1983, where he is working on the development of a computer-assisted test facility for radiometric evaluation of focal plane arrays. He has conducted investigations into IRCCD noise sources and the radiometric performance of the NASA SWIR devices.

He is currently pursuing the MSEE degree at the University of Pennsylvania.

Contact him at:

**Advanced Technology Laboratories
Moorestown, N.J.
Tacnet: 222-2950**

Hammam Elabd received his MS and PhD degrees in Electrical Engineering from Rensselaer Polytechnic Institute, Troy, NY, in 1979. Currently, he is a Member of the Technical Staff at RCA Laboratories, Princeton, NJ. He is involved in the development of visible and infrared imagers and cameras. He has worked extensively in the field of Schottky barrier IRCCD device development. He developed high responsivity PtSi and Pd:Si detector designs for RCA's IRCCD focal plane arrays, and was responsible for Pd:Si process development and VIS/NIR device design on the NASA programs.

Contact him at:

**RCA Laboratories
Princeton, N.J.
Tacnet: 226-2687**

Tony Moldovan received the MS degree in Solid State Physics from the University of Bucharest, Romania. In 1978, he received a PhD degree in Physics and Chemistry from the University of Pittsburgh. He worked in high-resolution flat panel displays and solar cells. At the present time he is working on CCD imagers. Dr. Moldovan is responsible for VIS/NIR filter lamination, silicon butt-edge definition, and optical cavity tuning on the NASA contracts.

Contact him at:

**RCA Laboratories
Princeton, N.J.
Tacnet: 226-2258**

Peter Levine received the BS and MSEE degrees from Cornell University in 1967 and 1968, respectively. He joined RCA Laboratories in 1968, where he is presently a Senior Member of the Technical Staff. Since 1971, he has been working on charge-coupled devices, including participation in the development of the CCD television comb filter. He participated in the process evaluation and design of a variety of imaging CCDs. Mr. Levine has been responsible for the design and implementation of low-noise video processing electronics for the 512x403 imager and the NASA VIS/NIR device.

Contact him at:

**RCA Laboratories
Princeton, N.J.
Tacnet: 226-2923**

Dorothy Hoffman received a BS degree in Chemical Engineering from Rensselaer Polytechnic Institute in 1947, and an MS degree in Chemical Engineering from Bucknell University in 1948. In 1962, Mrs. Hoffman joined RCA Laboratories as a Member of the Technical Staff. Since 1967, she has been in charge of a Thin Film Technology Service group. She is responsible for developing evaporated coatings used in various devices, including kinescope parts, optical waveguides, semiconductors, and optical elements. In addition, she helped create a central Corporate resource of computer know-how

on the design of optical interference coatings. Mrs. Hoffman's principal responsibility on the NASA programs has been optical bandpass filter design.

Contact her at:

**RCA Laboratories
Princeton, N.J.
Tacnet: 226-3013**

Bill Kramer received the BS degree in Chemical Engineering from West Virginia University in 1942. He joined RCA Lancaster in 1957 as a member of the Chemical and Physical Laboratory, specializing in glass problems. He spent the next several years in materials synthesis, specializing in photoconductive materials and their deposition. From 1970, his work has been entirely mass spectrometry and thin films. Mr. Kramer has devoted the last two years primarily to the NASA striped filter program.

Contact him at:

**New Products Division
Lancaster, Pa.
Tacnet: 227-3464**

Dick Longsderff received the BSEE degree from Tri-State University in 1959. He joined RCA Lancaster in 1959 as a product development engineer. He has held engineering positions in various electro-optics product lines (lasers, photomultipliers, camera tubes), and was named Manager—Manufacturing Methods and Industrial Engineering in 1980. In 1982, Mr. Longsderff was assigned the position of Manager, Process Engineering for the tube operations activity of the New Products Division. He is involved in the NASA striped filter development.

Contact him at:

**New Products Division
Lancaster, Pa.
Tacnet: 227-6696**

Multifeature methods for target detection

The first step is a global search for possible targets. The second step is to separate the target and non-target features.

Autonomous target detection requires a search algorithm that can rapidly process vast amounts of data to locate regions of interest that may contain a target. These smaller regions can then be examined more thoroughly to segment the targets from their immediate surroundings, or to reject the region as a non-target. In this article we describe the methods used for the global search and the local segmentation using multifeature techniques. The outputs of both these processes are binary images with target pixels set to 1 and non-target pixels set to 0. We will show the results of these algorithms when they are applied to digitized imagery of ships at sea.

Multifeature histogram computation

Some of the possible features we can use for this technique are intensity, edge magnitude, or texture. We can also use multis-

Abstract: *Autonomous target detection requires a search algorithm that can rapidly process vast amounts of data to locate a target. The two stages of target detection are global search and target/background segmentation, with Bayesian theory being used to determine whether a pixel is actually a target pixel. Targets are determined by using features such as intensity, edge magnitude or texture, and multisensor or multispectral intensities to segment the target from the background.*

sensor or multispectral intensities. An L -dimensional feature vector $\bar{F}(i, j)$ is defined for each pixel in the image. The k th component of the feature vector at a pixel represents the feature value of the k th feature at that pixel.

$$\bar{F}(i, j) = [F_1(i, j), F_2(i, j), \dots, F_L(i, j)]$$

An L -dimensional joint feature histogram is generated from the L feature images for each window of the image. The L -dimensional joint feature histogram is the number of pixels having feature vector $\bar{F} = (f, f, \dots, f)$. Each f_k ranges from 0 to $2^{N(k)} - 1$, where $N(k)$ is the number of bits used to represent the k th feature.

One advantage of using the joint histogram comes from the fact that there may be target/background conditions that are inseparable using two features independently, but are readily separable using the same two features jointly. A simple example of this is illustrated in Fig. 1. In this example, neither edge magnitude nor intensity can be used independently to separate the target from the background. However, the joint histograms clearly delineate the two areas.

Another advantage of using the joint histogram is the inherent ability to select the feature, or features, that will distinguish target from background. For example, if intensity and edge magnitude are the two features computed for the image, and target 1 differs from the background only in intensity, and target 2 differs from the background only in edge magnitude, the multifeature algorithms will act as an intensity

discriminator for target 1 and as an edge-magnitude discriminator for target 2.

Global search using multifeature thresholding

The multifeature threshold algorithm determines on a pixel-by-pixel basis which pixels are part of the target. Additional processing is required to detect clusters of target pixels to be processed by the local segmentation algorithm. Two assumptions are basic to the multifeature thresholding algorithm:

1. The target size is small in comparison to the background in the search window.
2. At least one of the features selected is statistically different between target and background for a sufficiently large percentage of the pixels in the target.

A vertically-sliding search window of M lines is placed on each of the feature images. M is chosen large enough so that condition (1) is satisfied. After the pixels in one line of data in the window are classified, the window is moved down by one line. The line that is classified is the center line of the window, except for the first half of the first window, and the last half of the last window.

The number of features, L , and the number of bits/feature, $N(k)$, must be small enough that the multifeature histogram is not too sparse for the background feature values. Under these conditions the target feature vectors should occur only a few times, and the background feature vectors

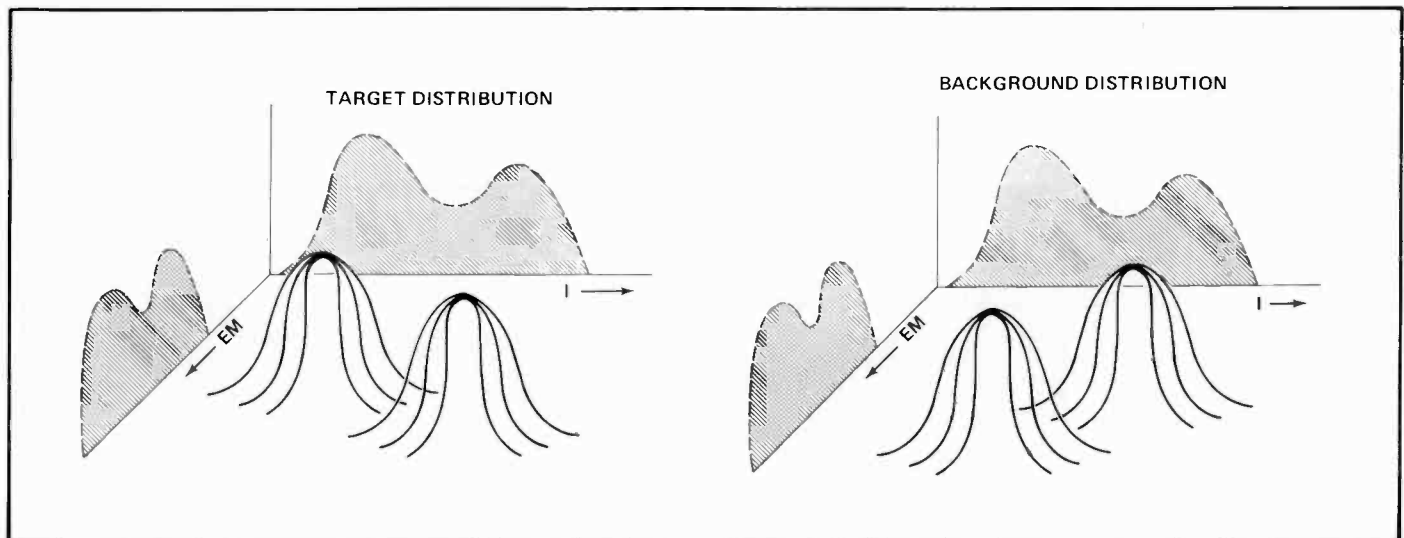


Fig. 1. Joint histograms improve separability.

should occur many times in the window. Figure 2 illustrates how the multifeature thresholding works for a simple one-dimensional feature histogram. A threshold ($TMAX$) is chosen based on target size relative to the window size. Pixels whose feature vector occurs fewer than $TMAX$ times in the histogram over the window are classified as target pixels. If the actual background and target distributions are as shown, then target pixels with features F^1 to F^{TMAX} will be missed. Background pixels with features F^{TMAX} to F^2 will be misclassified as target pixels. Increasing $TMAX$ reduces the number of misclassifications at the expense of more misses. The misclassified pixels will probably be scattered, and can be eliminated by examining pixel clusters. Therefore, it is desirable at this processing stage to accept more false alarms in order to minimize misses.

Figure 3 illustrates the global search algorithm using two features. The number of occurrences of the two-dimensional feature vectors are computed over the search window. Pixels in the center line of the window whose feature vector occurred below the threshold plane are called target pixels. The threshold plane can be a fixed small number whose size is a function of the window size and the feature distribution. This threshold value may be difficult to determine. A method of computing the threshold adaptively based on previous lines of data, and a specified false alarm rate in the background is being developed.

Figure 4 shows an original image, and Fig. 5 shows the binary output of the multifeature thresholding algorithm using intensity and Sobel edge-magnitude as the two features.

Local segmentation using multifeature histograms

Clusters of pixels that were found using the global search are examined more thoroughly to obtain a high-quality binary segmentation of the target from the background. The decision rule that labels each pixel as target (1) or background (0) is based on the statistical differences between the probability density functions of the feature vectors of the background and target within the region of interest. The region of interest consists of two areas; a target window, and a background window. The target window is a rectangular region that encloses the cluster of pixels found by the global search. The background window consists of the border around the target window, as shown in Fig. 6. Two basic assumptions are made:

1. The target is absent from the background window.
2. The background pixels in the target window have the same distribution as the background pixels in the background window.

The L -dimensional joint-feature histograms are computed over both windows. Bayes' theorem is used to determine the probability that a pixel in the target window is actually a target pixel based on the joint distributions in these two window regions. The Bayesian, or minimum risk, decision rule assigns a weight, or cost, to the misclassification of pixels. The Bayesian rule classifies a pixel as a target pixel if:

$$P(X = T : \bar{F} = \bar{f}) C(b : T) > P(X = B : \bar{F} = \bar{f}) C(T : B)$$

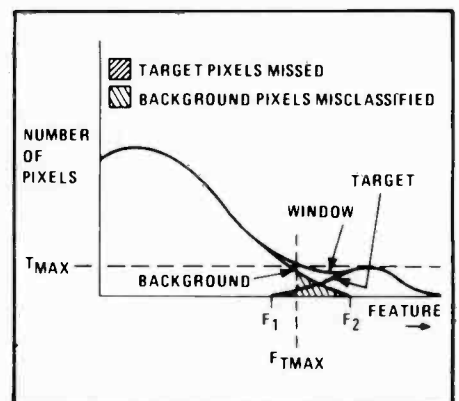


Fig. 2. Multifeature histogram segmentor.

where:

$$P(X = T : \bar{F} = \bar{f})$$

is the conditional probability that pixel $X(i, j)$ is a target pixel given that it has feature vector \bar{f} .

$$C(B : T)$$

is the cost of classifying a pixel as background given that it is a target pixel.

$$P(X = B : \bar{F} = \bar{f})$$

is the conditional probability that pixel $X(i, j)$ is a background pixel given that it has feature vector \bar{f} .

$$C(T : B)$$

is the cost of classifying a pixel as target given that it is a background pixel. Using Bayes theorem, this inequality becomes:

$$P(\bar{F} = \bar{f} : X = T) P(T) C(B : T) > P(\bar{F} = \bar{f} : X = B) P(B) C(T : B)$$

where:

$$P(\bar{F} = \bar{f} : X = T)$$

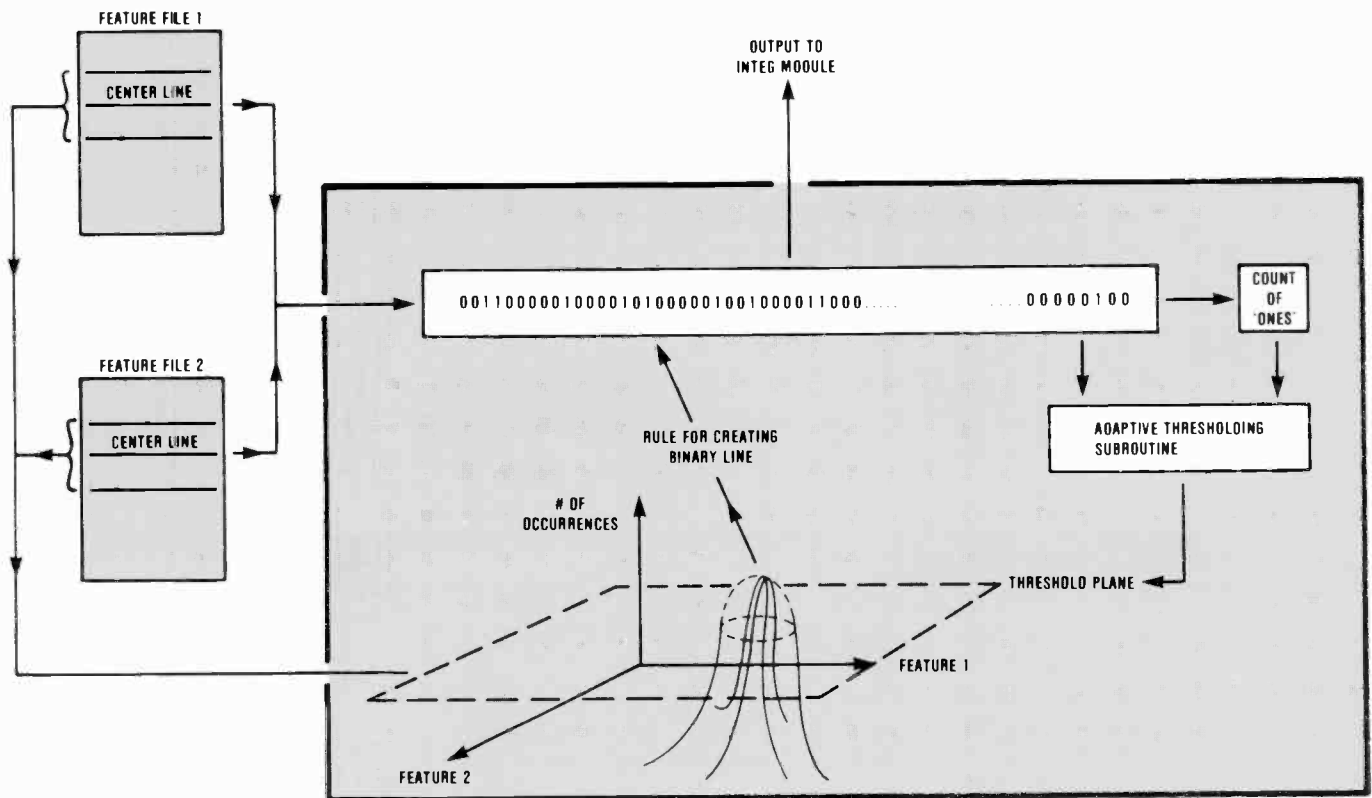


Fig. 3. Glogal search algorithm.



Fig. 4. Original image.



Fig. 5. Multifeature threshold image.

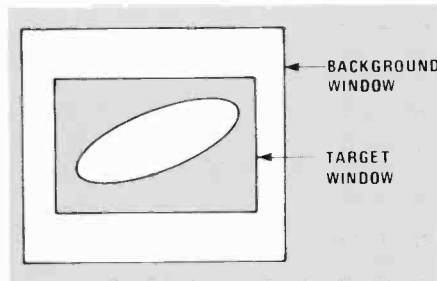


Fig. 6. Target and background windows for statistical segmentor.

is the conditional probability that the feature vector has value \vec{f} given that the pixel is a target pixel.

$$P(T)$$

is the *a priori* probability of target in the target window.

$$P(\bar{F} = \vec{f}; X = B)$$

is the conditional probability that the feature vector has the value \vec{f} given that the pixel is a background pixel.

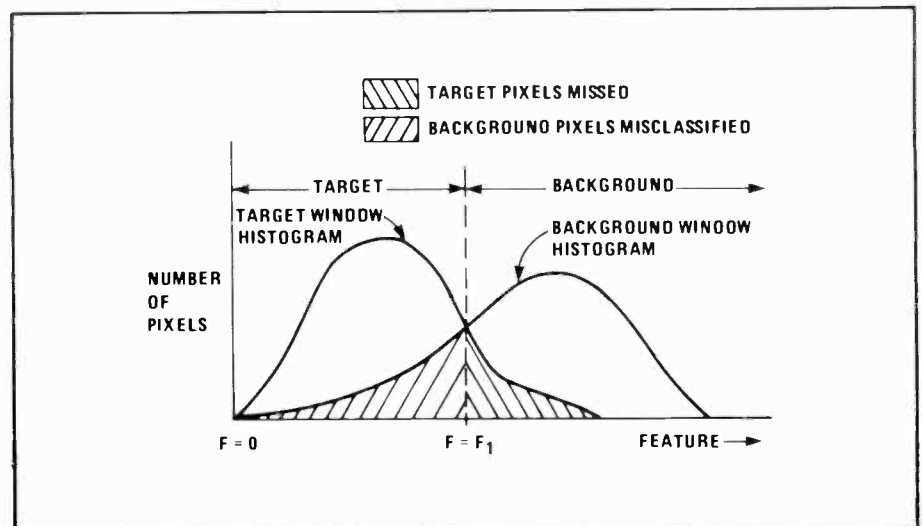


Fig. 7. Example of maximum likelihood decision rule for a single feature.

$$P(B)$$

is the *a priori* probability of background in the target window. These probabilities can be expressed in terms of the distributions over the target window and the background window. By assumption (1) above, the distribution of background pixels is approximated by the probability density function P^b , which is calculated from the histogram over the background window.

$$P^b = P(\bar{F} = \bar{f}; X = B)$$

The target window contains both target and background pixels. Under assumptions (1) and (2), the probability density function P^T , which is computed from the histogram over the target window, can be expressed as:

$$P^T = P(B)P(\bar{F} = \bar{f}; X = B) + P(T)P(\bar{F} = \bar{f}; X = T)$$

Written in terms of the target window density function P^T , and the background window density function P^b , the Bayesian decision rule classifies a pixel as target if:

$$P^T > \alpha A P^b$$

where:

α = the percent background in the target window. This can be approximated by the number of "0" pixels, as determined by the global search.

and:

$$A = (C(T:B) + C(B:T)) / C(T:B)$$

If the two costs are equal, then $A = 2$. This decision rule is called the maximum likelihood decision rule, and guarantees that the majority of the pixels will be classified correctly. Figure 7 is an example of the maximum likelihood decision rule where 50 percent of the target window is background ($\alpha = 0.5$). All pixels with feature values in the range $F = 0$ to $F = F$ will be classified as target because the probability of a target is greater than the probability of background ($P^T > P^b$). All pixels with feature values F greater than F^1 will be classified as background. The pixels corresponding to the area under the background histogram in the interval $F = 0$ to $F = F^1$ will be misclassified as target pixels. Likewise, the pixels corresponding to the area under the target histogram in the interval $F > F^1$ will be misclassified as background. Although the maximum likelihood decision rule guarantees that the majority of the pixels are correctly labeled, it may be desirable to miss a few target pixels in order to reduce problems caused by misclassifying background pixels. This

may be done by using different cost factors $C(T:B)$ and $C(B:T)$. Using different cost factors has the effect of moving the line $F = F^1$ in Fig. 7 to the left or right.

The results of the Bayesian segmentor applied to the target found by the multifeature thresholding algorithm in Fig. 5 are shown in Fig. 8.

Summary

The techniques described in this article address the first two stages of target recognition, namely the global search and the target/background segmentation. The next step in the process is to compute a set of features from the segmented objects that can be used to determine if indeed they are targets of interest. This process is by no means trivial, because the selection of appropriate features for class discrimina-

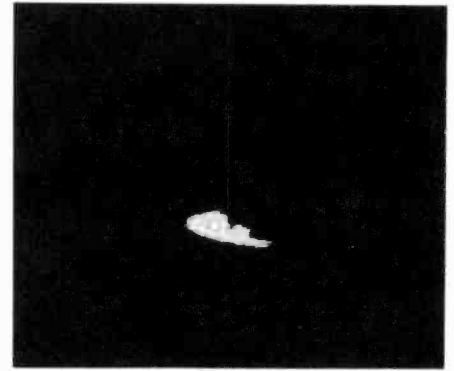
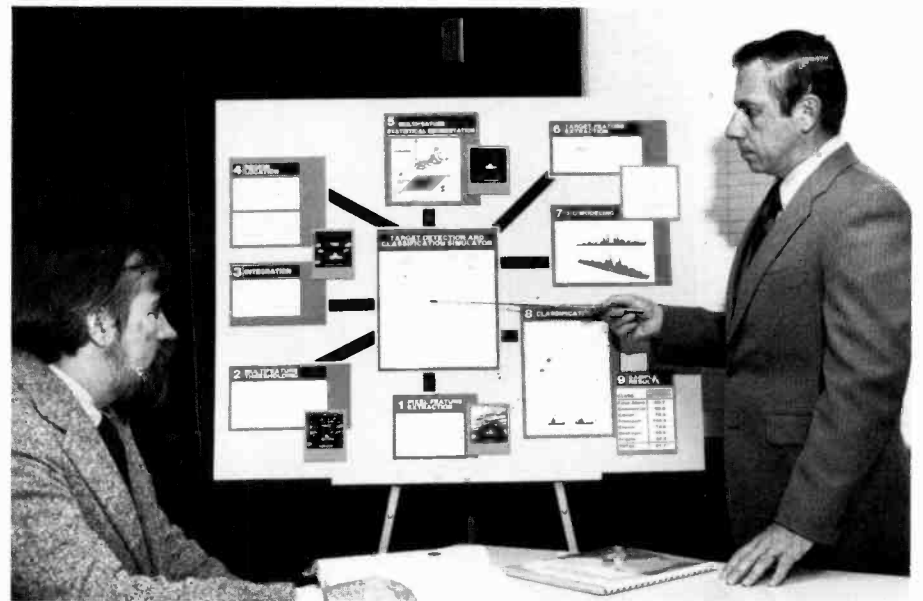


Fig. 8. Bayesian segmented image.

tion is mainly heuristic. Considerable success has been achieved for the ship-at-sea application corresponding to a low-altitude cruise missile scenario. The low altitude guarantees a small sensor depression angle, which minimizes the viewing angles that must be considered.



Loren Toombs is a Principal Member of Engineering Staff in the Image Technology Laboratory of the Advanced Technology Laboratories in Camden, NJ. Mr. Toombs joined RCA in 1970, and has worked primarily on computer simulations and image processing. This work has included two-dimensional filtering, two-dimensional compression, and pattern recognition. Currently, he is developing algorithms for automatic target cueing and classification using multifeature techniques.

Contact him at:
Advanced Technology Laboratories
Camden, NJ
Tacnet: 222-3403

Bernie Schaming is Unit Manager in the Image Technology Laboratory of the Advanced Technology Laboratories in Camden, NJ. Mr. Schaming joined RCA's Astro-Electronics Division in 1962 and transferred to ATL in 1964, where he has concentrated in the area of image processing since the early 1970s. He was responsible for RCA's development of video bandwidth compression algorithms, and more recently a multifeature statistical tracking algorithm. Presently, he is responsible for contracts and IR & D in the area of target detection and classification.

Contact him at:
Advanced Technology Laboratories
Camden, NJ
Tacnet: 222-3942

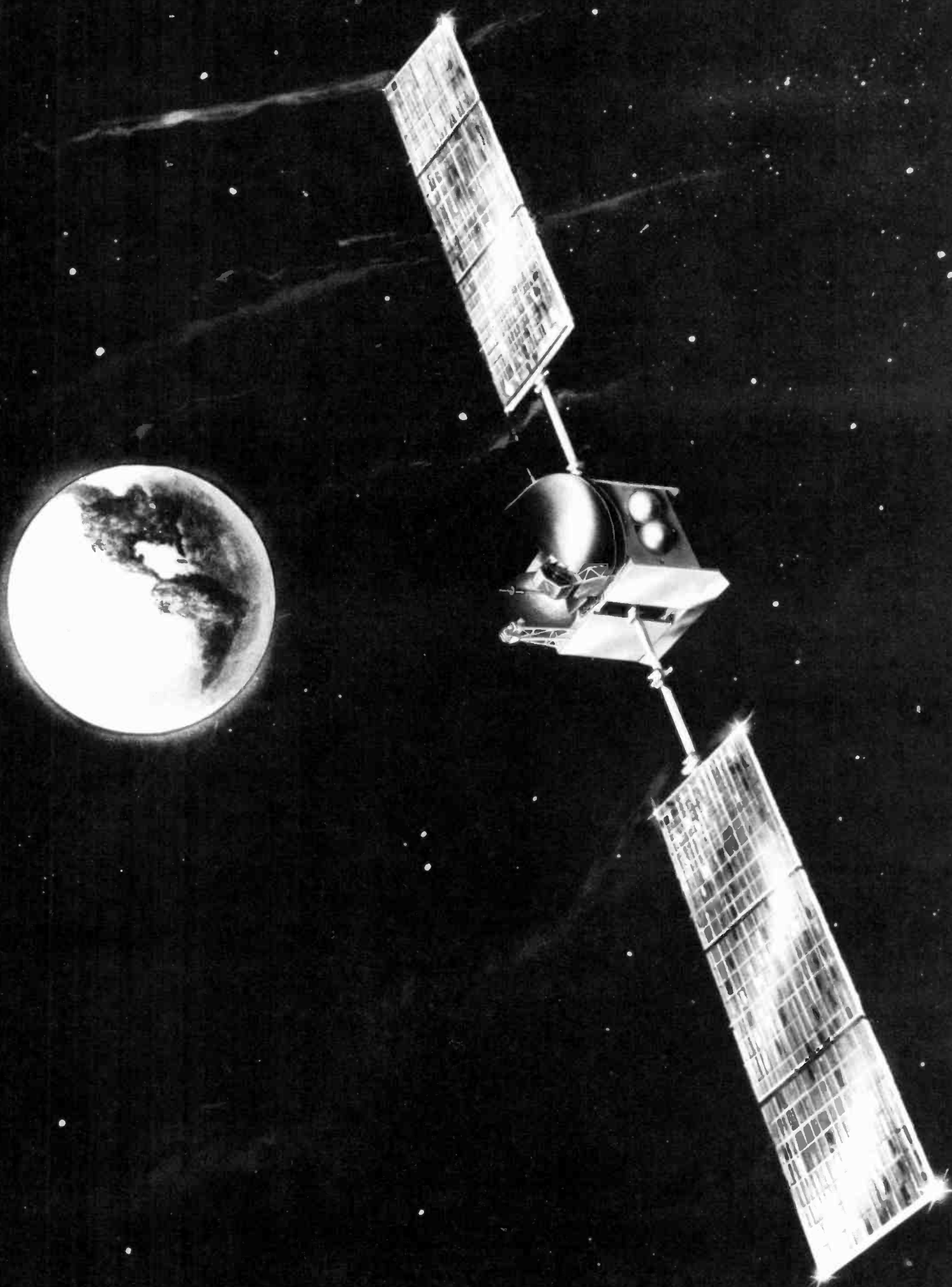


Fig. 1. Artist's rendition of Spacenet 1 satellite launched May 1984.

Nickel-hydrogen batteries come of age

Nickel-hydrogen batteries can provide higher specific energies and longer life than nickel-cadmium batteries for aerospace and other applications.

When RCA Astro-Electronics launched the Spacenet I communications satellite last May, it contained one of the first operational nickel-hydrogen (NiH₂) batteries to be used for a commercial application in space.

The sealed NiH₂ cell design is a hybrid combining the nickel electrode from nickel-cadmium technology and the platinum-black hydrogen electrode from fuel-cell technology. These two electrodes provide an anode and cathode with an extremely long and stable life. The separator material most widely used, fuel-cell-grade asbestos, is also quite stable in the caustic potassium hydroxide battery electrolyte, providing long-life capability for this design. Other unique characteristics of this cell design include energy densities in the range of 40 to 60 watt-hours/kg (vs. 30 to 35 for

nickel-cadmium), high-rate charge and discharge capability, the ability to withstand overcharge and overdischarge, and maintenance-free operation. Potential uses for this expensive—but long-life and maintenance-free—sealed battery include utility load-leveling and undersea applications.

Background

The most common on-board power source for spacecraft applications is the photovoltaic conversion of sunlight into electrical power. During periods when the solar cells are eclipsed by the earth, power is supplied by storage batteries that have been charged from the solar cells during periods of sunlight.

The most widely used storage batteries for this application have been nickel-cadmium. However, the higher weight-energy density of NiH₂ and the higher permissible depth-of-discharge for the NiH₂ system for equal life gives nickel-cadmium a weight disadvantage for the higher-power and longer-life missions now desired. The limitations of the nickel-cadmium system further include gradual degradation of the organic separators; cadmium penetration of the separators; and a life-sensitivity to high depth-of-discharge, overcharge, and overdischarge.

The NiH₂ system does not appear to have any of these limitations. Recognizing the potential of this system, two parallel development programs were initiated in the early 1970s to bring NiH₂ technology to the status of "flight hardware." One program, financed principally by INTELSAT at COMSAT Labs, resulted in the "COMSAT*-design" cells that RCA and INTELSAT are flying in geostationary satellites today.¹ The other program, financed

by the USAF, resulted in the "Air Force design" NiH₂ cells, which flew in one classified mission in 1977 and are now being evaluated by RCA and others for more severe low-earth-orbit spacecraft use.^{2,3}

The first satellite to use the COMSAT-design cells was a Navy experimental satellite, NTS2, launched in 1977 and successfully operated until 1984. A complete discharge of the battery before satellite turn-off in 1984 showed no degradation from its 1977 performance.⁴ Six additional years of continued testing, component and manufacturing technique development, system development, and program management "convincing" were required before the second and third satellites containing these batteries, INTELSAT V flights 6 and 7, were launched in 1983.

RCA's Spacenet communications satellite (Fig. 1), manufactured for the GTE Spacenet Co., and launched in May 1984,⁵ contains two 22-cell, 40-ampere-hour NiH₂ batteries (Fig. 2). RCA Astro now has over a dozen more geosynchronous-orbit satellites under construction with NiH₂ batteries scheduled for launch during the next two years.

Normal Operation

The electrochemical reactions of the nickel-hydrogen cell for normal operation, overcharge, and reversal are listed in Table 1.⁶ The half-cell reactions at the positive nickel-oxide electrode are similar to those occurring in the nickel-cadmium system. At the negative electrode, hydrogen gas is oxidized to water during discharge and is reformed, during charge, from the water by electrolysis. The overall reaction is hydrogen reduction of nickelic hydroxide to nick-

Abstract: *When RCA-Astro Electronics launched the Spacenet I communications satellite last May, it contained one of the first operational nickel-hydrogen batteries to be used in space. By virtue of this milestone, RCA established itself as one of the leaders in the use of this relatively new (less than 15 years old) technology. In this article, we discuss the design of the nickel-hydrogen battery cell, its electrical characteristics, its advantages over the nickel-cadmium battery, and its possible failure modes. Future aerospace and terrestrial applications of the NiH₂ battery are also discussed.*

*Trademark of Communications Satellite Corporation.

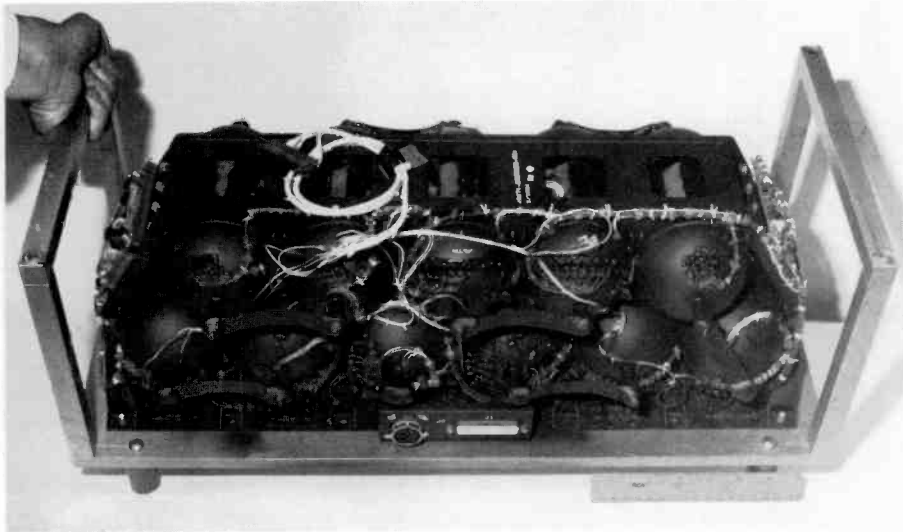
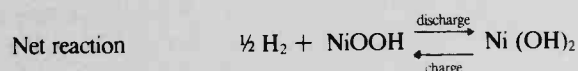
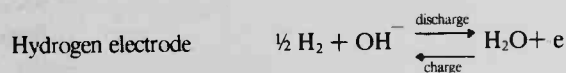
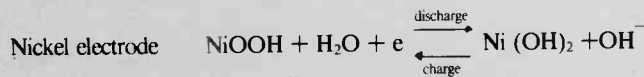


Fig. 2. 11-Cell 40-ampere-hour battery module flown on Spacenet. Each battery consists of two such modules. Spacenet carries two batteries connected in parallel.

Table 1. Electrochemical reactions of NiH_2 cell

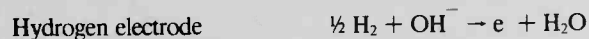
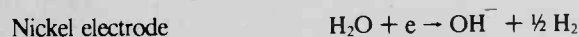
Normal operation:



Overcharge:



Reversal:



elous hydroxide on discharge with no net change in electrolyte concentration or in the amount of water within the cell.

Overcharge

Electrolysis occurs on overcharge with oxygen generated at the positive electrode and

with hydrogen at the negative electrode. Oxygen is chemically recombined with hydrogen to form water at the catalytic platinum electrode. Again, there is no change in the electrolyte concentration or the amount of water in the cell with continuous overcharge. The oxygen recombination rate at the platinum electrode is

very rapid, so even at high rates of overcharge there is no significant buildup of oxygen in the hydrogen gas (oxygen partial pressure of less than 1 percent is typical); thus pressure does not build up, and overcharge is not harmful.

Reversal

During cell reversal, hydrogen is generated at the positive electrode and consumed at the negative electrode at the same rate. Therefore, the cell can be continuously operated in the cell reversal mode without pressure buildup or a net change in electrolyte concentration. This is a unique feature of the system.

Cell Construction

The COMSAT and Air Force cell designs are similar in many respects. The main features of each design, as shown in Figs. 3 and 4, respectively, are as follows:

- COMSAT design: Pairs of positive "back-to-back" electrodes, with negatives opposed across a gas screen. Asbestos separator between the outsides of the positive pairs and the platinum side of the negatives.
- Air Force design: Alternating electrodes with asbestos, "zircar," or combination separators extending past the electrodes to contact the wall wick. Gas transportation is through the center core and directly across the gas screen between the positive and the teflon-coated hydrophobic back of the negative.

Both designs use Inconel pressure vessels 0.020 in. thick. The pressure vessels are designed for burst strengths in excess of 2400 psi. Maximum cell operating pressure is 900 psi for both designs. In the COMSAT design, a hydrophobic teflon layer is coated on the inner wall of the pressure vessel. In the Air Force design, zirconium-oxide flame sprayed on the inner wall acts as a wick to maintain electrolyte distribution.

The COMSAT design uses a circular electrode with a flat section on one edge for tab (electrical) connections and a small central hole for support. The Air Force electrodes are a circular "pineapple slice" shape, with a large center hole for support and tab passage and connections. Both electrodes are shown in Fig. 5.

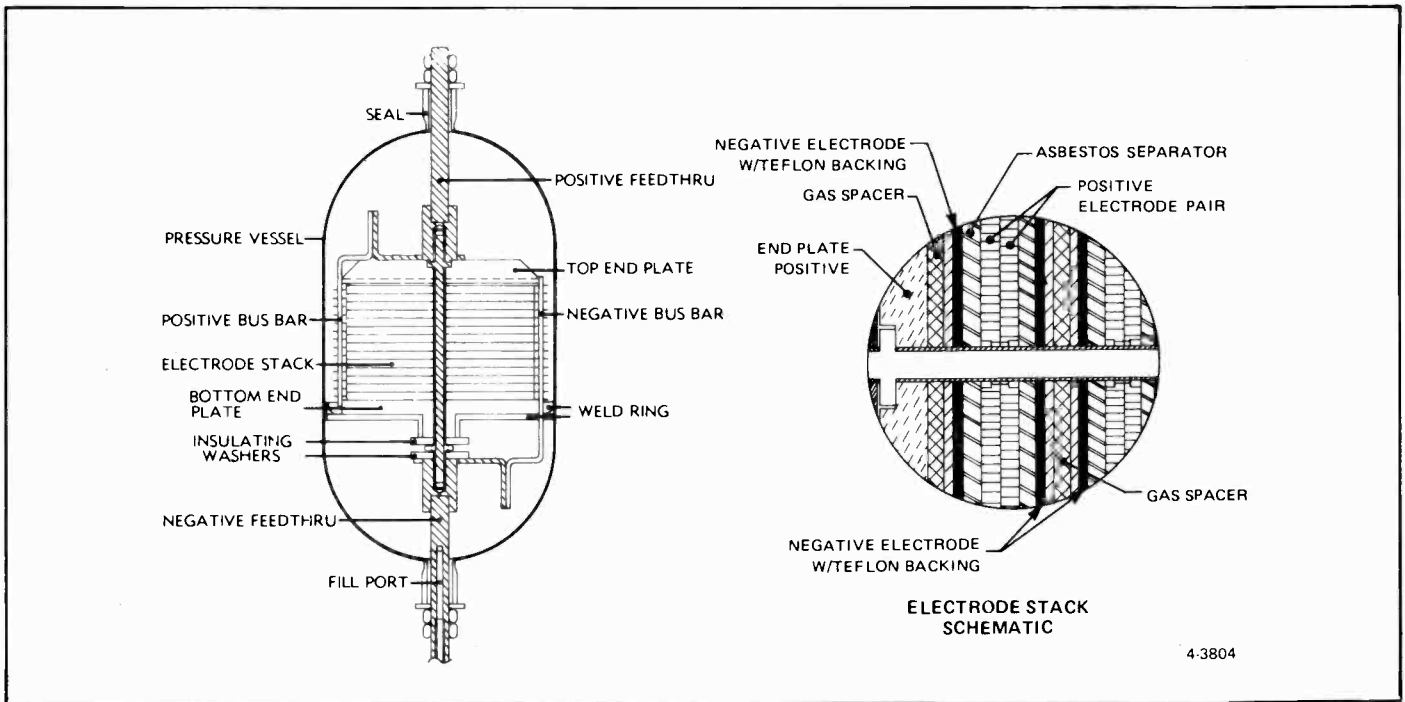


Fig. 3. Nickel-hydrogen cell—Comsat design.

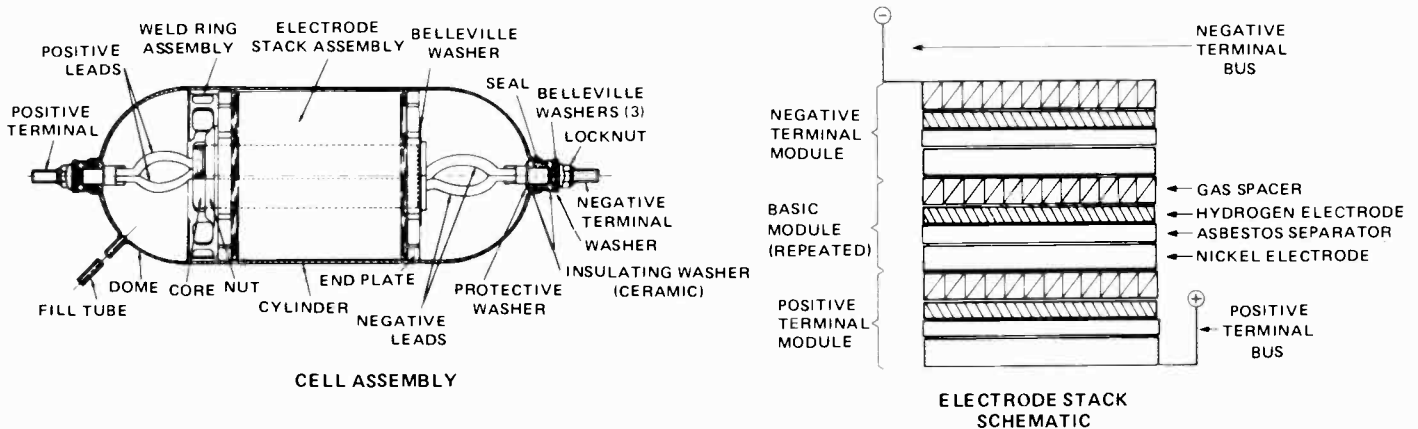


Fig. 4. Nickel-hydrogen cell—Air Force design.

Performance Characteristics

Performance of the Spacenet 40-ampere-hour NiH_2 cells (manufactured by Eagle Picher Ind., Joplin, Mo.) during charge are shown in Fig. 6. Note the higher end-of-charge voltage at lower temperatures, which is similar to the characteristics of nickel-cadmium cells. The straight-line relationship between charge input and cell internal pressure is of interest; this is a unique characteristic of NiH_2 cells, providing a method of determining state of charge. Figure 7 shows pressure and voltage of the 40-ampere-hour cells during charge and overcharge (200 percent). Note that the pressure and voltage level off once full charge is reached—an important safety feature of this system.

Discharge performance of the 40-ampere-

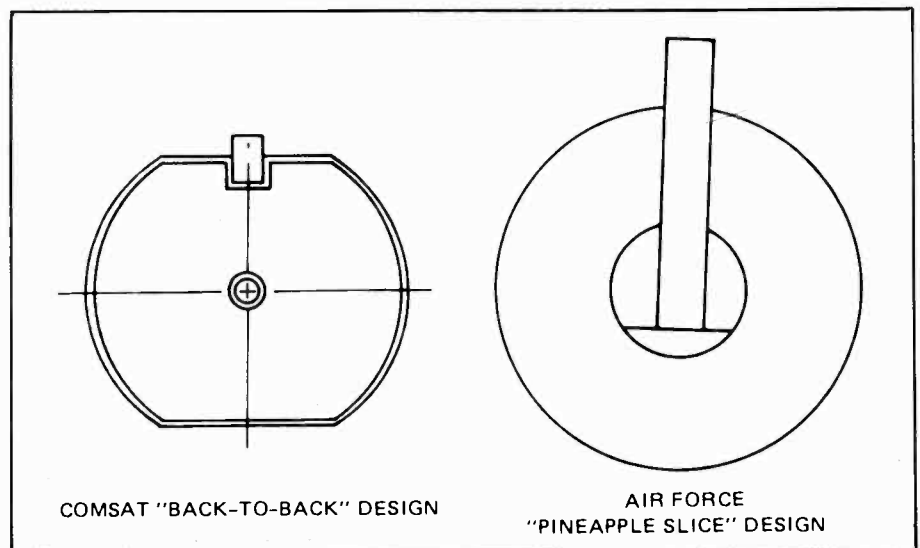


Fig. 5. Nickel-hydrogen cell—positive electrode design.

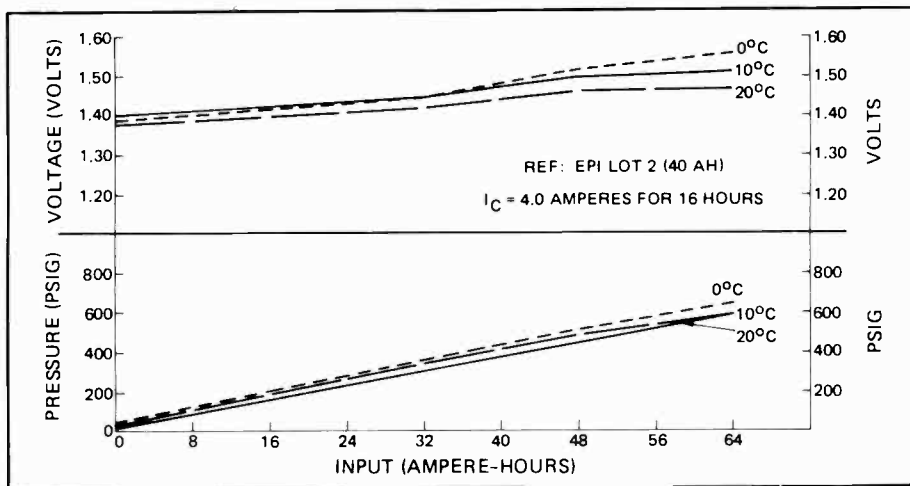


Fig. 6. Typical Spacenet cell voltage and pressure vs. input at 0°C, 10°C, and 20°C.

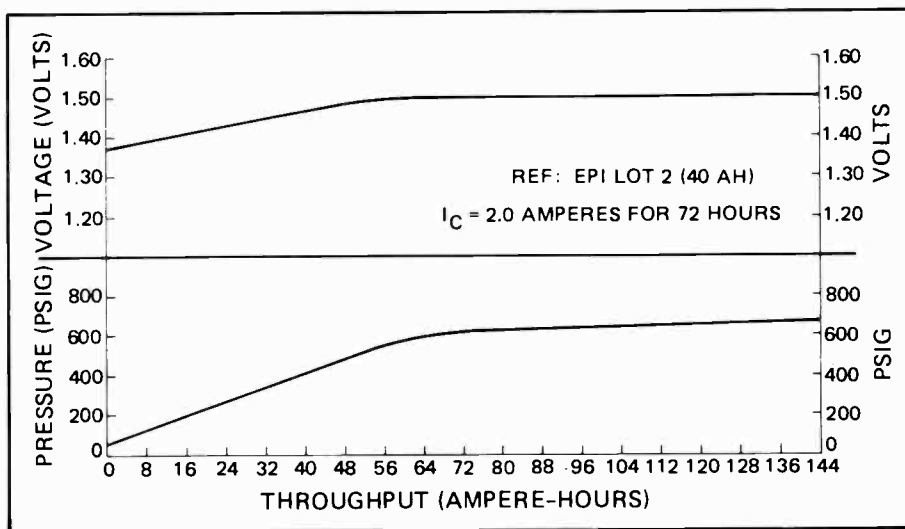


Fig. 7. Typical Spacenet cell voltage and pressure vs. ampere-hour throughput during overcharge at 10°C.

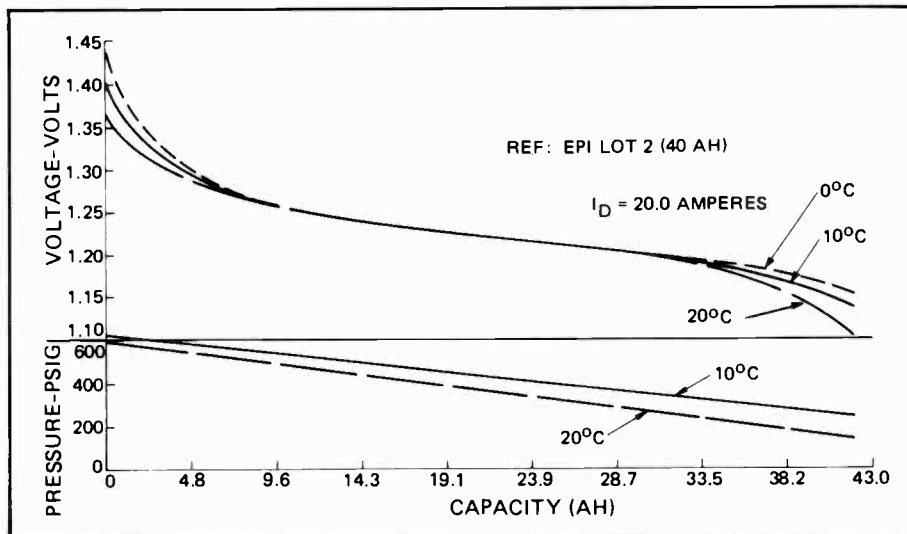


Fig. 8. Typical Spacenet cell voltage and pressure vs. ampere-hours removed at discharge at 0°C, 10°C, and 20°C.

hour cells is shown in Fig. 8. Higher capacity at lower temperatures in the 20° to 0°C range is characteristic of these cells. Again, a straight-line relationship between internal cell pressure and state of charge is evident.

The number of charge/discharge cycles that the NiH₂ system can provide will vary with operating conditions such as temperature and depth-of-discharge. Recent articles reported more than eight years of ongoing cycling (more than 1100 cycles) in the lab under simulated geosynchronous-orbit operating conditions for the NTS2 life-test (COMSAT design) battery.⁴ Up to 17,000 cycles have been reported, at 25 to 50 percent depth-of-discharge, in simulated low-earth-orbit cycling of Air Force cells.⁷ At RCA, over 4000 cycles have been obtained from the Air Force cells at 80 percent depth-of-discharge; however, the results have not been consistent for those cells, and the database is too small to commit them to flight use at this time in low-earth orbit. Additional cells are now undergoing test in our laboratory at 40 and 60 percent depth-of-discharge.³

Failure Modes

NiH₂ technology is only 10 to 15 years old. Therefore, it is possible that some failure modes have not yet been identified. However, the life provided by these cells and batteries in the laboratory and in orbit show that the failure modes, for the most part, have been addressed satisfactorily. These are some of the possible failure modes and their corrective measures:

- Positive electrode expansion. Expansion of the positive electrodes with time has been a leading cause of failure reported for nickel-cadmium cells. The expansion forces electrolyte out of the separators, increasing cell internal resistance, creating "hot spots," and eventually causing shorting. The use of recently developed electrochemically impregnated nickel electrodes in the NiH₂ cells has greatly reduced the reported swelling.
- Separator degradation. The asbestos or zirconium oxide separator materials used in these cells are very stable in the potassium-hydroxide electrolyte at normal operating temperatures.
- Electrolyte redistribution. This has been handled by minimizing positive electrode swelling, by the choice of separators, and, in the case of high-rate Air Force-designed cells, by providing a plasma-

sprayed zirconium-oxide wall wick. The wall wick provides for electrolyte redistribution should "puddling" or evaporation and condensation of electrolyte occur during high-rate, high depth-of-discharge cycling.

- Hydrogen-oxygen recombination. One major advantage of the NiH₂ system is that the gases recombine benignly during overcharge or overdischarge, preventing damage to the cells. One concern, however, is the prevention of localized rapid recombination of hydrogen and oxygen at the platinum electrode, which could result in localized heating, "blow out" areas of separator, and possibly result in internal short circuits. Various techniques of gas and electrolyte management, including careful separator selection and special handling during electrolyte filling and early conditioning cycles have been instituted by the manufacturers and users to prevent this type of failure.

Failure modes peculiar to nickel-cadmium cells, such as cadmium migration through the separators causing shorts and separator breakdown in the electrolyte causing carbonate buildup, are not present in this design. Work is continuing under the sponsorship of NASA, the USAF, and private industry to identify and eliminate any further failure mechanisms.

Conclusions

The NTS2 flight battery has exceeded eight years of life with no degradation. We expect that the usable life of the batteries will exceed 10 years at relatively deep depths of discharge in orbit. If this proves to be the case, storage battery technology will have finally progressed to the point at which batteries will not be among the limiting components of geostationary satellite lifetime.

Demands for even longer missions and for higher power will increase the use of NiH₂ cells in the 1980s and into the 1990s in space. Government funding is being applied to improve the manufacturability and reduce the cost of Air Force designed cells, improve the reliability of both designs through advanced separator development, and develop multiple cell designs in single (common) pressure vessels.^{8,9,10,11} Any or all of these developments will further serve to

accelerate the use of this relatively new technology.

Other possible applications of the long-life, sealed, maintenance-free NiH₂ system include large storage batteries for load leveling for electric utilities, storage of solarcell-generated electrical power, and submarine applications.^{12,13,14} Many other uses will develop as the cost of these cells decreases and as the confidence based on additional successful months and years of operation of these cells increases.

Acknowledgments

The author wishes to thank Herbert Bilsky, Stephen Gaston, and Eugene Pearlman for their technical support for this paper, and to acknowledge the entire Astro team's contributions to the successful application of nickel-hydrogen technology to satellite use.

References

1. J. D. Dunlop and J. F. Stockel, "Nickel-Hydrogen Battery Technology—Development and Status," *Journal of Energy*, Vol. 6, No. 1, pp. 22-33, January 1982.
2. E. Levy, Jr., "Nickel-Hydrogen Battery Technology—A Tenth Anniversary Review," *Proceedings of the 18th Intersociety Energy Conversion Engineering Conference*, pp. 1530-1534, August 1983.
3. S. F. Schiffer, "Life-Cycling Testing of Air Force Design Nickel-Hydrogen cells Using a Simulated Low-Earth Orbit Cycling Regime," *Proceedings of the 19th Intersociety Energy Conversion Engineering Conference*, pp. 252-256, August 1984.
4. J. F. Stockel and D. B. Cooper, "Geosynchronous Performance of Nickel-Hydrogen Cells," *Proceedings of the 19th Intersociety Energy Conversion Engineering Conference*, pp. 505-508, August 1984.
5. S. J. Gaston, "The GSTAR and Spacenet Nickel-Hydrogen Batteries for Geosynchronous Orbit Applications," *Proceedings of the 19th Intersociety Energy Conversion Engineering Conference*, pp. 257-262, August 1984.
6. J. Dunlop, "Nickel Hydrogen Batteries," *McGraw-Hill Handbook of Batteries and Fuel Cells*, Chapter 22, 1984.
7. M. J. Mackowski and V. C. Mueller, "Cycling Characteristics and Failure Modes of Prototype Nickel-Hydrogen Cells," *Proceedings of the 19th Intersociety Energy Conversion Engineering Conference*, pp. 146-151, August 1984.
8. N. Puester, "Phase I Value Engineering Study Resulting in Increased Producibility of Air Force Design Cells," *Proceedings of the 17th Intersociety Energy Conversion Engineering Conference*, pp. 786-789, August 1982.
9. O. Gonzalez-Sanabria and M. A. Manzo, "Separator Development and Testing of Nickel-Hydrogen Cells," *Proceedings of the 19th Intersociety Energy Conversion Engineering Conference*, pp. 279-286, August 1984.
10. R. L. Cataldo, "Design of a 1-kWh Bipolar Nickel-Hydrogen Battery," *ibid.*, pp. 264-269, August 1984.
11. G. Van Ommering and C. W. Koehler, "Bipolar Nickel-Hydrogen Battery System Design," *ibid.*, pp. 625-630, August 1984.
12. V. J. Puglisi, A. S. Berchelli, C. P. Donnel, "Nickel-Hydrogen Battery for Load-Leveling Application," *Proceedings of the 15th Intersociety Energy Conversion Engineering Conference*, pp. 1198-1203, August 1980.
13. J. E. Clifford and E. W. Brooman, "Assessment of Nickel-Hydrogen Batteries for Terrestrial Solar Applications," SAND 80-7191, Sandia National Laboratories, Albuquerque, NM, February 1981.
14. G. W. Work, P. A. Karpinski, "Energy Systems for Underwater Power," Marine Technology Conference and Exposition, New Orleans, October 1979.



Stephen Schiffer is a Principal Member, Technical Staff, in the Power Systems Engineering Group at RCA Astro-Electronics. He received his Bachelor's and Master's degrees in Chemical Engineering from the Polytechnic Institute of Brooklyn, New York, in 1963 and 1968, respectively. He has worked in battery design and development for more than 21 years and has been with Astro since May 1982. Steve has authored numerous articles on battery technology, including a chapter in the *Handbook of Batteries and Fuel Cells* (McGraw-Hill, 1984).

Contact him at:
RCA Astro-Electronics
Princeton, NJ
Tacnet: 229-3277

Fat Albert peers over the horizon

Even flying at 10,000 feet, Seek Skyhook IB has to contend with earthbound boats, cars, and trucks, and then there is the occasional mysterious "sea crawler"...

Low-flying aircraft can penetrate long distances into our ground radar surveillance areas without detection. These undetected aircraft pose serious problems to the Air Force and Customs Service. Line-of-sight limits of conventional ground-based radars can be overcome in a number of ways, most of which are very costly. RCA Service Company has developed an aerostat (tethered balloon) platform and lightweight radar payload as a cost-effective solution to providing low altitude coverage out to 150 nautical miles. The system is officially known as Seek Skyhook IB, but is most frequently referred to by the press as Fat Albert. Systems located near Key West and Cape Canaveral, Florida are now providing radar coverage 24 hours a day.

A shocking start

RCA's involvement with tethered balloons or aerostats can be traced back more than 17 years. Early projects sponsored by De-

Abstract: *Seek Skyhook IB is an aerostat (tethered balloon) radar platform designed to provide low-altitude radar coverage out to 150 nautical miles. This article discusses the system and the problems that had to be overcome to make it viable.*

© 1984 RCA Corporation
Final manuscript received May 2, 1984
Reprint Re-29-6-10

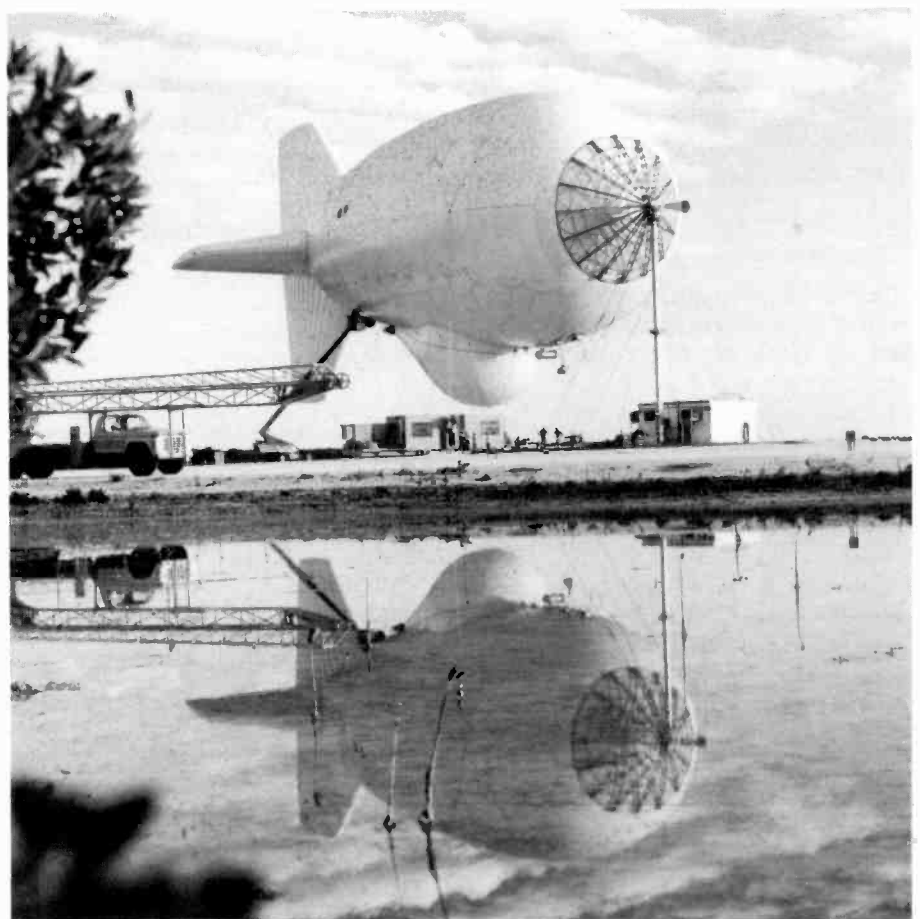


Fig. 1. Aerostat moored at Cudjoe Key Air Force Station. Pressurization system is being serviced from an aerial lift. The winch platform with 25,000 feet of tether is directly behind the aerostat. A truck-mounted aerial lift used to service the upper surface of the aerostat is parked in the left foreground.

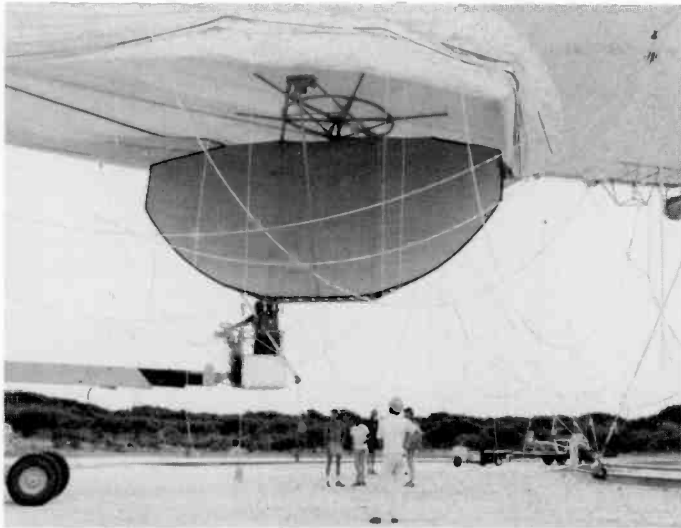


Fig. 2. Aerostat radar. The windscreen has been opened and reefered to show the radar antenna, which is 22 feet across. Servicing is normally accomplished through an access port in the inflated windscreen.

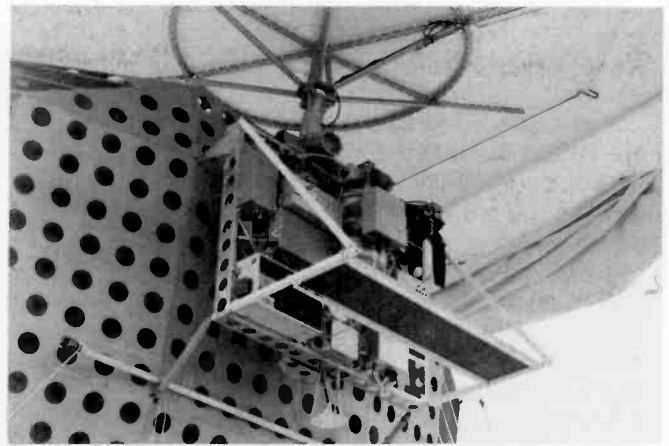


Fig. 3. Aerostat radar. Radar subsystems are assembled on a backplane for easy maintenance from the service platform. A large tubular mounting ring (shown at the top) is laced to the aerostat belly. The two-axis gimbal used for antenna stabilization is partially visible between the antenna and mounting ring. The only slip rings required for this configuration are for 3-phase, 400-Hz power.

fense Advanced Research Projects Agency (DARPA) were devoted to developing a reliable and stable platform that could lift 1000-pound payloads 10,000 to 15,000 feet. An aerostat provided an ideal application for radar surveillance because equipment costs and operating costs were both projected to be a full order of magnitude less than if aircraft were used as the platforms. A development site was built at Cudjoe Key, Florida. RCA was originally responsible only for the aerostat and its support equipment. However, in July 1976 RCA assumed operation and maintenance of the radar payload as well. Within one week after assuming operation of the radar, lightning hit the aerostat and it fell into the Gulf of Mexico. The radar was recovered and the pieces refurbished or rebuilt without the aid of any of the original vendor's engineering drawings. Within six months the radar was not only flying, but working better than the original. This success led to contracts for a number of improvements, culminating in the current high-performance Seek Skyhook Radar AN/DPS-5.

Height leads to many problems

Flying at 10,000 feet, the radar can detect aircraft at an altitude of 500 feet out to 150 nautical miles. By the same token, the radar also sees massive amounts of land and sea clutter—reflections from topographic artifacts—as well as cars, trucks, boats, etc. Doppler filtering is used to suppress returns from nearly stationary clutter, but it is not effective against fast-moving surface vehicles and certain types of clutter

with a wide velocity spectrum. Ground-based radars have a similar problem, but due to the earth's curvature, ground and sea clutter are observed over only a small inner region of their coverage.

Data automation increases the problem

Air Force observers viewing Plan Position Indicator (PPI) scopes were originally employed to detect any targets of interest and forward track data to the Regional Operations Control Center (ROCC) at Tyndall AFB, Florida. Manning three PPIs at a site on an around-the-clock basis is very expensive. The Air Force therefore levied a requirement for data automation. An attempt was made to use the AN/FYQ-47 Common Digitizer, which is standard equipment for most Joint Surveillance System (JSS) sites. The many real targets (vehicles and boats), together with clutter spikes, quickly overloaded the data capacity of the FYQ-47, the voice channels used for data transmission, and the ROCC. Interim automated operation was achieved only by greatly limiting the geographical areas of coverage.

Where's the aircraft

The technical challenge was clear—find the aircraft in the background of residual clutter and surface vehicles. The current state of the art offers many approaches, but most would significantly increase the weight or power consumption of the radar, making it impossible to lift with an aerostat.

System constraints

The aerostat system must be able to remain on station at 10,000 to 12,000 feet altitude for up to one week without refueling or other routine maintenance. With balloons of reasonable size (250,000 ft³), lightweight tethers and efficient power generation, the radar payload is limited to a maximum of about 1000 pounds, 3 kW in power consumption, and a 22-foot antenna diameter. A magnetron transmitter operating at S-Band (3 GHz) was originally chosen for its high efficiency and low weight. The noncoherent pulse train generated by the magnetron was made coherent-on-receive by storing a phase sample of the transmitted pulse and using it to reference the received signal phase. In order to minimize airborne equipment weight and complexity, the reference sample and the received signals are digitized and relayed to the ground over wideband microwave channels for subsequent Doppler processing and target extraction.

An evolutionary approach, rather than complete radar redesign, was initiated. It consisted of two major items—improving land and sea clutter rejection and improving extraction of the desired targets.

Improved clutter rejection

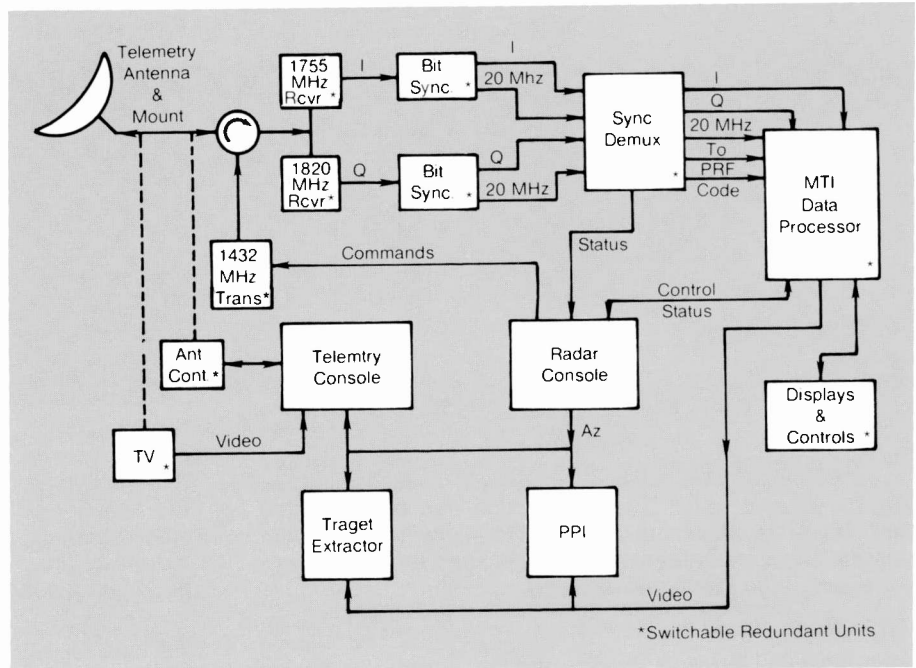
Some of the most significant improvements in Doppler cancellation of land and sea clutter were achieved by:

- Replacing the conventional magnetron with a coaxial magnetron
- Increasing the resolution of the analog-

Radar description

The aerostat-borne portion of the AN/DPS-5 surveillance radar weighs only 1000 pounds. It is housed in a pressurized windscreen, and is gravity-stabilized by a two-axis gimbal attached to the underside of the balloon. A block diagram of the airborne system is shown in Fig. 1. Received signals and a reference sample from the transmitter are phase-detected and digitized for transmission to the ground station. Two 20-megabit/second telemetry downlink channels are employed—one for in-phase and one for quadrature data. Housekeeping and synchronizing signals are also inserted in these data streams. A single telemetry uplink channel is used to control the airborne system.

A block diagram of the radar ground station is provided in Fig. 2. A steerable antenna is manually positioned to track the telemetry signals radiated from the aerostat. Each channel is amplified, demodulated and sent to a bit synchronizer. The synchronizer/demultiplexer then establishes ground station



synchronization using the preamble code. It also extracts the radar status and mode data, prf information, azimuth information, and computes the biterror rate. Radar status information is displayed at the radar console. Commands to change various radar functions can also be

sent from this radar console via the uplink telemetry channel. The telemetry console contains the necessary controls and monitors for operating the telemetry system and numerous other aerostat systems such as pressurization, power generation, etc.

to-digital converters from 10 to 12 bits

- Using airborne PreCOR corrections
- Adding a "clutter shifter"

The last two items are novel, and warrant further explanation.

In a fully coherent system the phase of a nearly stationary target changes very little from pulse to pulse. Any errors introduced by the I/Q (in-phase and quadrature) detector and the A/D converters are at a very low frequency and are further attenuated by the Doppler filter.

In a coherent-on-receive system (which is necessary with a magnetron transmitter), each transmitted pulse has a random phase. The random phase component is subtracted out in the ground processor by using a phase sample of the transmitted pulse. Any errors in the I/Q detector and A/D converters, however, are random from pulse to pulse and are not further suppressed by the Doppler filter. The coherent-on-receive system thus requires much higher compo-

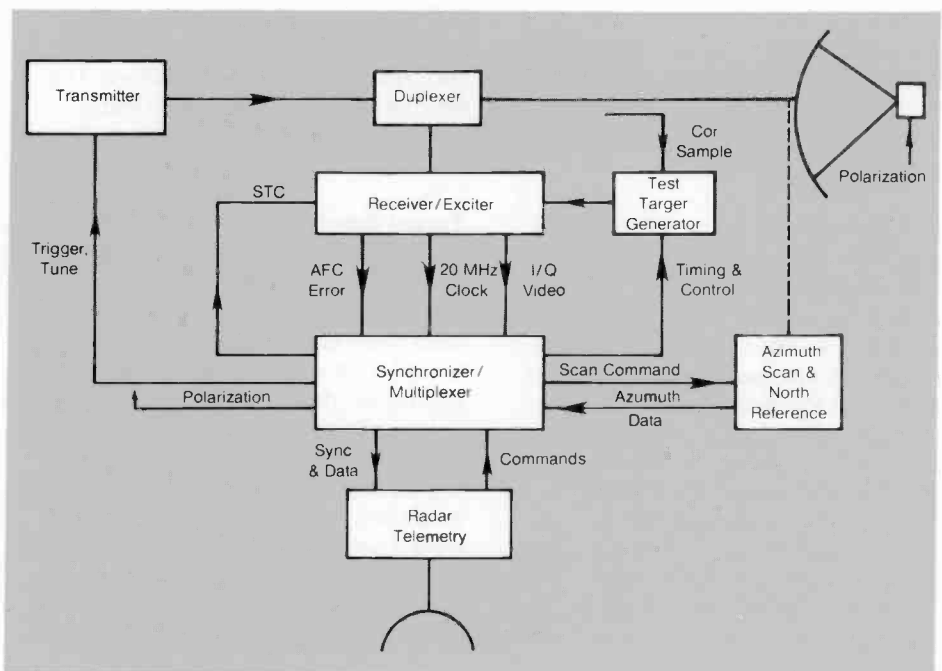
nent accuracy than the fully coherent system to achieve the same clutter cancellation. This problem is greatly reduced by the PreCOR corrector installed in the airborne unit. Two delayed transmitter samples are needed for this correction. The receiver phase is first changed with a digitally controlled shifter so as to bring the first transmitter sample to within a few degrees of a coherent reference. The second transmitter sample and all received radar data are then fed through the receiver and normal coherent-on-receive channel. Using this system, relatively large errors in the I/Q detector and D/A converter can be tolerated with little cancellation loss.

Most of the area covered by present radars is over water. Wave motions due to the winds and currents (Gulf Stream) bias the Doppler spectrum significantly from zero velocity. This bias greatly reduces the sea clutter cancellation. Residual or uncanceled clutter is always very high when the radar looks directly into waves created by high winds. By shifting the mean Doppler

frequency as a simple function of wind speed and direction, a 10 to 15 dB improvement in sea clutter rejection has been achieved.

Blind speeds

Doppler radars have blind speeds, or dead zones, where the radial target velocities correspond to multiples of the radar pulse repetition frequency (prf). It is well known that higher-order blind speeds can be eliminated by staggering the prf. This stagger feature was incorporated in the first aerostat radars, but was never satisfactory. The problem stemmed from instabilities of the common magnetron when operated with a non-uniform prf. An interim solution was used in which the prf was changed on successive scans (rather than every pulse). The cyclic target loss every few scans, however, caused very serious problems with the target extractor. By improving the modulator and going to a coaxial magnetron, stability was improved sufficiently so that



Radar signals are processed in the MTI data processor. On site, radar data can be observed on plan position indicators (PPIs). It is also converted to standard TV format and recorded for a permanent record. A target extractor is used to send radar reports and track reports over

long distance telephone lines to the regional control centers. At present, two target extractors produced by Litton Data Systems are being evaluated. One is a production system, the other is an advanced state-of-the-art system.

clutter cancellation with 5-pulse stagger is now virtually as good as for a fixed prf. This one improvement made useful automatic target extraction performance practical.

Target extractor handles the rest

Any residual clutter spikes and moving targets are converted to radar plot reports on a scan-by-scan basis. Experience has shown that spurious plots can easily overload the control centers. Further correlation of track on a scan-to-scan basis is required to eliminate random reports and reports from vehicles (boats, cars, and trucks) traveling below aircraft speed. Two target extractors produced by Litton Data Systems, the Radar Beacon Digitizer (RBD) and the Advanced Tracking System (ATS), are being used and evaluated for this application. The problem is severe, because real world clutter does not always follow expected textbook data.

One interesting phenomenon found under certain (usually calm) sea conditions is called a sea "crawler." The crawler has a nearly straight path with a speed of 20 to 60 knots. Crawlers in the same general area usually have parallel tracks, and may last many minutes. Since these speeds are much higher than either the wind or waves, they were originally thought to be high-speed boats (traveling between the Florida

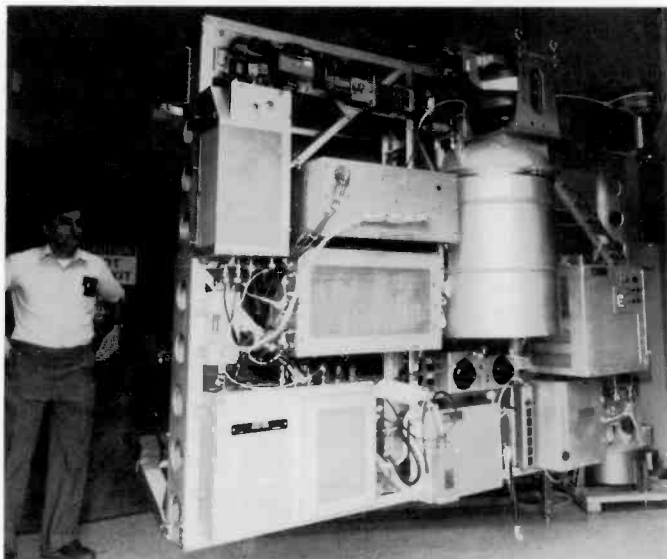


Fig. 4. Radar back plane. In normal maintenance, any failed or suspect major subsystem (boxes) is replaced with a functional one from a "hot spare" system. The most difficult unit to change is the transmitter/modulator, which weighs over 200 pounds. The windscreen access port and a winch have been designed to accomplish this quickly and safely.



Fig. 5. Aerostat ground station. Cabinets on the right contain the MTI processor and radar telemetry and the synchronizer/demultiplexer subsystems. The radar and telemetry operating consoles are in the center. They are configured to support two-aerostat operation. Racks on the left contain equipment for monitoring and controlling other aerostat systems such as pressurization and power generation.

MTI data processor

The moving target indicator (MTI) data processor receives and processes 12-bit digital I and Q data from the airborne radar, then converts the processed data to radar video for distribution to video users. Processing reduces noise, land clutter, and sea clutter, resulting in enhanced visibility of airplanes and other targets of interest. The most important processing functions are:

Transmitter phase correction. During each radar interpulse period (IPP), 2890 I and Q pairs are received by the processor. The first word pair received is the result of sampling the radar transmitter phase as related to the receiver stable oscillator (STALO). This phase sample is used to correct each received word pair during that IPP. This is accomplished by performing a complex multiplication every 600 nanoseconds, and is necessary to remove the random phase of the

transmitted pulse each time the magnetron is triggered. This process produces coherent-on-receive (COR) video, and allows the Doppler filtering to remove the low-velocity clutter components.

Doppler shifting. Sea clutter has a significant average Doppler shift when the waves have an inbound or outbound velocity component relative to the radar. Because of these Doppler shifts, sea clutter may then appear at the output of the narrow band MTI filter and obscure targets of interest. The Doppler shifter provides a frequency shift that is a function of prevailing wind speed and the cosine of the antenna angle relative to the prevailing wind. This in effect subtracts the mean Doppler shift caused by the wind, and shifts the sea clutter Doppler velocity back to zero average velocity. A land/is provided to inhibit Doppler correction over land or areas where sea returns will not produce a mean Doppler shift.

MTI filter. The MTI filter is implemented by cascading two 2-pole, 2-zero recursive high-pass filters. The filter has five manually selectable notch widths of 50, 100, 125, and 150 Hz.

Target detection and integration. A linear amplitude detector is approximated by first rectifying both I and Q and then taking the larger (I or Q) plus one-half the smaller. This detected data is then processed by a sliding window integrator that can select either 4, 8, or 16 pulse windows. Improvements in minimum signal of up to 9.4 dB can be achieved. Use of a sliding window type of integrator minimizes the with the 16-pulse integraskewing of azimuth centroids as a function of variation in signal amplitude.

Constant-false-alarm rate. Conversion to logarithmic video is accomplished by use of ROM look-up tables. Two automatic thresholds are generated to implement the

Table 1. Radar characteristics

Coverage and Accuracy		Receiver	
Range (instrumented)	10 to 150 nautical miles	RF Sensitivity time control	0 to 15 dB in steps of 1.0 dB
Target altitude coverage	0 to 12,000 feet	Noise figure	2.1 referenced to the antenna terminals
Range resolution	0.08 nautical miles	Dynamic range	81 dB (including STC)
Range accuracy	0.25 nautical miles	IF frequency	30 MHz
Azimuth resolution	1.0%	Detection	Baseband producing in phase (I) and quadrature (Q) video
Azimuth accuracy	0.25%		
MTI improvement factor	45 dB	Synchronizer/Multiplexer	
Precipitation clutter suppression	15 dB	Type	digital
Transmitter		A/D conversions for I&Q	11 bits + sign bit
Type	Coaxial magnetron	Sample rate	1.66 MHz
VMS-1178 (Varian)		Uplink channels	32
Tuning range	3.1 to 3.5 GHz	Housekeeping functions	70 bits
Peak power	1.0 MW	Digitized analog housekeeping	32 functions
Average power	500 W	Radar Telemetry	
Pulse width	1.0 sec.	<i>Command uplink</i>	
Pulse repetition frequency (fixed or staggered)	480.7 pulses/sec. (average)	carrier frequency	1432 MHz
Antenna		deviation	±100 kHz
Type	Shaped beam reflector	modulation	FM
Polarization	Selectable horizontal or circular	<i>I data downlink</i>	
Gain	38.7 dB (min.)	carrier frequency	1820 MHz
Beamwidth		deviation	±8 MHz
azimuth	1.1°	modulation	PCM/FM
elevation	3.5° with cosecant squared shaping	<i>Q data link</i>	
Azimuth sidelobes	-20 dB (max.)	carrier frequency	1755 MHz
Rotation rate	5 rpm	deviation	±8 MHz
		modulation	PCM/FM

constant-false-alarm rate (CFAR) video. The first threshold removes the mean by generating a threshold that is the average value in a 64-cell sliding range window (approximately 3.1 nautical miles long and centered on the cell being thresholded). The second threshold is generated in a similar manner, but has operator gain and offset adjustment controls to allow setting of the desired false alarm rate.

Digital data conversion to video.

The processor has six D/A converters that convert processed digital data to analog video outputs. Radar videos with and without MTI (Doppler filtering) and with and without CFAR processing are available. Several amplitude compression curves are available to match user needs.

Built-in test and monitoring features.

Provision is made for monitoring data at 40 pairs of test points distributed along the data paths

through the processor. Test points occur in pairs because of a certain duality of data paths (I/Q, NON-MTI/MTI, etc.). At operator option, any one of the 40 pairs of tristate buffers can be enabled, gating data from the selected pair of test points to the two display buses. Each bus connects to a dedicated D/A converter whose output may be conveniently displayed on a dual-channel oscilloscope. The two buses also interface with a microcomputer that converts the binary data to either octal or decimal, as selected by the operator, for display on two LED displays. Any of the 2890 range cells can be selected for display. This display is updated once every 512 IPPs.

Each processor incorporates an I/Q test data generator (TDG) whose output can be selected for processor input. Under operator control, the TDG precisely defines static and dynamic may data inputs. The TDG is used with the previously described display equipment to verify proper

operation the MTI data processor and to troubleshoot when a malfunction is detected.

The MTI data processor has 100 percent equipment redundancy. It incorporates two complete and identical processors that can be used in several ways. For example, both processors could be driven in parallel by the same airborne radar and provide two different types of filtering (e.g., one optimized to detect aircraft, and the other to detect ships). Alternatively, one processor could be selected to drive all video users and the second processor could be used as a backup or taken down for maintenance. Another configuration in which a processor is driven by an operating radar that is on the aerostat, while the other processor is driven by a second radar being tested or serviced on the ground.

Keys and Cuba). However, observers in vectored aircraft were never able to identify the source. The most reasonable explanation for the crawlers at present is that they are reflections from facets at the inter-

sections of different sets of ocean swells. An intersection can move considerably faster than the waves if the intersection angle is small. Regardless of their source, the trackers can edit out the crawlers by

employing a minimum speed threshold of about 75 knots.

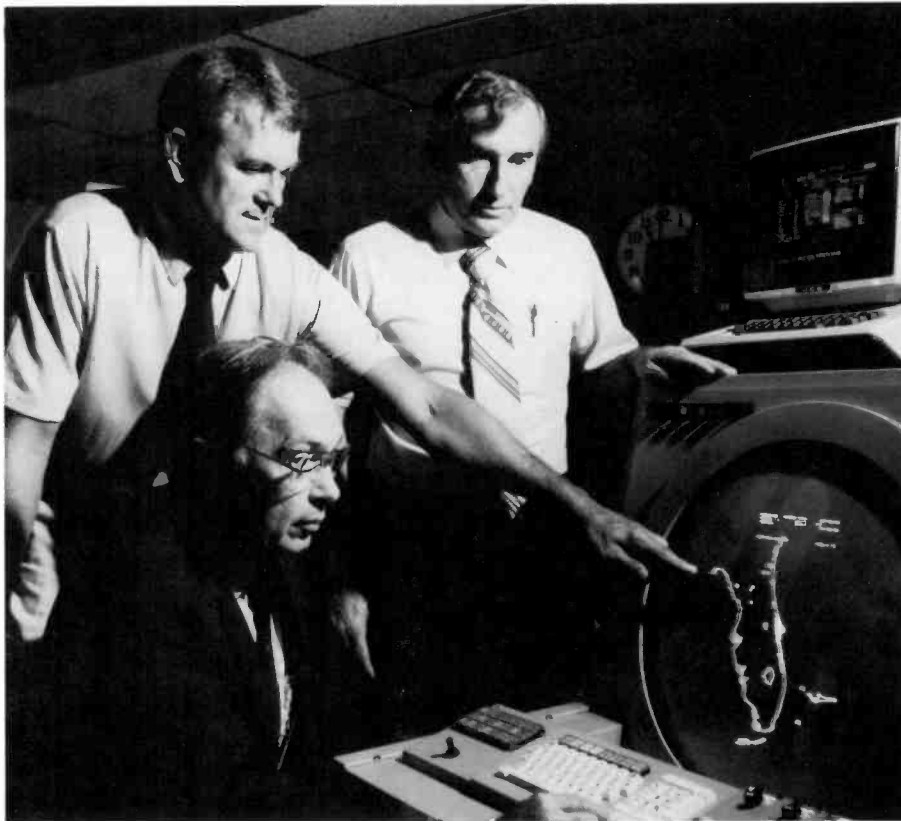
One man's junk may be another man's target

Many of the slow moving targets that are rejected for air surveillance are of great interest to the Navy, Coast Guard, and Customs Service. With different processing these tracks can be made available to an additional class of users at little increase in overall cost. Oceanographers have also shown interest in the sea clutter returns, which may contain useful data on currents, internal waves, and wave height and direction.

Conclusion

Feedback of operational problems to system and design engineers has improved performance significantly, and has brought the aerostat radar to full operational capability. Two sites are currently providing 24-hour low-altitude surveillance of the Florida Straits, and more sites are being considered.





Authors Mertens (seated), Gelzinis (left), and Houyouse (right) in front of the target extractor displays.

Larry Mertens is a graduate of Columbia University, where he received the B.S., M.S., and D. Eng. Sci. degrees in Electrical Engineering. He joined RCA Defense Electronic Products

in 1953, and had a variety of assignments in advanced development, systems engineering, and digital communications. He transferred to the RCA Service Company in Florida in 1962,

and has been responsible for analysis of missile instrumentation and the development of the aerostat system. He is currently Manager, Technical Analysis and Chief Scientist. Contact him at:

**RCA Service Company
Missile Test Project
Patrick AFB, Florida
(305) 494-7411**

James Houyouse joined the Missile Test Project in 1964. He transferred to Aerostat Systems in 1978. His primary task was the development of the MTI data processor for the Seek Skyhook Phase IB radar system. He is now involved in the implementation of radar improvements such as IFF and data automation.

Contact him at:
**RCA Service Company
Aerostat Systems
Patrick AFB, Florida
(305) 494-7601**

Pete Gelzinis received the BEE from Villanova University in 1950, and the MSEE from Drexel University in 1954. He has been with RCA since 1954, when he started working with Missile and Surface Radar at Moorestown, NJ. He participated in the design of the AN/FPS-16, BMEWS, TRADEX, and ALCOR tracking radars. Joining RCA Aerostat Systems at Patrick AFB, Florida in 1977 as a senior engineer, he contributed to the design and field evaluation of the aerostat-borne radar. Currently, he is with the Missile Test Project at PAFB.

Contact him at:
**RCA Service Company
Missile Test Project
Patrick AFB, Florida
(305) 494-5173**

Patents

Astro-Electronics

Kujas, E. F.
Negative hydrogen electrode comprising an alloy of palladium and ruthenium—4460660

C.E. Profera/H.H. Soule, Jr.
Phase Reconfigurable Beam Antenna System—4471361

Communications Systems Division

Hacke, J. F./Banks, A. J./Bazin, L.J.
Square-wave symmetry corrector—4461962

Hudson, K. C.
Semiconductor laser scanning system—4460240

Thompson, C. R.
Digital recording of television components with improved transition spacing—4464683

Consumer Electronics

Brauer, E. A.
Stylus cleaner pad orientation in disc record player—4464742

Fitzgerald, W. V. Jr.
Regulated power supply incorporating a power transformer having a tightly coupled supplemental power transfer winding—4466051

Greenstein, B.
Method and apparatus for quantitatively evaluating the soldering properties of a wave soldering system—4467638

Helm, J. H.
Video disc player having turntable retention mechanism—4464744

Hicks, J. E.
Horizontal output transistor protection circuit—4459517

Hughes, L. M.
Video disc player having door lock mechanism—4467466

McNeely, M. L.
Video disc preform and method of making a disc therefrom—4460656

Parker, R. P.
Kinescope black level current sensing apparatus—4463385

Prusak, J. J./Patel, B. P.
Video disc caddy—4463849

Rainey, J. H./Boltz, C. D. Jr.
Video disc caddy—274905

Turner, R. L./Jennings, R. E.
Rack for transporting recorded discs—4461386

Turner, R. L./Prusak, J. J.
Apparatus for manufacturing disc record package—4465453

Weaver, C. A.
Apparatus for attaching a matrix to an electroforming device and method therefor—4468290

Whipple, B. A./Dunn, V.S.
Method for preparing a molding composition—4465617

Government Communications Systems

Corsover, S. L./Ammon, G. J./Reno, C. W.
Multi-beam optical record and playback apparatus having an improved beam splitter—4459690

Crowley, A. T.
Phase frequency detector using shift register—4459559

Crowley, A. T./Lisowski, R.M.
Universal digital frequency synthesizer using single side band techniques—4464638

Crowley, A. T.
Phase locked loop frequency synthesizer including fractional digital frequency divider—4468632

Laboratories

Bloom, S.
CRT with quadrupolar-focusing color-selection structure—4464601

Bogner, B. F.
Radial transmission cancellation device—4466090

Chartier, M. S.
Digital gain control system—4464723

Christopher, L. A./Reitmeier, G. A./Smith, T. R./Strolle, C. H.
Window-scanned memory—4460958

Connolly, J. C./Botez, D.
Terraced heterostructure semiconductor laser—4461008

Faith, T. J. Jr./Irven, R. S./Plante, S. K.
Method for mounting a sapphire chip on a metal base and article produced thereby—4457967

Gale, M. T./Knop, K. H.
Dynamic accuracy X-Y positioning table for use in a high precision light-spot writing system—4464030

Goldberg, S. B.
Amplitude control apparatus—4468631

Gorog, I.
Signal pickup cartridge—4459692

Gorog, I.
Video disc caddy—4463850

Haferl, P. E.
Horizontal drive and nonlinearity correction circuit—4468593

Hasili, J. P.
Line cathode heating and protection circuit—4464611

Huang, H./Mawhinney, D. D.
Monolithic voltage controlled oscillator—4458215

Huang, H./Kumar, M./Sechi, F. N.
Predistortion circuit for a power amplifier—4465980

Janton, W. M.
Waveguide tunable oscillator cavity structure—4459564

Lewis, H. G. Jr.
Clock generation apparatus for a digital television system—4463371

Lim, C. C.
Piezoelectric ultrasonic voltage generator for a television receiver—4459505

Maa, J.
Patterning of submicrometer metal silicide structures—4460435

Nelson, J. R./Wissing, W. K./Dunn, V. S.
Formulation of electrically conductive plastics—4465616

Pike, W. S.
Adaptive control signal filter for audio signal expander—4465981

Prabhu, A. N.
Indium oxide resistor inks—4467009

Pritchard, D. H.
Television signal filtering system—4466016

Reitmeier, G. A.
Adaptive television signal estimator—4464686

Ross, M. D.
Noise reduction circuitry for audio signals—4462048

Samuels, G.
Apparatus for spraying a liquid on a spinning surface—4457259

Scheible, H. G.
Wave soldering apparatus and method—4463891

Schiff, L. N./Freeman, S.
Time window key system for video scrambling—4464678

Schroeder, A. C.
Sampling arrangement for a television ghost signal cancellation system—4458269

Stavitsky, D./Beres, E. A.
Injection molding apparatus—4462780

Strolle, C. H.
Memory scanning address generator—4462024

Wargo, R. A.
Method and apparatus for operating a microprocessor in synchronism with a video signal—4464679

Wargo, R. A./Perlman, S. S.
Automatic color burst magnitude control for a digital television receiver—4466015

Whitley, G. J.
Apparatus for securing a component to a printed circuit board—4462435

Whitley, G. J.
Apparatus for detecting the presence of components on a printed circuit board—4463310

Whitley, G. J./Rayl, M.
Component lead bending apparatus—4464829

Missile & Surface Radar

Abeyta, I.
Circuit for coupling signals to or from a circuit under test—4465971

Landry, N. R.
Dispersion correcting waveguide—4458229

Michaelis, T. D.
Encoder controlled apparatus for dynamic braking—4460857

Tower, J. R.
Multi-chip imager—4467342

Wasson, R. A.
Fail-safe sensor circuit—4467386

New Products Division

Ritzman, I. G.
Method of removing a glass backing plate from one major surface of a semiconductor wafer—4465549

Solid State Division

Balaban, A. R./Steckler, S. A.
Low frequency digital comb filter system—4464675

Brackelmanns, N. W./Hulstrunk, W.
Fast switching transistor—4460913

Harford, J. R.
Integrated circuit overload protection device—4463369

Harwood, L. A./Shanley, R. L. 2nd
Amplifier incorporating gain distribution control for cascaded amplifying stages—4464633

Kaplan, L. A.
Power amplifier circuit employing field-effect power transistors—4463318

McIntyre, R. J./Webb, P. P.
Avalanche Photodiode array—4458260

McIntyre, R. J./Webb, P. P.
Silicon avalanche photodiode with low keff—4463368

Schade, O. H. Jr.
Trimming circuits for precision amplifier—4462002

Schmitt, E. T./Ronan, H. R. Jr./Schuler, M. R.
Fixture for testing semiconductor devices—4460868

Solid State Technical Center

Dingwall, A. G.
Electronic circuits and structures employing

enhancement and depletion type igtets—4463273

Stewart, R. G./Dingwall, A. G.
Memory system with redundancy for error avoidance—4464754

Stewart, R. G./Dingwall, A. G.
Memory system with error detection and correction—4464755

Video Component and Display Division

Brown, M. K./Richard, K. S.
Rigid cathode support structure for an in-line electron gun assembly—4460845

Hoffman, B. L.
Vacuum gripping apparatus—4460208

Krufka, F. S.
System and method of accurately controlling the electrode voltage of a welding device—4464556

Maddox, W. J.
System for applying a high voltage source to a CRT through a capacitive load—4467224

Pearlman, S.
Reducing glare from the surface of a glass viewing window—4460621

Ragland, F. R. Jr.
Color picture tube having improved temperature compensating support for a mask-frame assembly—4460843

Schlack, R. E./Richard, K. S.
Cathode support structure for an in-line electron gun assembly—4468588

Wilbur, L. P. Jr./Wardell, M. H. Jr.
Color selection electrode mounting structure having an off-set washer—4467242

Yakmovitz, K. J.
Television receiver and test set voltage analyzer—4459551

Special Contract Inventors

Yarnitsky, Y./Livny, A.
Jig for use in machining stylus blanks—4466555

Pen and Podium

Recent RCA technical papers and presentations

To obtain copies of papers, check your library or contact the author or his divisional Technical Publications Administrator (listed on back cover) for a reprint.

Astro-Electronics

D. L. Balzer

Shuttle Compatible Orbit Transfer Subsystem—Presented at the 35th IAF Congress, Lausanne, Switzerland Presented (10/7/84)

G. A. Beck

The NASA Advanced Communications Technology Satellite (ACTS)—Presented at the 35th IAF Congress, Lausanne, Switzerland (10/7/84)

L. A. Freedman (AE)/P. B. Pierson (ATL)/ O. L. Graham (NASA JSC)

Digital Television for Space Applications—Presented at EASCON '84', Washington, DC (9/11/84)

J. N. LaPrade/D. Ferguson/J. Duthie

Dual Band Telemetry Transmitter for Broadcast Satellite Application—Presented at MILCOM, Los Angeles, Cal. (10/21/84)

R. C. Maehl

Low Cost Planetary Spacecraft Based on an Existing Satellite Design—Presented at the 35th IAF Congress, Lausanne, Switzerland (10/7/84)

S. Palocz

Utility Requirements for Serviceable Platforms—Presented at the 35th IAF Congress, Lausanne, Switzerland (10/7/84)

A. Rosenberg

Accommodation of a Lidar Sounder on a Polar Meteorological Satellite—Presented at the NASA Sponsored Workshop, Stanford University, Palo Alto, Cal. (10/1/84)

C. R. Voorhees/G. A. Clark

Discussion of Modal Test Techniques as Applied to a Spacecraft Structure—Presented at the SAE 1984 Aerospace Congress and Exposition, Long Beach, Cal. (10/15/84)

L. Yermack

Direct Broadcast Satellite Design Solution—Presented at the 35th IAF Congress, Lausanne, Switzerland (10/7/84)

Automated Systems

G. L. Edgar/D. A. Gore

Techniques for the Early Detection of Gear

and Bearing Failures in Helicopter Drive

Trains—Presented at the American Helicopter Society's National Specialists Meeting on Testing Technology, Williamsburg, Va. (10/29/84)

J. C. Tranfaglia

Hybrids and Computer Aided Design (CAD)—Presented at the Applicon Users' Group, San Francisco, Cal. (10/17/84)

J. C. Tranfaglia

BRAVO Software—Presented at the Applicon Users' Group, San Francisco, Cal. (10/17/84)

Government Communications Systems

H. R. Barton/B. Tiger/F. M. Winton

Sampling in System State Availability Modeling—Presented at the Quality in Electronics (QIE) Symposium and Proceedings, Raleigh, N.C. (9/26/84)

J. Cervini/J. Springer

A High Speed ESM Processor for Target Identification—Presented at the Tri-State Combat Identification Systems Conference and Proceedings, Johns Hopkins University, Laurel, Md. (10/23/84)

T. S. Chichester

Automating Engineering Communication—Presented at the IEEE Professional Communications Conference IEEE, and published in the *Transactions on Professional Communications*, Atlantic City, N.J. (10/10/84)

D. G. Herzog/S. L. Corsover/B. L. Compton

A Highly Accurate 2.5 GHz Pixel Image Generation Recording System—Presented at the SPIE 20th Annual Symposium, San Diego, Cal. (8/21/84)

D. T. Kjellquist

The Personal Computer & Procurement Process—Presented at the RCA Symposium, Lancaster, Pa. (9/11/84)

J. L. Lynerd

Tactical Military Equipment Logistics Support Analysis (LSA) and Reliability Centered Main(RCM) Program—Presented at the 19th International Tenance Logistics Symposium, Minneapolis, Minn. (8/21/84)

B. Milstein

Information Center Training at RCA GCS—Presented at the Philadelphia Area Information Center User Group, Philadelphia, Pa. (10/17/84)

M. H. Riddle

Modulated Pilot Tone—RCA Tech Note (5/20/84)

M. H. Riddle

High Density Magnetic Tape Recording for Mass Storage—RCA Tech Note (6/6/84)

M. Rosenblatt

Low Rate Multiplexer—Presented at MILCOM 84, Los Angeles, Cal. (10/21/84)

J. J. Wynne

Integrated Communications Displays—Presented at the Man/Machine Interface Seminar, MIT, Boston, Mass. (9/20/84)

L. T. Yeh

Validity of One Heat Transfer Correlation to Various Shaped Ducts via Hydraulic Diameter Concept—Presented at the International Electronic Package Conference, Baltimore, Md. (10/29/84)

Government Systems Division

H. W. Kaiser/J. S. Pridmore/R. K. Smeltzer (RCAL)

RCA Radiation Hard CMOS/SOS Technology Status—Presented at Radiation Hardened Electronics Technology Meeting, Dallas, Tex. (10/17/84)

B. Mudge

Machine Vision for Motion Analysis—Presented at the IEEE Computer Society 13th Workshop on Applied Imagery Pattern Recognition, Silver Springs, Md. (10/23/84)

Laboratories

L. R. Avery

Electrostatic Discharge: Mechanisms, ProtecTechniques, and Effects on Integrated Circuit Reliability—Published *RCA Review*, Vol. 45 (6/84)

R. S. Crandall

Modeling of thin-film solar cells: Nonuniform field—Published in *Journal of Applied Physics* 55 (12) (6/15/84)

T. J. Faith, Jr./R. S. Irven

Bond-Integrity Testing of Sapphire Chips Mounted with Eutectic Preforms—Published in *IEEE Transactions on Components, Hybrids, and Manufacturing Technology*, Vol. CHMT-7, No. 2 (6/84)

T. J. Faith/J. J. O'Neill, Jr./W. A. Hicinbothem, Jr.

Contact resistance improvements by implantation through an Al mask—Published in *Applied Physics Letters* 45 (5) (9/1/84)

T. J. Faith/C. P. Wu

Elimination of hillocks on Al-Si metallization by fast-heat-pulse alloying—Published in *Applied Physics Letters* 45 (4) (8/15/84)

L. Jastrzebski/A. G. Kokkas

SOI By CVD: An Overview of Material Aspects and Implications of Device Properties—Published in *Mat. Res. Soc. Symp. Proc.* Vol. 23 (1984)

M. A. Lampert/R. U. Martinelli

Solution of the Non-Linear Poisson-Boltzmann Equation in the Interior of Charged, Spherical and Cylindrical Vesicles I. The High-Charge Limit—Published in *Chemical Physics* 88, pp. 399-413 (1984)

H. W. Lehmann/B. J. Curtis/R. Fehlmann

A throttle valve for automatic pressure control in sputtering and reactive sputter etching—in *Vacuum*, Vol. 34, No. 7, pp. 679-681 (1984)

Published P. A. Longeway/H. A. Weakliem/R. D. Estes

Mechanism of the Direct Current Plasma Discharge Decomposition of Disilane—Pub-

lished in *J. Phys. Chem.*, Vol. 88, pp. 3282-3287 (1984)

R. C. Ross/J. L. Vossen

Plasma-deposited thin-film step coverage calculated by computer simulation—Published in *Appl. Phys. Lett.* 45 (3) (8/1/84)

J. R. Sandercock

Experimental Observation of Surface and Interface Modes by Light Scattering—Published in *Journal De Physique, Colloque C5*, supplement au no. 4, Tome 45 (4/84)

R. K. Smeltzer/C. W. Benyon, Jr.

Dielectric Integrity of the Gate Oxide in SOS Devices—Published *RCA Review* Vol. 45 (6/84)

D. J. Szostak and B. Goldstein

Photovoltage profiling of hydrogenated amorphous Si solar cells—Published in *J. Applied Physics Letters* 56 (2) (7/84)

Missile and Surface Radar

J. A. Bauer

Design Considerations With Leadless Chip Carriers—Presented at ISHM Surface Mounting Workshop, Dallas, Tex. (9/17/84)

F. J. Buckley

The IEEE Software Engineering Process—Published in *IEEE Micro*, Vol. 4, No. 4 (8/84)

P. Das

Microprocessor Operation of Fault Detection in VHSIC Based Programmable Signal Processor—Presented at the Int'l. Society for Mini and Microcomputers, New York, N.Y.,

and published in the *Proceedings* (10/22-24/84)

J. W. Douglas

Multiple Disks and Tapes on Applicon Systems—Presented at the Applicon Users' Group Fall Technical Meeting, Santa Clara, Cal. (10/14-19/84)

G. S. Edelson

Sidelobe Reduction of the Random Array by Third Moment Diversity—Presented at the Valley Forge Research Center Friday Seminar Series, University of Pennsylvania (1½/84)

R. A. Faust, Jr.

The MMI Emulation Facility—Presented at MIT, Boston, Mass. (9/20/84)

F. H. Ireland

MSR's Man-Machine Systems Organization—A Miniprofile—Published *RCA TREND*, Vol. 24, No. 4 (9/84)

G. W. Kaisar

AEGIS Cruiser CG-47 Class Maintainability Consideration—Presented at the ITEA '84' Symposium, Washington, DC, and published in the *Proceedings* (11/6/84)

W. J. Paterson

MIL-STD-1862B Implementation Considerations—Presented at the AE-9 Committee Meeting, Orlando, Fla. (10/15-18/84)

A. W. Wainwright, Jr.

Working With the Programmer's Reference Manual—Presented at the Applicon Users' Group Fall Technical Meeting, Santa Clara, Cal. (10/14-19/84)

Engineering News and Highlights

Taylor named Staff VP, Systems Integration



The appointment of **Lloyd A. Taylor** as Staff Vice President, Systems Integration, RCA Electronic Products and Laboratories, has been announced by **Roy H. Pollack**, Executive Vice President. Mr. Taylor will report to **Dr. Harry J. Woll**, Staff Vice President and Chief Engineer, RCA Electronic Products and Laboratories.

In this post Mr. Taylor will coordinate the development of new electronics products, including digital TV, with the design and fabrication of new solid state products to achieve an overall improvement in the Corporation's operations and market position. This activity will involve vertically integrating aspects of the RCA Consumer Electronics Division, the New

Products Division, the Solid State Division, and RCA Laboratories in Princeton, N.J.

Mr. Taylor was previously Vice President of Technology for Commodore International Limited. Prior to that time, he was Group Vice President of the Semiconductor Components Group, Northern Telecom Ltd., and Vice President of Technology for Bell-Northern Research Ltd. for seven years. Mr. Taylor has over twenty years experience in solid state systems.

He is a graduate of the University of Idaho with an Electrical Engineering degree, and he earned a Master's degree, also in Electrical Engineering, at the University of Southern California.

David Shore named head of SDI



David Shore has been named Division Vice President, Strategic Defense Initiative, by **Paul E. Wright**, Division Vice President and General Manager, RCA Government Systems Division.

Mr. Shore, who has served since 1981 as Division Vice President of Business Development, now has responsibility for all of the division's activities related to the nation's new anti-ballistic missile defense effort. A 30-year RCA employee, Mr. Shore has a wide range of experience in programs concerned with ballistic missile defense. He directed several of the division's complex system studies, including the TALOS Land-Based Defense System, a guidance system for ICBMs, an RCA-sponsored study of defenses against ICBMs, the Wizard anti-ICBM system, and the Ballistic

Missile Early Warning System (BMEWS). In the BMEWS program, he directed the design of the overall system.

Mr. Shore was named Division Vice President of Advanced Programs Development in 1975. He had held the same position for two years before that with the RCA Government and Commercial Systems organization. Earlier, he served for two years as Division Vice President, Government Plans and Systems Development.

A graduate of the University of Michigan, where he received a Bachelor's degree in Aeronautical Engineering in 1941, Mr. Shore received a Master's degree in Physics from Ohio State University in 1950.

John Serafin named GCS Program Operations VP



John F. Serafin has been appointed Division Vice President, Program Operations, by **Lawrence J. Schipper**, Division Vice President and General Manager, RCA Government Communications Systems.

Mr. Serafin is responsible for directing the planning, control, and performance of all programs at the operation. He came to RCA in 1979 as Manager, Projects, in the Government Communications Systems organization. In 1981 he became Manager, Integrated Communications Systems, and in 1982, Director, ICS, with responsibility for developing new business while maintaining high performance on current programs.

Before coming to RCA, Mr. Serafin was employed for 19 years at Ford Aerospace Corp. in Willow Grove, Pa., holding several engineering and management positions, including Manager of Advanced Programs.

Mr. Serafin received Bachelor's and Master's degrees in Electrical Engineering from Drexel University, and he served as an officer in the U.S. Army Corps of Engineers from 1957 to 1959. A member of the Navy League, Mr. Serafin also belongs to the United States Naval Engineers, the Armed Forces Communications Electronics Association and the American Defense Preparedness Association.

Philip Martin to head GSD unit



Philip J. Martin has been named Division Vice President, Business Development, by **Francis H. Stelter Jr.**, Division Vice President, Marketing. Mr. Martin is responsible for the domestic business development of the division. He maintains executive liaison with the Department of Defense, NASA and other federal agencies, and he assists the division's business units in developing and implementing plans for attaining major business goals in the government market.

Regional offices in Washington, D.C., Los Angeles, Cal., Dayton, Ohio, Burlington, Mass., Huntsville, Ala., and Red Bank, N.J. are also Mr. Martin's responsibility. He succeeds David Shore, who was promoted to the position of Division Vice President, Strategic Defense Initiative.

Before his appointment, Mr. Martin was Division Vice President, Business Development and Strategic Planning, for RCA Service Company, a position he had held since July 1981. He was also Division Vice President of Government Services Marketing for RCA Service Company from September 1979 to July 1981.

Mr. Martin received a Bachelor's degree in Physics from St. Joseph's University, and a Master's degree in Electrical Engineering from Drexel University. He also is a graduate of the management development program at Harvard's Graduate Business School.

Staff announcements

Jack K. Sauter, Group Vice President, announces his organization as follows: **Edward A. Boschetti**, Division Vice President and General Manager, Distributor and Special Products Division; **William E. Boss**, Division Vice President, Distributor and Commercial Relations; **D. Joseph Donahue**, Vice President, Consumer Electronics Operations; **Charles A. Quinn**, Division Vice President and General Manager, Video Component and Display Division; **Stephen S. Stepnes**, Division Vice President, Consumer Electronics Marketing; and **Arnold T. Valencia**, Division Vice President and General

Manager, VideoDisc Division, and President, RCA Distributing Corporation.

Americom

Patrick F. Egan, Manager, CTO, Eastern Operations, announces the appointment of **Kenneth H. Hoffman** as Supervisor, Pittsburgh CTO.

Astro-Electronics

Louis Gomberg has been appointed Director, Remote Sensing Satellite Programs by **Charles A. Schmidt**, Division Vice President and General Manager, RCA Astro-Electronics, East Windsor, N.J.

Consumer Electronics

D. Joseph Donahue, Vice President, Consumer Electronics Operations, announces his organization as follows: **James E. Carnes**, Division Vice President, Engineering; **Keith U. Clary**, Division Vice President, Consumer Electronics Employee Relations; **David E. Daly**, Division Vice President, Consumer Electronics Product Planning; **Michael B. Evans**, Division Vice President, Consumer Electronics Finance; and **Leonard J. Schneider**, Division Vice President, Manufacturing Operations.

James E. Carnes, Division Vice President, Engineering, announces the appointment of **Theodore L. Allen** as Manager, Project Operations.

Leonard J. Schneider, Division Vice President, Manufacturing Operations, announces his organization as follows: **Bennie L. Borman**, Division Vice President, Manufacturing; **Larry A. Cochran**, Director, Monitor Operations; **Dennis L. Dwyer**, Director, Production Planning, Distribution and Transportation; **John P. Keating**, Division Vice President, Purchasing; and **James R. Smith**, Division Vice President, Product Assurance.

Globcom

Dominick A. Intartaglia, Vice President, Business Development, announces the appointment of **Robert C. Atkinson** to the newly created position of Director, New Service Planning and Development.

Joe Terry Swaim, Vice President, Switched Services Engineering and Operations, announces the appointment of **Beth M. Eckenrode** as Manager, Project Control.

Government Systems Division

H. Andre Carron, director, Manufacturing Operations, announces his organization as follows:

H. S. Barr, Manager, Manufacturing Administration; **Robert M. Birkland**, Manager, Plant Engineering; **Larry A. Colangelo**, Manager, Government Manufacturing; **Richard J. Grimm**, Manager Manufacturing Systems; **George H. Lines**, Manager, Fabricated Products; **Charles F. O'Donnell**, Manager, Materials; **Fred Pfifferling**, Manager, Technical Operations; **L. Clair Phillips**, Manager, GWEN Planning and Production; **Vincent F. Renna**, Manager, Commercial Manufacturing; and **Nathan Shectman**, Manager, Manufacturing Projects.

Richard J. Haug, Manager, Photomask, Equipment and Facilities Operations, announces his organization as follows: **Robert A. Geshner**, Manager, Photomask Operations; **Ronald A. White**, Manager, Facilities and Safety Engineering; and **Richard J. Haug**, Acting Manager, Equipment Engineering.

RCA Laboratories

Bernard J. Lechner, Staff Vice President, Advanced Video Systems Research, announces the appointment of **Peter J. Burt** as Head, Advanced Image Processing Research.

Arthur Kaiman, Director, Digital Products Research Laboratory, announces the appointment of **G. David Ripley** as Head, Consumer Software Research.

Curtis R. Carlson, Director, Information Systems Research Laboratory, announces his organization as follows: **Philip K. Baltzer**, Head, Knowledge-Based Systems Research; **James J. Power**, Head, Home Data Systems Research; **Glenn A. Reitmeier**, Head, Home Communications Research; and **Thomas M. Stiller**, Fellow, Technical Staff.

Charles J. Nuese, Director, Integrated Circuit Research Laboratory, announces the appointment of **Lawrence A. Goodman** as Head, Advanced Silicon Technology Research.

Missile and Surface Radar

Donald E. Dalgleish has been named Director of Product Operations at RCA Missile and Surface Radar in Moorestown, N.J. by **William V. Goodwin**, Division Vice President and General Manager.

Solid State Division

Carl R. Turner, Division Vice President and General Manager, Solid State Division, announces the appointment of **Robert P. Jones** as Division Vice President, Power Products.

R. Adrian Bishop, Manager, Product Marketing and Applications—Memory and Microprocessors, announces his organization as follows: **Edmund J. Blicke**, Manager, Product Marketing—Automotive and Industrial; **William**

H. Schilp, Jr., Section Manager, Applications Engineering—Memory and Microprocessors; and Paul K. Sferazza, Manager, Product Marketing—Computer and Telecommunications.

Video Component and Display Division

Albert M. Morrell, Manager, Product Development, announces his organization as follows: Robert L. Barbin, Manager, Mount Development; Richard H. Godfrey, Manager, Tube Design; Carl W. Penird, Manager, Display Engineering; and Anthony S. Poulos, Manager, Type Engineering.

William R. Miller, Manager, Equipment Development, announces the appointment of John H. Prusak as Manager, Mount and New Process Equipment.

Professional activities

Yang receives M.S.

Jialing Yang received his Master of Science degree from the Mechanical and Aerospace Department of Rutgers University in September.

P.E. Licenses

David P. O'Rourke has been awarded a Pennsylvania Registered Professional Engineer's license (PE-033899-E)

Perlman receives award

Barry S. Perlman, Manager, Design and Test Automation, received the Hall of Fame award from INTEREX, the International Association of Hewlett-Packard Computer users, at their recent Technical Computer Conference in San Jose, California. Dr. Perlman was recognized for his work in helping to establish the HP/1000 International Users Group and serving as President of the Board of Directors.

Pankove receives appointment

Jacques I. Pankove, Integrated Circuit Research Laboratory, was recently appointed to a two-year term on the Advisory Editorial Board of Solar Energy Materials, 1984-1986.

Kumar chairs METSAC

Mahesh Kumar, Microwave Technology Center, is the 1984-85 Chairman of the Metropolitan Sections Activities Council (METSAC), which coordinates the activities of the Long Island, New York, North Jersey, and Princeton IEEE Sections.

Broadcast Systems Wins Emmy

RCA Broadcast Systems Division was awarded a 1984 Emmy for its pioneering role in the development of Circular Polarization for Broadcast Television. John Cannon, President of the National Academy of Television Arts and Sciences, presented the Emmy to Joseph C. Volpe, Vice President and General Manager, RCA Broadcast Systems Division. It was the ninth Emmy awarded to RCA for its technical and engineering contributions to the television industry. The Antenna Engineering activity has been a pioneer in the development and manufacture of broadcast antennas for radio and television stations, including those for circularly polarized broadcasting for which this Emmy is awarded.

Library automation workshop

Gerry Moss, Manager, Technical Information Systems, hosted the RCA Librarians' Workshop held at the RCA Technical Excellence Center in Princeton on November 1 and 2. The theme was library automation. The workshop also included a discussion of problems in one-person libraries, and the speakers reflected the move to automation. Robin Deal of Americom described the field test of microcomputer software, and Jim Goodman of the Labs described plans for automating the Labs' library and the merging of all of the RCA library collections into one database. Susan Tamer of Consumer Electronics library in Indianapolis led a discussion of techniques to improve library service in one-person libraries.

The librarians are preparing a manual of library procedures that will be available to librarians who join the RCA staff or non-librarians who have responsibility for a library collection.

MSR wins award

RCA Missile and Surface Radar has received an award in recognition of its achievement in placing more than \$1.2 million in orders with small disadvantaged businesses in the 1983 calendar year.

The Minority (Small Disadvantaged) Business Enterprise Award is an RCA Corporate award given annually to each business unit within the company that meets or surpasses its set goal for small disadvantaged business subcontracting. Goals are set each year by the corporation as a percentage of each business unit's total projected annual spending. "Nearly 75 percent of the vendors used here during 1983 are classified as small and small disadvantaged businesses," said William L. Reid, Manager of Purchasing at RCA Missile and Surface Radar. Mr. Reid serves as the Small Business and Small Disadvantaged Business Liaison Officer at RCA-MSR. "This award shows our success in meeting our goals," Mr. Reid said. "Our \$1.2 million in orders surpasses

the goal that we were expected to meet."

The award plaque was presented to Mr. Reid, on behalf of the Materials Management Department, by William V. Goodwin, Division Vice President and General Manager, at a recent ceremony in the plant. RCA Missile and Surface Radar received this award last year for surpassing its 1982 goal for small disadvantaged business subcontracting.

Courtney receives Coast Guard medal

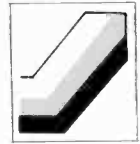


John E. Courtney, Senior Member of the Engineering Staff, Engineering Department, Missile and Surface Radar, received the Coast Guard Arctic Service Medal from Commander W. A. Caster, Commanding Officer, *USCGC Northwind*, in July.

Mr. Courtney represented MSR in the testing of the Advanced Autonomous Array (A³), a free-floating passive sonar system under development with the Navy Electronics Systems Command. The tests took place in the Norwegian and Greenland seas, up to 200 miles above the Arctic Circle, over a six-week period from the end of February to Mid-April 1984.

The A³ system, which maintains contact via a radio link from a surface buoy, was deployed from *USCGC Northwind*, a Coast Guard icebreaker, so that tests could take place up to and within the ice pack.

Commander Caster's commendation letter to Mr. Courtney read in part, "Wind chill factors of minus 55 degrees were encountered during deck operations. All hands shared the hardships and endured harsh arctic conditions to ensure successful mission completion. Gale force winds, freezing temperatures, and flying ice, which was literally torn from the tops of waves by the wind, caused the task force to seek refuge in the lee of Iceland on more than one occasion. *Northwind*, however, remained on station and completed all tasks assigned. In recognition of your outstanding performance, diligence, and devotion to duty, you are hereby authorized to wear the Coast Guard Arctic Service Medal."



1st Quarter CE Technical Excellence Awards



Parks



Heiny



Winton



Allen



McClain



Anderson



Henson



Nero

Robert A. Parks—for developing an audio IC test system using digital synthesis of test signals and FFT processing of sampled measurements.

Edward J. Heiny and Robert A. Winton—for developing electrical hardware and computer software to facilitate the function of the United Tensile Tester in the Products Protection Labs, significantly improving its accuracy and automating its function. This improved system resulted in a 300 percent increase in test data accuracy and a 70 percent reduction in required man hours for data reduction.

John K. Allen and Kevin E. McClain—for developing a significant and timely alignment/test time reduction program on a major master-

board assembly that resulted in substantial capital and manufacturing cost savings.

William D. Anderson and Michael A. Henson—for designing and verifying a filter and gain control for luminance peaking in digital television. This project was undertaken even though the vendor had stated that goals for the peaking filter characteristics and linear gain control were not practical.

Leroy W. Nero—for developing the ROSE IHVT primary winding design, including time-to-failure theoretical analysis and subsequent experimental verifications.

Larry G. Moore and Roland P. Patterson—for designing, writing, and testing the software in the system controller of the modular audio/video entertainment system.

Peter F. Gero—for playing the pivotal role in diagnosing and solving membrane switch performance and field reliability problems. This included extended on-site process development.

2nd Quarter CE Technical Excellence Awards



Albean



Fraley



Muterspaugh



Snell



Gilbert



Gorgal



Morgan

Dave Albean, Morgan Fraley, Jim Gibson, Max Muterspaugh, Marc Snell—for developing multi-channel sound capability for television. The demands on the team were severe because the state-of-the-art was new and the normal development and problem solving time had to be shortened. Not only was it necessary to design the television receiver decoding circuitry, but it was also necessary to design the transmitter signal encoding system. The decoder module is currently part of the CTC131, and part of the encoding system is being used by WNBC, Channel 4, New York, for broadcast. The individual contributions were vitally important, and were required to meet the project goals. The team effort resulted in a very successful presentation to RCA distributors at the May Special Products Presentation in Las Vegas.

Dan Gilbert—for the design and installation of robotic systems to automatically unload portable plastic cabinet fronts, backs, and 25-inch console masks from 14 plastic injection

molding presses. The robotic systems had to interface with six different models of equipment spanning eighteen years of technology. The project was completed one month ahead of the revised schedule and within budget, and improvements were made in product quality, material handling, and production capacity. The major direct labor savings achieved have allowed the Indianapolis plant to produce at a cost advantage over outside vendors.

Robert Gorgol—for the start-up of the first microprocessor-controlled injection molding press. The normal production process for injection molding involves 16 parameters, of which 12 are adjusted by the press set-up person. Through exhaustive testing and experimenta-

tion, Mr. Gorgol reduced the process parameters to ten constants and two variables. The press was purchased to produce high voltage transformer tertiary bobbins. These parts require extremely close tolerances, and were previously considered too difficult to be produced by the Indianapolis plant. The project demonstrated the feasibility of molding precision parts in-house, and will be used as a basis for bringing other close-tolerance parts inside.

Edward Morgan—for the conception, design, and implementation of a device that inexpensively duplicates the controlled motion of a painting robot arm. This device duplicates the programmability, versatility, and dynamic con-

trol attributed to contemporary robots without the path programming capabilities. This was accomplished for about 20 percent of the cost of similar purchased units and for less than 15 percent of the cost of a true robot. The successful implementation of this device has made the testing of paint processing variables feasible on a practical scale. Testing of paint used in production can now be performed. In addition, research into critical painting parameters that directly affect product finish is now possible. The application of this simulator has led to a more thorough understanding of the variables that affect quality and consistency during the finishing process.

SSD Technical Excellence Awards



Krysko



Longenberger

Dave Krysko—for his contributions to the photo resist area. Dave helped to design and install an automatic system that stopped the operation of the cannon aligners when wafers were not centered on the chuck. Operation of the equipment with wafers off center had for some

time been a cause of wafer breakage. He also recently completed design improvements on the suss aligner, allowing its use on thyristors.

Marty Longenberger for his contributions to the automatic TO-3 assembly line. Most notably, the modifications to the shinkawa and slee software programs to allow efficient and trouble-free operation of this equipment. Innovations include both software and hardware design and implementation on mounters, bonders, sealer and handling system.

Rick Friend—for his work in designing, laying out, and implementing the 480-volt substation expansion project in Fab II. When the COS/MOS equipment was being converted to 4-inch capability in late 1982, the required diffu-

sion furnaces were only available in 480 volts. Since no 480 volt service was available in the CMOS Fab II area, Rick modified three lightly loaded 480-volt single-phase welding circuit transformers to three-phase service. This provided the required power prior to receiving the equipment. The project also involved the installation of a new 480-volt transformer to replace the modified welding circuits. This provided power for COS/MOS in the event of a transformer failure, and also provided an alternate source of power for Penthouse #2. The loss of any of these services would shut down the Plant until power could be restored. This paid off handsomely last April when the Plant was struck by lightning.

2nd Quarter GSD TEC winners



Katsumata



Mehling

Kun Katsumata—for creativity and dedication in defining an efficient, generic architecture for a Multiple Instruction Set Processor (MISP), CPU hardware, and microcode. His timely development provides a viable in-house 1750A processor, a requirement for impending VHSIC-1 insertion projects. In addition, the MISP can be configured as either an 1862B or 1750A processor, placing MSR in a strong competitive position for addressing future DOD computer procurements.

Thomas H. Mehling—for outstanding contributions to AEGIS Combat System readiness and operational excellence. His services were specifically requested during March and April 1984 to assist in preparations for a special post-deployment operational test designed to challenge USS *TICONDEROGA*'s air defense capabilities. His ability to diagnose subtle and unusual problems and provide instantaneous solutions was a major factor in the extraordinary performance levels achieved.

Joseph P. Pryzbylkowski—for design and implementation of an interactive computer graphics system that significantly enhances the development, manufacture, and test of wire-wrapped modules and back planes. The system provides discipline and flexibility in geometric data generation for a variety of wire-wrapped products. Mr. Pryzbylkowski's development has reduced the time and skill levels necessary to perform this operation, with significantly improved design accuracy and quality.

Frank J. Reifler—for significant contributions to basic radar tracking theory through application of asynchronous filtering for separation of range and angle measurements. This filtering technique, developed previously by Dr. Reifler for smoothing of passive track and burnthrough data, promises full target tracking performance at roughly one-half the data rates currently required. This performance is particularly significant in terms of its potential impact on tracking radar energy management.



Pryzbylkowski



Reifler

Dr. Elmer W. Engstrom, former RCA President



Dr. Elmer W. Engstrom, 83, a former President of RCA and head of the corporation's research laboratories in Princeton, N.J., died on Tuesday, October 30, after a long illness. Dr. Engstrom retired from RCA in 1969, following a 39-year career with the company.

He served as President of RCA from 1961 to 1965. In the ensuing two years he was Chairman of the Executive Committee of the Board and Chief Executive Officer. He relinquished

the latter title in 1968, but remained as Chairman of the Executive Committee until his retirement.

During the early years of his retirement, Dr. Engstrom served as a Consultant to RCA and remained a member of its Board of Directors until 1971. Prior to his election as President of RCA, he had been a Senior Executive Vice President of the Corporation for six years.

Dr. Engstrom advanced to the top levels of responsibility within RCA from a background of research, engineering, and technical management. He was graduated in 1923 from the University of Minnesota with a Bachelor of Science degree in Electrical Engineering. Upon graduation, he joined the General Electric Company and was assigned to engineering development work on radio transmitting and receiving equipment in Schenectady, N.Y. In 1930, the radio and engineering activities of G.E. were transferred to RCA, and Dr. Engstrom joined the Corporation as Division Engineer in charge of Photophone sound motion picture apparatus. Soon afterward, he assumed engineering responsibilities for RCA's broadcast receiver development and production.

Beginning in the early 1930's Dr. Engstrom supervised RCA's program of TV research and development. He brought to the project

the concept of television as a complete system, instituting one of the early large-scale examples of the systems engineering concept that is now standard in major technical programs. In the postwar years, as head of RCA Laboratories, he applied the same concept in directing the development program for the all-electronic, compatible color television system.

In 1942, when all the research activities of RCA were brought together in Princeton, N.J., Dr. Engstrom became Director of General Research. He held a series of progressively higher positions, culminating in his appointment in 1955 as Senior Executive Vice President. He served in that capacity until he became President of RCA in 1961.

During World War II, Dr. Engstrom was responsible for research in the fields of radar, radio, airborne electronics, television and acoustics.

He was awarded honorary degrees by 18 colleges and universities, and also received numerous industry awards and medals. In 1966, he was the recipient of the Founders Award of the Institute of Electrical and Electronics Engineers for "leadership in management and integration of research and development programs and for his foresighted application of systems engineering concept in bringing television to the public."

A personal note

Just 51 years ago in the month of November, I arrived in Camden in response to a letter offering me a position on the research staff of RCA. So on that day I met Elmer Engstrom, the Director of Research, and began a professional relationship that continued until his retirement 33 years later, and a personal relationship that spanned 51 years.

On the evening after the death of Elmer Engstrom, I reflected on the events we had shared for a little over a half century. First, I thought of the many times he had encouraged me to pursue a variety of research projects. Then I remembered the time after our twins were born when he quietly confided that he soon would be a father.

Together we faced the challenges of

the battle for standards of a compatible color-television system, when he and I spent so many nocturnal hours in preparing for his and my appearances as witnesses before the Federal Communications Commission. When these hearings ended, he and I, accompanied by our families, spent two months in Europe, where we received the disappointing news that the FCC had rejected our proposals. Then we and our colleagues labored together for three more years to bring about a satisfactory conclusion.

I remember the Saturday evening many years ago when, after three hours of discussion at my home, we decided to tell David Sarnoff that one of his birthday presents was damaged beyond repair.

I remember my disappointment in 1957 when the presidency of RCA was

vacated and Elmer Engstrom was not selected for the position.

I remember the evening in November 1961, when Elmer Engstrom came to my home and in five minutes informed me that he was to be elected to the presidency of RCA on the first of December, and he asked me to assume responsibility for his current duties. One month later, I had the pleasure, pride, and privilege of announcing his election to the assembled guests at the dinner to honor the 25-year members of the RCA Laboratories staff.

I remember my dismay as I saw him in his past few years of life and I remember because it hurt so, that I failed to visit him when he needed comfort. I try to remember all the best of our past moments, and forget the rest.—

George H. Brown

Charles J. Young, RCA facsimile pioneer



C.J. Young, left, and H.G. Greig.

Charles Jacob Young, a retired RCA Laboratories scientist who held more than 65 patents in the field of facsimile transmission and applications of electronics to graphic arts, died on October 2 in the Medical Center at Princeton, N.J., after a long illness. He was 84.

Mr. Young was Associate Director of the

Acoustical and Electro-mechanical Research Laboratory when he retired in 1965 from RCA Laboratories, Princeton, N.J. Among the major developments to which Mr. Young contributed were the early transmission of text and pictures over long distances, widely used in the newspaper and news magazine field, and the

invention of the Electrofax copying process. The system was subsequently licensed by RCA to several photocopier manufacturers.

He was born December 17, 1899, in Cambridge, Mass., his parents were Josephine Edmonds Young and Owen D. Young, who was later Chairman of the Board of the General Electric Co. as well as the first Board Chairman of RCA Corporation from 1919 to 1929.

During World War I, Mr. Young served with the American Red Cross Ambulance Corps in Italy. He was graduated from Harvard University in 1921 and subsequently took postgraduate work in electrical engineering at the Harvard Engineering School.

In 1939, Mr. Young was a recipient of the Modern Pioneer Award of the National Association of Manufacturers for distinguished achievement in the field of science and invention. In 1982, together with Harold G. Greig, he received the Kosar Memorial Award from the Society of Photographic Scientists and Engineers for their joint development of the Electrofax process.

He was a Fellow of the Institute of Electrical and Electronics Engineers, a life member of the Academy of Natural Sciences of Philadelphia, a member of Sigma Xi and the Harvard Club of New York City. At his death, he was President of the Community Corp. of Van Nessville, N.Y., where he had a home.

The accompanying photo shows C. J. Young, left, and H. G. Greig, co-developers of the Electrofax dry photo process at the David Sarnoff Research Center of RCA in Princeton, N.J., examining a photo print produced with a hand-operated Electrofax system. The Electrofax process could produce photo contact prints and master copies of microfilm records, letters, diagrams and other documents in permanent form in a fraction of a minute, and used a highly photosensitive paper developed by the RCA scientists. The speed of the process permitted experimental development of a mechanized continuous-strip system for reproduction.

David S. Rau, RCA pioneer

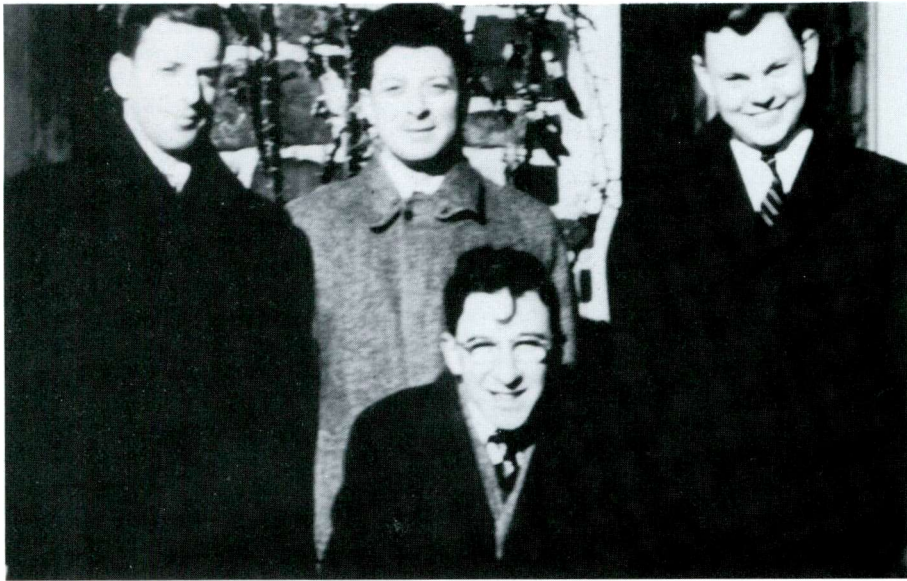
David S. Rau began his RCA career as one of RCA's first student engineers at the Rocky Point high-power transmitting station. He graduated from the U.S. Naval Academy in 1922 with a degree of Bachelor of Science. After a period as Chief Engineer of the Radio Corporation of the Philippines, a wholly-owned subsidiary, and subsequent assignments at major radio stations, Mr. Rau was assigned to the New York Headquarters staff of RCA Communications, Inc. as a Station Design Engineer. During World War II he was on active duty in the office

of the Director of Naval Communications as head of the Shore Radio Stations section, with promotions to the rank of captain. During this time he attended courses in Advanced Radio Engineering at George Washington University. Upon return to RCA Communications he was assigned management duties in facilities design engineering, advancing to Vice President and Chief Engineer. He was a Fellow of the Institute of Radio Engineers, a member of the Board of Editors for the *RCA Review*, and a member of the Board of Technical

Advisors for the RCA Institutes.

Mr. Rau retired in 1964. In 1969 he received the IEEE Communications Technology Group Achievement Award, and in 1978 he was chosen to appear in the first edition of *Leaders in Electronics*, published by McGraw-Hill. On May 14, 1984, as part of its centennial celebration, IEEE presented Mr. Rau with a volume of *A Century of Honors* in recognition of his contributions to electrical progress. Mr. Rau died on July 14, 1984 at the age of 85.

Dr. Carl I. Shulman



Graduate College, Princeton University, 1944. At rear, left to right—Three former Members of Technical Staff, RCA Laboratories: Jerome Kurshan, now Manager, Administrative Projects; Carl I. Shulman, subsequently Professor of Electrical Engineering, City College of the University of the City of New York; Robert R. Bush, subsequently Professor and Chairman of the Psychology Department, University of Pennsylvania, Philadelphia. In front—Howard K. Schachman, Rockefeller Institute, subsequently Professor and Chairman of the Department of Molecular Biology, University of California, Berkeley.

Dr. Carl I. Shulman, 67, died on October 15 following heart surgery. He joined RCA in 1940, and transferred to Princeton as a Member of the Technical Staff of RCA Laboratories when it was established there in 1942. He was part of a small group doing research on electron tubes, an effort not only important to a key RCA business segment at that time, but also vital to World War II military needs.

One of the earliest demonstrations of radar had been conducted by Dr. Irving Wolff, who

subsequently became RCA's Vice President, Research. There was great need to invent and develop electron tubes for radar that were capable of higher-frequency operation, higher power output, and easier modulation. Shulman's early work at RCA had these objectives, and led to publications on: "Frequency Modulation and Control by Electron Beams," with L. P. Smith; "A Frequency-Modulated Magnetron for Super-High Frequencies," with G. R. Kilgore and J. Kurshan; and "Small Signal

Analysis of Travelling Wave Tubes," with M. S. Heagy.

In subsequent work at RCA, Dr. Shulman applied his background in electronic phenomena to the developing solid state field. This led to a publication in *Physical Review* on the "Measurement of Shot Noise in CdS Crystals." In 1955, after a brief assignment with RCA in Lancaster, he joined the Electrical Engineering faculty at City College in New York and continued his career there, retiring with the title of Professor Emeritus. During that time he completed the requirements for a Ph.D. in Physics, awarded to him by Princeton University in 1957.

Dr. Shulman was a low-key, thoughtful, and considerate individual. In his days at RCA he moved in a small circle of friends, but a circle of tremendous intellectual stimulation, loyalty, respect, appreciation, and support. And he, more than anyone else in the group, exemplified these qualities. Dr. Shulman and several of his close friends of that period are shown in the accompanying photograph, taken in 1944.

In 1961, Dr. Shulman was one of the founders of MSI Electronics, a manufacturer of tuning diodes and equipment for measuring the properties of semiconductors. He was a member of the Board, and he worked on integrally-cooled hot-carrier detectors, wide open frequency receiving systems using cyclotron resonance of electrons in a tapered magnetic field as the detecting mechanism, and laser microwave interaction in electro-optic materials. He contributed to a better understanding of measuring doping profiles under an oxide in MOS wafers, and was heavily engaged in minority carrier lifetime measurements in silicon and MOS wafers using mercury contacts. He also developed a theory for a four-point probe with mercury contacts.